DESIGN AND MANUFACTURING OF ELECTRICALLY CONDUCTIVE COMPOSITES VIA MICROVASCULAR CHANNELS

A THESIS SUBMITTED TO
THE GRADUATE SCHOOL OF NATURAL AND APPLIED SCIENCES
OF
MIDDLE EAST TECHNICAL UNIVERSITY

BY

HAMED TANABI

IN PARTIAL FULFILLMENT OF THE REQUIREMENTS
FOR
THE DEGREE OF DOCTOR OF PHILOSOPHY
IN
MECHANICAL ENGINEERING

DECEMBER 2017

Approval of the thesis:

DESIGN AND MANUFACTURING OF ELECTRICALLY CONDUCTIVE COMPOSITES VIA MICROVASCULAR CHANNELS

Submitted by **HAMED TANABI** in partial fulfillment of the requirements for the degree of **Doctor of Philosophy in Mechanical Engineering Department, Middle East Technical University** by,

Prof. Dr. Gülbin Dural Ünver _____
Dean, Graduate School of **Natural and Applied Sciences**

Prof. Dr. M. A. Sahir Arıkan _____
Head of Department, **Mechanical Engineering**

Assoc. Prof. Dr. Almıla GüvençYazıcıoğlu _____
Supervisor, **Mechanical Engineering Dept., METU**

Examining Committee Members:

Prof. Dr. F. Suat Kadıoğlu _____
Mechanical Engineering Dept., METU

Assoc. Prof. Almıla GüvençYazıcıoğlu _____
Mechanical Engineering Dept., METU

Assoc. Prof. Dr. Merve Erdal _____
Mechanical Engineering Dept., METU

Prof. Dr. Levend Parnas _____
Mechanical Engineering Dept. TED Uni.

Prof. Dr. Can Çoğun _____
Mechanical Engineering Dept. Çankaya Uni.

Date: **13.12.2017**

I hereby declare that all information in this document has been obtained and presented in accordance with academic rules and ethical conduct. I also declare that, as required by these rules and conduct, I have fully cited and referenced all material and results that are not original to this work.

Name, Last name: HAMED TANABI

Signature:

ABSTRACT

DESIGN AND MANUFACTURING OF ELECTRICALLY CONDUCTIVE COMPOSITES VIA MICROVASCULAR CHANNELS

Tanabi, Hamed
Ph.D., Department of Mechanical Engineering
Supervisor: Assoc. Prof. Dr. Almıla Güvenç Yazıcıoğlu

December 2017, 104 pages

Owing to their tunable properties and wide range of applications, conductive composites are one of the most important, interesting, and active areas in advanced composite research. For instance, among numerous types of health-monitoring and damage-sensing sensors that can be integrated into composites, electrically conducting sensors offer a simple, cost-effective, and durable option for structural health monitoring in fiber reinforced composites. Despite these advantages, the development of internal electrical sensors in composite systems is limited due to sensitivity and reliability of the sensor. The unique electrical and mechanical properties of carbon nanotubes (CNTs) render CNT reinforced nanocomposites as potentially attractive materials for strain-sensing and monitoring purposes in various industries. The dispersion state of CNT's in polymeric matrix has a significant role on the physical and the mechanical properties of the resulting CNT reinforced nanocomposites. In this study, a series of experiments was designed to investigate the effect of dispersion process parameters and CNT concentration, as well as their interactions on electrical and mechanical and strain sensing properties of CNT-epoxy nanocomposites. Composite samples were produced under different CNT-resin dispersion conditions based on a design of experiments approach, and were characterized using tensile testing, conductivity measurements and micrography. Also, electrical

conductivity of the fabricated nanocomposites was improved with aligning of nanotubes under a magnetic field. In order to create electrical conductive networks in composite specimens, hollow micro-channels were made using vaporization of sacrificial components and then were filled with CNT-epoxy conductive filler. The use of such conductive pathways for in situ strain monitoring of a composite specimen was also investigated. It was found that the strain sensitivity of the prepared conductive channels is nearly two times of conventional strain sensors.

Keywords: carbon nanotubes, CNT-epoxy nanocomposites, electric conductivity, strain sensor, vascularized composites

ÖZ

KOMPOZIT MALZEMELERDE MIKROVASKÜLER KANALLAR YARDIMIYLA ELEKTRIK İLETKENLIĞI OLUŞTURULMASI

Tanabi, Hamed
Doktora, Makina Mühendisliği Bölümü
Tez Yöneticisi: Doç. Dr Almıla Güvenç Yazıcıoğlu

Aralık 2017, 104 sayfa

İletken kompozitler, ayarlanabilir özellikleri ve geniş uygulama alanına sahip olmalarından dolayı ileri dereceli kompozit alanındaki çalışmalarda en önemli, ilgi çekici ve aktif kullanıma sahip kompozitlerdir. Örneğin, kompozitlerin içerisine entegre edilebilen çeşitli sağlık taraması ve hasar analiz sensörleri arasında, elektrik ileten sensörler elyaf katkılı kompozitlerde yapısal sağlık taraması için basit, uygun maliyetli ve dayanıklı bir seçenektir. Bu avantajlara rağmen kompozit sistemlerinde içsel elektrik sensörlerinin gelişmesi hassasiyet ve güvenilirlik sebebiyle sınırlıdır. Karbon nanotüplerin eşsiz elektriksel ve mekanik özellikleri karbon nanotüp katkılı nanokompozitleri çeşitli sanayilerde gerinim algılama ve tarama amaçları için potansiyel ilgi çekici malzemeler haline getirmiştir. Karbon nanotüplerin polimerik matriks içerisinde dağılım durumu oluşan karbon nanotüp katkılı nanokompozitlerin fiziksel ve mekanik özellikleri üzerinde önemli bir role sahiptir. Bu çalışmada, karbon nanotüp epoksi-nanokompozitlerin elektriksel, mekanik ve gerinim algılama özellikleri üzerindeki etkileşimlerinin yanısıra dağılım proses parametreleri ve karbon nanotüp konsantrasyonlarının etkilerini araştırmak için bir seri deney yapılmıştır. Kompozit örnekleri deney tasarımı yaklaşımına dayanılarak farklı karbon nanotüp-reçine dağılım koşullarında üretilmişler ve çekme testi, iletkenlik ölçümleri ve mikrografi kullanılarak karakterize edilmişlerdir. Ayrıca üretilen nanokompozitlerin elektriksel iletkenlikleri magnetik bir alan altında nanotüplerin

yanyana dizilmesiyle arttırılmıştır. Kompozit numuneleri içerisinde elektriksel iletkenlik ağları oluşturmak için içi boş mikro kanallar sacrificial bileşenleri buharlaştırarak oluşturulmuş ve daha sonra bu kanallar karbon nanotüplü-epoksi iletken katkı malzemeyle doldurulmuştur. Kompozit numunesinin gerinim taraması için iletkenlik yollarının kullanımı ayrıca incelenmiştir. Hazırlanan iletken kanalların gerinim hassasiyetinin konvansiyonel gerinim sensörlerinin yaklaşık iki katı olduğu bulunmuştur.

Anahtar kelimeler: mikrovasküler kanallar, mekanik testler, Karbon nanotüp, kompozit malzemeler, elektrik iletkenliği

To My Family

ACKNOWLEDGMENTS

First of all, I am deeply grateful to my supervisor Assoc. Prof. Dr. Merve Erdal for her invaluable supervision, guidance and criticism and especially her extreme support not only during this study but also in whole period of my graduate study. Besides my advisor, I would like to thank the rest of my thesis committee: Prof. Dr. Levend Parnas, Prof. Dr. Can Çoğun, and Assoc. Prof. Dr. Almıla Güvenç Yazıcıoğlu, for their encouragement, insightful comments.

My special and heartily thanks to my friends, Dr. Barış Sabuncuoğlu, Masued Latifinavid and Matin Ghaziani for assisting me during this study with their valuable experience and ideas. I am also deeply thankful to Napelon Shemouil for encouraging and supporting me during this study. I place on record, my sincere gratitude to Tuğçe Aydıl and her lovely family for their great help and support.

I wish to thank my loving and supportive wife, Samaneh, and my daughter, Elsa, who is four at the time of writing, has also needed to show patience when her dad was working on this dissertation.

TABLE OF CONTENTS

LIST OF TABLES

TABLES

LIST OF FIGURES

FIGURES

NOMECLATURE

h_d :fiber disturbance height

k : gauge factor , $k = \frac{\Delta R/R_0}{\varepsilon}$

L_{cnt} : length of nanotubes

L_{RP} : length of resin pocket

l_c : length of conductor

R : electric resistance [Ω]

R_0 : initial electric resistance [Ω]

R_t : theoretical contact resistance at ballistic limit electric resistance [Ω]

R_{jct} : nanotube-nanotube junction contact resistance [Ω]

ε : tensile strain

ε_b: tensile strain at breaking point

λ : electron mean free path , assumed to be 1 μm

σ : electric conductivity $[S/m]$

σ_t : transformed electric conductivity $[S/m]$

σ_m : ultimate tensile strength $[MPa]$

θ: nanotube's orientation angle

θ_d: fiber disturbance angle

CHAPTER 1

INTRODUCTION

1.1 Background

Electrically conductive composites are one of the most important and active areas in advanced composite research. For example, among numerous types of structural health-monitoring and damage-sensing sensors that can be integrated into fiber reinforced composites, electrically conducting sensors offer a simple and cost-effective option for structural health monitoring in fiber reinforced composites. The remarkable electrical and mechanical properties of carbon nanotubes (CNTs) render CNT-reinforced nanocomposites as potentially attractive materials for strain-sensing and monitoring purposes. With the inclusion of CNTs, the viscosity of the polymer matrix is increased dramatically such that fabricating of CNT-filled composites by infusion molding techniques were found to be limited to CNT content below 0.3 wt.% mainly due to unacceptably high resin viscosities.

Recently, vascularized composites (at which hollow channels are fabricated within the composite part) have gained attention in the literature and several research studies have been conducted, aiming to develop techniques for health monitoring and self-healing through vascular channels. In this study, filling the microvascular channels with a conductive material is introduced as an option to create electrically conductive networks in fiber reinforced composites.

1.2 Literature review

1.2.1 Vascularized Continuous Fiber Reinforced Composites

Vascularized fiber reinforced composites are continuous fiber reinforced polymeric composites with embedded vacant vascular channels which can be filled with different mediums such as for various applications. These vascular channels can be made using various techniques with different diameters raging from micro up to macro.

1.2.1.1 Potential Use and Applications

Micro-vascular channels integrated within the fiber reinforced composites, that are filled with appropriate fillers can be used for varying functionality including thermal management [1,2], self-repair and healing [3,4], and damage detection [5].

Coppola et al. [6] developed an active cooling system by pumping cooling fluid into vascular channels embedded in carbon fiber reinforced composites. They showed that the time to failure of actively cooled composites via vascular channels was dramatically longer than that for non-cooled samples under thermo-mechanical compression loading.

Patrick et al. [4] conducted an evaluation of in situ self-healing in fiber-reinforced composites using microvascular networks formed via the vaporization of sacrificial components. The self-healing process in a micro vascularized fiber-reinforced composite is shown in Figure 1. They showed that vascular architectures not only provide efficient and repetitive delivery of healing agents, but also provide increased resistance to the initiation and propagation of delamination.

Vascular channels can also be used to detect fatigue cracks under composite structures. For example, in Comparative Vacuum Monitoring (CVMTM), developed by Structural Monitoring Systems Ltd., vascular channels are used for monitoring the health of large composite aircraft structures [7,8]. This system consists of hollow channels with a typical diameter of less than 1 mm inside the composite structure. These channels are connected to sensors and other measurement equipment located

external to the structure. Air within alternating channels is vacuumed to create states of low pressure. Therefore, a sensor system consisting of a series of channels that alternate between low and ambient pressure can be created. This approach is based on the principle that a growing delamination crack will break neighboring channels and connect them to each other, resulting in flowing air from the channel at ambient pressure into the neighboring low pressure channel. This pressure change is detected by sensors and makes it possible to determine the location and size of delamination cracks inside structures. However, the sensitivity of CVM sensors to detect delamination damage inside composite structures is not well understood but is currently being evaluated [9].

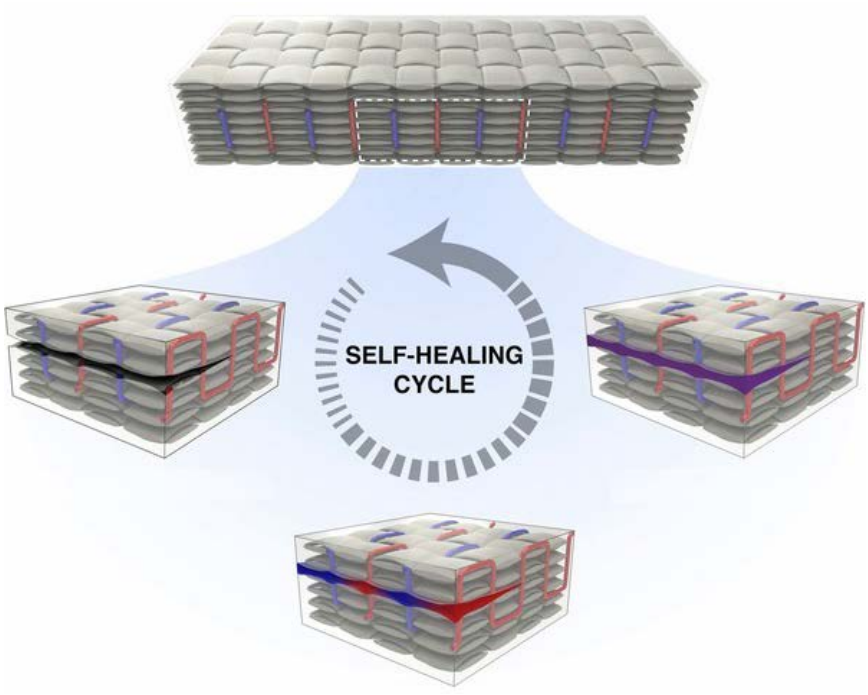

Figure 1. Self-healing cycle in a vascularized fiber reinforced composite. (a) Composite laminate consists of vascular channels filled with healing medium (red is epoxy, blue is hardener), (b) Delamination crack ruptures the vasculature causing to release healing liquids agents from fractured micro channel orifices. Molecular diffusion and polymerization (purple) of the healing agents leads to restoration of structural integrity over multiple healing cycles [4].

1.2.1.2 Production Methods for Vascularized Continuous Fiber Reinforced Composites

In fiber reinforced polymer composite materials, vascular networks are generally fabricated by embedding non-removable hollow tubes or removable solid cores. In both techniques, tubes or cores are placed between fabrics. The fabrics are then impregnated with a polymer and allowed to cure. When the cores are solid, channels are revealed by removing the core from the laminate, either manually or by melting it out. Figure 3 shows the procedure of fabricating microvascular composites using these mentioned techniques. Table 1 summarizes the main features of the fabrication techniques used to create microvascular channels in fiber reinforced composites.

These techniques are limited to straight channels, a challenge overcome by the VaSCs [10,11]. In this method, embedding sacrificial fibers into woven fabrics enables the seamless fabrication of 3D microvascular composites that are both strong and multifunctional [10,11]. With VaSCs, sacrificial polylactide (PLA) fibers are weaved into fiber preforms or fabrics using weaving machines [10] or manually using a sewing needle [11]. Geometric features of fibers such as length, diameter, and curvature are varied to meet the desired design criteria. The fabric is then impregnated with an appropriate polymer and cured at an elevated temperature. After curing, the sample is trimmed to expose the ends of the sacrificial fiber. The fiber is then removed by heating the sample at 200°C for 24 h to vaporize the PLA, yielding empty channels and a 3D vascular network throughout the composite structure. Figure 4 shows the VaSC fabrication procedure schematically.

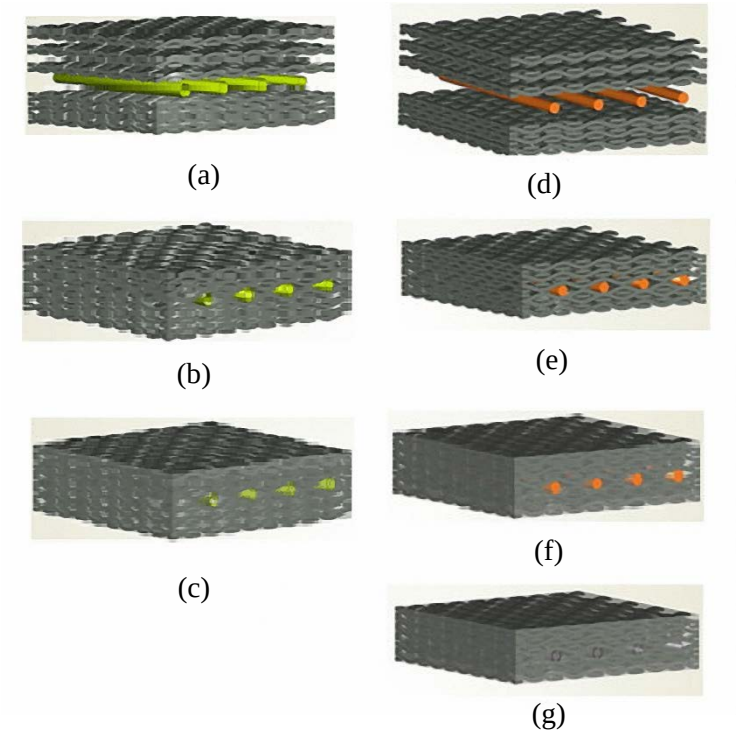

Figure 2. Fabrication of vascular channels in fiber reinforced composites, using non-removable hollow tubes (a-c) and removable solid cores (d-g). (a, d) placing core between fabrics, (b, e) impregnating fibers with resin, (c) cured laminate with embedded hollow tubes, (f) cured laminate with embedded solid cores, (g) removing solid cores to make hollow channels in cured laminate.

Table 1. Key features of manufacturing methods used for fabricating microvascular channels in fiber reinforced composites

Fabricating technique	Channels diameter	Limitations	Reference
Hollow glass fiber (non-removable)	0.3-3 (mm)	Not suitable for thermal management applications Limited to straight channels Not suitable for carbon fiber reinforced composites	[9]
Hollow glass tube (non-removable)	5-60 µm	Not suitable for thermal management applications Limited to straight channels Macro scale channel diameters	[12]
Hollow metal tube (non-removable)	1.5 (mm)	Not suitable for self-healing applications Limited to straight channels Macro scale channel diameters	[3]
Hollow polymer tube (non-removable)	1-25.4 (mm)	Not suitable for thermal management applications Limited to straight channels Macro scale channel diameters	[13]
polymer wire (removable)	0.28-1.2 (mm)	Limited to straight channels May result in deforming of channel shape	[5]
Metallic wire (removable)	0.25-0.75 (mm)	Limited to straight channels	[14]

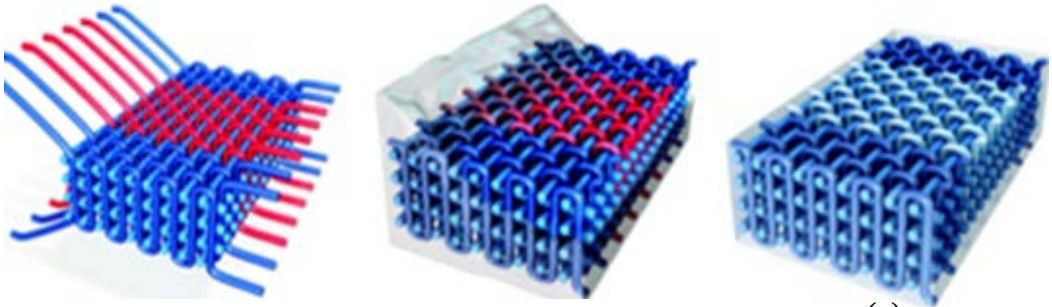

Figure 3. Fabrication of vascular channels using VaSC, Schematic diagrams of (a) a 3D structure involves straight yarns (light blue) with interwoven Z fiber tows (dark blue) and sacrificial components (red); (b) preform is impregnated with epoxy resin and let to cure; (c) formation of a hollow microvascular network by thermal depolymerization and vaporization of sacrificial components [10]**.**

1.2.1.3 Effect of vascular channels on composite structural properties

The effect of vascular channels on the mechanical properties of fiber-reinforced composites has been well studied. Kousourakis et al. [9] examined the effect on hollow channels of different shapes, sizes, and orientations on the in-plane tensile and compressive properties of carbon/epoxy laminates. They also established simple models to predict the modulus of elasticity and tensile strength of vascularized composites under longitudinal and transverse loading conditions while considering the reduction in cross-sectional area due to the existence of hollow channels.

Kousourakis et al. [9] also reported that channel shape (circular and elliptical) and dimension (up to 1 mm) had no noticeable effect on the tensile and compressive strengths when the channels were in the longitudinal direction. However, when vascular channels were oriented transverse to the load direction, the channel shape had a significant effect on the strength. In addition, a significant strength reduction, greater than 50%, was shown for samples with transversely oriented channels.

Figure 5 shows the tensile failure modes of specimens containing transverse elliptical channels prepared using silicon tubes. As shown in Figure 5b, the tensile ply rupture in specimens containing the small channels occurred at a channel, although this did not alter the failure mechanism compared to the un-vascularized sample. When the channel diameter exceeded a critical size (1 mm), the tensile

failure mode changed to a ply rupture (Figure 5c). This transition in the failure mode corresponded to a substantial drop in tensile strength for the largest channel size.

Coppola et al. [11] studied the effect of the tailoring pattern of vascular channels (straight and waved) made by the VaSC method (diameter of 0.5 mm) on the in-plane tensile properties of a 3D orthogonally woven glass/epoxy composite. They created vascular composites with straight and wavy trajectories. They found that vascular channels had a negligible effect on the strength, modulus, and damage development when integrated such that no misalignment of the reinforcing fibers occurred (i.e., the channels were straight), regardless of loading orientation. They also observed an increase in fiber misalignment (Figure 6) due to the placement of channels (i.e., wave channels) that correlated with larger reductions in strength and modulus properties and increased cracking in regions directly surrounding the channel, especially for transverse loads.

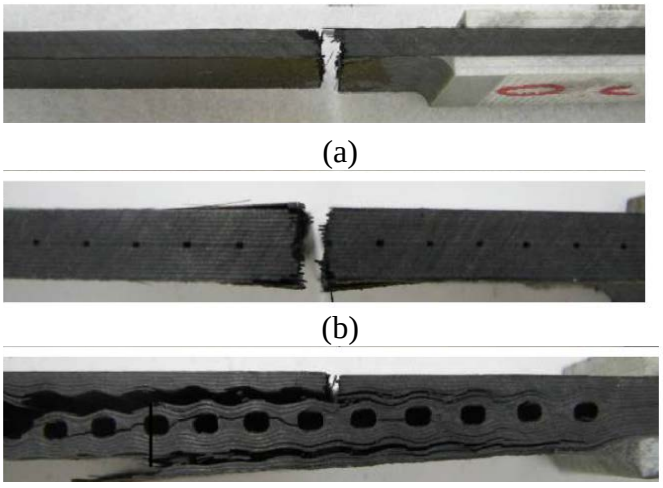

Figure 4. Tensile failure modes of laminate specimens containing transverse vascular channels (a) ply rupture in specimen without channels, (b) ply rupture in specimen with 0.58 mm elliptical channels and (c) ply rupture and longitudinal splitting cracks in specimen with 2.98 mm elliptical channels [9].

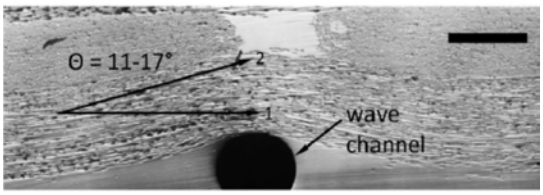

(a)

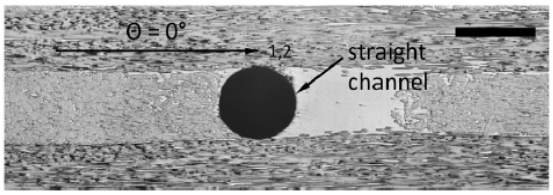

(b)

Figure 5. Comparing weft tow misalignment due to the (a) wave channel, and (b) straight channel [11]. Scale bar represents 0.5mm.

1.2.2 Electrically conductive composites

Owing to their tunable properties and wide range of applications, conductive composites are one of the most important, interesting, and active areas in advanced composite research. For instance, among numerous types of health-monitoring and damage-sensing sensors that can be integrated into composites, electrically conducting sensors offer a simple, cost-effective, and durable option for structural health monitoring in fiber reinforced composites.

1.2.2.1 Production of conductive composites

Electrically conducting composites can be prepared using either naturally conducting reinforcing materials, such as carbon fiber [15,16], or the addition of conducting fibers [17] or particles [18–20] in the insulating matrix.

The use of nanocarbon particles, e.g., carbon nanotubes (CNTs), as conductive phase has been recently proposed for preparing conductive composites. The dispersion of CNTs in an epoxy matrix is generally performed using ultrasonic and/or shear mixers. In a typical preparation method [21,22], a required amount of CNTs is mixed with epoxy using mechanical stirring at 2000 rpm for more than 30 min at room temperature. Then, a hardener is added into the epoxy-CNT suspension

and stirred at 500 rpm. A combination of ultrasonication and shear mixing is used for dispersing the CNTs after they are first dispersed in an ultrasonic ethanol bath at room temperature for 1 h. The solution is then mixed with the resin and stirred for 1 h at 2000 rpm at 80°C. The ethanol is evaporated in a vacuum oven at 80°C for 1 h, and the mixture is stirred again for 1 h at 2000 rpm [23]. After adding the hardener, the mixture is stirred again at 2000 rpm for 15 min.

The bulk conductivity of nanocomposites is quite sensitive to the curing temperature, mixing speed, and mixing time used in the fabrication process, ranging from the order of 10^{-6} S/m to 1.0 S/m depending on processing conditions used [24]. Hu et al. [24] studied the effect of dispersing processes on the conductivity of composites. They dispersed 2 wt.% multi-walled carbon nanotube (MWCNT) in an epoxy matrix with and without a dilute solution with different mixing conditions (Table 2). According to this study, the electrical conductivity of the nanocomposite was clearly affected by the fabrication process.

Table 2. Processing conditions for various samples

sample	Sequence of addition of ingredients	Mixing speed	Mixing time	Curing	Measured electric conductivity (S/m)
A	(A1) Epoxy + CNT A1 + hardener	720 rpm 80 rpm	1 h 10 min	80 ºC for 3 h	0.025
B	(B1) Epoxy + ethanol+ CNT B1 + hardener	720 rpm 80 rpm	1 h 10 min	(B1) 80 ºC for 2 h 22ºC for 48 h	--
C	(C1) Epoxy + ethanol+ CNT C1 + hardener	720 rpm 80 rpm	1 h 10 min	(C1) 80 ºC for 2 h 80 ºC for 2 h	0.015
D	(D1) Epoxy + CNT D1 + hardener	2000 rpm 2000 rpm	1 min 1min	80 ºC for 3 h	0.03
E	(E1) Epoxy + CNT E1 + hardener	2000 rpm 2000 rpm	4 min 1min	80 ºC for 3 h	0.015
F	(F1) CNT + Epoxy F1 + hardener	2000 rpm 2000 rpm	4 min 1min	80 ºC for 3 h	0.003
G	(G1) Epoxy + hardener G1 + CNT	2000 rpm 2000 rpm	20 sec 1min	80 ºC for 3 h	0.08
H	(G1) Epoxy + hardener G1 + CNT	2000 rpm 2000 rpm	20 sec 1min	80 ºC for 3 h	0.80

1.2.2.2 Applications

The use of CNTs as a conductive phase has been more recently proposed for preparing conductive composites for self-monitoring applications.

Wu et al. [5] explored the ability of an embedded carbon nanotube network prepared by sizing glass fibers with a CNT-based agent to sense damage and fill cracks in vascularized composites. Since a crack can be detected by analyzing the electrical resistance of the sample under a tensile test, the healing medium was injected through hollow axial channels into the composite specimens. However, for large composite specimens where all the fibers were sized by the conductive agent, the method was not feasible for detecting the crack location in a sample.

Grammatikos and Piapetis [25] exploited the electrical properties of both conventional and CNT-enhanced carbon fiber-reinforced polymers (CFRPs) in order to identify their sensing capabilities as characterized by strain variation and global damage. They found that the incorporation of the nanophase composite significantly increased the sensitivity of the electrical resistance measurements. For example, with plain CFRPs, a 3% increase of $\Delta R/R_0$ was recorded as compared to approximately 40% of the nanomodified composites. In other words, the nanomodification resolved the minimal strain- or damage-induced changes.

1.2.2.3 Limitations on the electrical conductivity performance

Although the use of conductive nanoparticles can increase the conductivity of composite structures and improve the strain sensitivity of samples, their self-monitoring properties are primarily affected by the filler dispersion pattern inside the reinforcing fibers. It is important to note that although an individual CNT particle is nanofiller, a resin-particle suspension will arise consisting of agglomerated particles with an average diameter of 150–200 nm, which may increase the risk of filtration. Any non-uniformity caused by filtration results in a large scatter of the electrical conductivity [26].

1.3 Motivation

Micro-vascularized composites have recently gained considerable attention because of their ability to form multifunctional structural composites. However, to date, the creation of electrically conductive pathways via microvascular networks has not been reported.

1.4 Objective

In this study, the vaporization of sacrificial components (VaSCs) was used to create hollow micro-channels in continuous glass fiber reinforced composites. These micro-channels were filled with electrically conductive fillers to create conductive networks in composite specimens. These conductive pathways were then applied as internal strain sensors.

1.5 Scope of thesis

In this study, a shear mixing process is used to disperse CNTs into an epoxy matrix. The effect of mixing process parameters on electrical conductivity, tensile strength, and the piezoresistivity of a CNT/epoxy nanocomposite is investigated experimentally. Based on the results, two regression models are established to predict the electrical conductivity and tensile strength of the CNT-epoxy nanocomposites. The robustness and accuracy of the models are verified by implementing verification tests. Details of the designed experiments, regression models, and verification tests are presented in Chapter 2. In Chapter 3, magnetization is used to produce an aligned CNT/epoxy nanocomposite. The electrical conductivities of the aligned and randomly distributed CNT nanocomposites are compared. The piezoresistivity of a CNT/epoxy nanocomposite with aligned CNTs is modeled in Chapter 4. Details on the techniques for manufacturing electrically conductive composites with microvascular channels are provided in Chapter 5. Chapter 6 summarizes the main conclusions of this study and provides key recommendations for future work.

CHAPTER 2

EFFECT OF SHEAR MIXING PROCESS PARAMETERS ON ELECTRICAL, MECHANICAL AND STRAIN SENSING PROPERTIES OF CNT / EPOXY NANOCOMPOSITES

2.1 Introduction

Unique properties of carbon fillers (carbon nanotubes, carbon blacks, etc.) such as high thermal and electrical conductivity [27–30], flame redundancy [31,32] coupled with their superior mechanical properties [33,34] render them potentially attractive fillers for advanced composites. In literature, carbon nanotubes (CNTs) have gained considerable attention since minimal CNT loadings could provide significant electrical conductivity as well as improvement in mechanical properties of the produced nanocomposites [35–37].

It has been known for some time that the mechanical, electrical and thermal properties of nanocomposites strongly depend on the dispersion state of CNTs in polymer matrix [38–40]. The research on the effect of CNT addition on the mechanical properties of CNT-epoxy composite indicates that there is an optimum content of CNT above which there is a decrease in tensile strength and/or modulus of elasticity of the composite. This issue is due to non-effective dispersion of CNT in resin matrix and existence of high amount of agglomerated CNT particles [34,38,41]. Research also shows that the electrical conductivity of CNT filled nanocomposites for the same CNT concentration can vary with two order of magnitudes among the samples prepared using different dispersion techniques [42].

Ultra-sonication and/or shear mixing are commonly used for dispersing CNTs in epoxy matrix [21,43,44]. The existence of strong Van der Waals forces among CNTs and high tendency of CNTs to agglomerate [39,43] are some of the challenges that render the effective dispersing of CNTs in a polymer matrix a continuing research issue. Chemical treatment of CNTs [45,46], using chemical surfactants[47,48] and adding dilute solutions [49,50] have been found to ease the dispersing process but did not necessarily have a positive effect on the electrical conductivity of the final nanocomposites [24,51]. The shear mixing conditions during the preparation of the CNT-resin suspensions (for composite production) were found to be effective on composite electrical conductivities [24] and in some cases, improved the electrical percolation threshold by one order of magnitude [52].

CNT reinforced composites have the potential to attain structural health monitoring capabilities by exploiting the variation of electrical conductivity and its relation to strain and/or damage within the nanocomposite [25,26]. The electrical conductivity depends on formation of electrically conductive pathways within the composite due to the presence of CNT. During the stretching (loading) of the nanocomposite, CNT agglomerates are dragged along with the polymer matrix and pulled apart since the bonds between CNT agglomerates and the polymeric matrix are stronger than the bonds within the CNT agglomerate [53]. If there is no failure (permanent deformation, internal cracking, etc.), releasing the composite (unloading) will restore contact between the CNT agglomerates (which were pulled apart previously). Since the electrical resistivity of the nanocomposite is affected by the distance between the conductive particles (i.e. CNT), it can be used as a measure of strain, and indirectly, a composite health monitoring tool.

Although the sensitivity of the electrical and mechanical properties of CNT-epoxy to resin-filler dispersion was investigated in several studies [24,52,54]; none of them present a reliable model which could show the effect of fabrication parameters and their interactions on the properties of nanocomposites.

In this chapter, the effect of shear mixing parameters (time and speed) on electrical conductivity and tensile strength of the epoxy/CNT samples at different CNT concentrations was investigated. Response Surface Methodology (RSM) was

used to design the experiments and the results were analyzed statistically to understand the most influential process parameters and their interactions. For this purpose over 100 samples were fabricated for electric conductivity measurements and over 50 tensile tests were performed for mechanical characterization of the nanocomposites. In this study, optical microscopy was also used to study the morphology of fillers in liquid matrix. The dispersion state of CNT in epoxy matrix was defined through quantitative indicators instead of using not measurable terms such as well or poorly dispersed. Also, the electrical and mechanical properties of nanocomposites were discussed in details considering the corresponding macrostructure. This study also considers the effect of CNT's dispersion state on piezoresitivity of CNT/epoxy nanocomposites that has never been considered in the previous studies.

2.2 Preparation and Characterization of CNT-epoxy suspensions

2.2.1 Materials and samples preparation

Nanocomposite samples were manufactured consisting of electrically conductive nanoparticles in a polymeric matrix consisting of epoxy resin (Araldite LY564, Huntsman) and hardener (Aradur 3486, Huntsman). Multi-Wall Carbon Nanotubes (MWCNTs), provided by Nanografi Co. Ltd. (Turkey), with an average diameter of 10 nanometer and average length of 1.5 micrometer (aspect ratio = 150) were used as the conductive nanoparticles. The CNT/epoxy suspensions were prepared by shear mixing of the components in a cylindrical vessel using a mechanical stirrer (MTOPS, MS3020D). A 3-blade turbine impeller with a pitch angle of 45° was used for shearing. Impeller blade numbers and blade geometry were selected to have an efficient axial flow pattern and minimum vortex, and to minimize the samples volume [55,56]. The vessel was equipped with four equally spaced flat wall baffles. Wall baffles provide top to bottom mixing by converting tangential flows to vertical

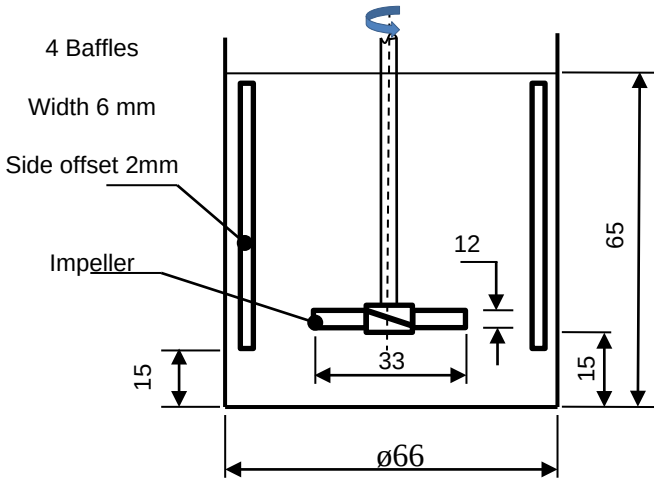

Figure 6. Dimensions and layout of shear mixing setup. Dimensions are in mm.

flows which prevents swirling motion, minimizes vortexing and air entrainment [57]. Figure 7 shows the geometrical configuration of the mixing equipment.

The vessel was filled with 150 gr of epoxy resin. Then the pre-weighted CNTs were added in several steps while stirrer was run at desired speed. At the end of the process, hardener was added with hardener-epoxy weight ratio 35:100. The suspension was further mixed for one minute at the same speed. Finally, in order to release trapped air the suspension was degassed under vacuum.

2.2.2 Design of experiments using response surface methodology

Response surface methodology (RSM) is a series of statistical and mathematical techniques used for modeling and analyzing the effect of known factors on a response with the objective of optimizing the response [58]. Using RSM, the response can be modeled as a second order polynomial of the form:

$$y = \beta_0 + \sum_{i=1}^{n} \beta_i x_i + \sum_{i=1}^{n} \beta_{ii} x_i^2 + \sum \sum_{i<j} \beta_{ij} x_i x_j + \epsilon \qquad (1)$$

where x_i and x_j are the factors; β_0, β_i , β_{ij} and β_{ii} are the regression coefficients which are estimated using least squares method and $\in$ characterizes the error observed in the response y.

The presented model (Equation 1) is a general model containing all predictor factors, their interactions and higher order (quadratic) terms. The significance of each term can be checked by running statistical tests (F test) and non-significant terms can then be eliminated from the model.

In this work, a series of experiments were designed using Response Surface Methodology to study the effect of shear mixing parameters (mixing time and mixing speed) on the electrical conductivity and the tensile strength of the epoxy/CNT composite samples at various CNT filler concentrations. The statistical software MINITAB 16 was used for the design of experiments as well as the statistical analysis of the results. The factors with their respective levels and the design matrix are presented in Table 3 and Table 4, respectively. Based on the design matrix, 20 samples were manufactured for analysis and characterization.

2.2.3 Morphological study of CNT-epoxy suspensions

The quality of the dispersion process was studied through the morphology of the prepared suspension samples. 1 cc samples were taken out from the epoxy/CNT suspensions at specified time instances during the mixing operation. The samples were laid upon glass laminates and images were captured from each sample through optical microscopy at a magnification of 400. On each sample, 5 images at different locations of the sample were captured. The images were analyzed using the ImajeJ software [59] in which CNT clusters were distinguished from the matrix background by converting the captured imagery into binary format. The number of detected clusters for cluster areas greater than$20\ \mu m^2$, and the cluster areas in each image were determined. The results were used to analyze the dispersion state of CNT in epoxy, and correlate the dispersion conditions with the composite properties.

Table 3. Experimental factors and levels

Factors	**Levels**		
	-1	0	1
Concentration (wt.%)	0.2	0.35	0.5
Mixing speed (rpm)	500	1250	2000
time (min)	10	35	60

Table 4. RSM design matrix

Run Order	mixing speed level	mixing time level	CNT concentration level
1	-1	-1	-1
2	1	-1	-1
3	-1	1	-1
4	1	1	-1
5	-1	-1	1
6	1	-1	1
7	-1	1	1
8	1	1	1
9	-1	0	0
10	1	0	0
11	0	-1	0
12	0	1	0
13	0	0	-1
14	0	0	1
15	0	0	0
16	0	0	0
17	0	0	0
18	0	0	0
19	0	0	0
20	0	0	0

2.3 Characterization of CNT-epoxy Nanocomposites

2.3.1 Measurement of electrical conductivity of CNT-epoxy nanocomposites

Nanocomposite samples were prepared by casting the prepared CNT-epoxy suspensions into thin, rectangular aluminum molds (dimensions 55 mm × 10 mm × 5 mm). The molds were placed in the oven following casting and cured at 80 °C for 8 hours. After curing, samples were de-molded, and the long ends were trimmed, polished using Sic sand paper and washed with acetone for smooth end sections. The end sections were then painted with silver and let dry at room temperature.

The electric resistance of the samples along their length was measured using Two Point Probe Technique [60] with a Keithley 2000 Digital Multimeter. Figure 8 presents the aluminum mold, specimens and the electrical resistance measurement configuration in which the probes are brought into contact with the silver-coated ends.

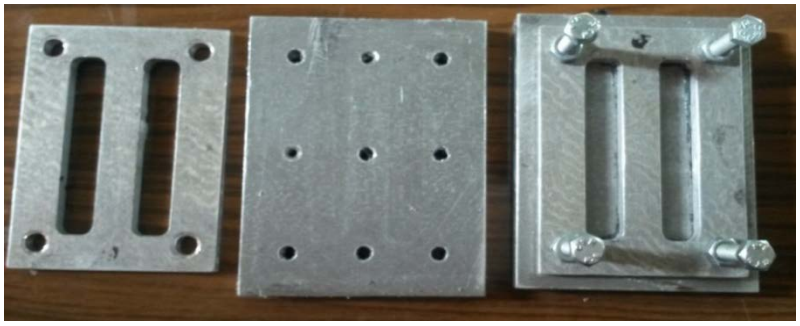

(a)

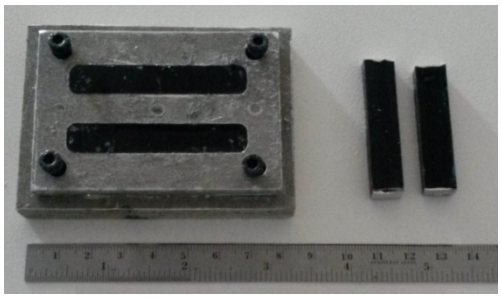

(b)

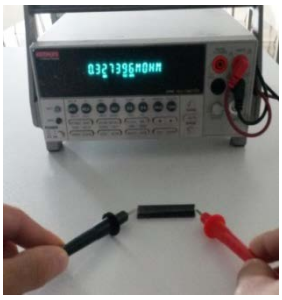

(c)

Figure 7. Preparation of nanocomposite samples for electric conductivity measurement, (a) mold setup, (b) specimens with silver-coated ends, (c) electrical resistance measurement

The dimensions of the composite samples were measured using a digital caliper. Electrical conductivity is calculated using the measured parameters in Equation (2) as

$$\sigma = \frac{L}{R \times A} \tag{2}$$

where σ is the electric conductivity, L is the sample length, R is the DC resistance (ohms) and A is the cross section area of the sample.

2.3.2 Mechanical Characterization of CNT-epoxy Nanocomposites

Uniaxial tensile tests were performed to study the electrical response of the prepared nanocomposites to strain. The tensile strength of the specimens was also recorded during the tests. Dog-bone shaped test specimens with a gauge length of 50 mm, a width of 13 mm and a thickness of 5 mm were prepared by casting CNT-epoxy suspensions into aluminum molds (Figure 9). Samples were cured at 80 °C for 8 hours. After de-molding, the ends of the samples were trimmed, polished, washed

and painted with silver. Two copper wires (connected to the multimeter probes) were attached to the silver-coated ends using aluminum tape. Tensile tests were run according to ASTM D638 under displacement control by straining at a rate of 0.5 mm/min using a universal tensile test machine (Tenson). Wood stickers were used to create an electrical isolation barrier between the metal grips of the tensile machine and the conductive samples. To measure the strain, an extensometer with a gauge length of 50 mm was used. The force-elongation and electric resistance data were monitored and recorded using Labview software (National Instruments). The experimental set up and the test specimen are shown in Figure 10.

Figure 8. Aluminum molds designed for casting tensile test samples. Dimensions are according to the ASTM D638.

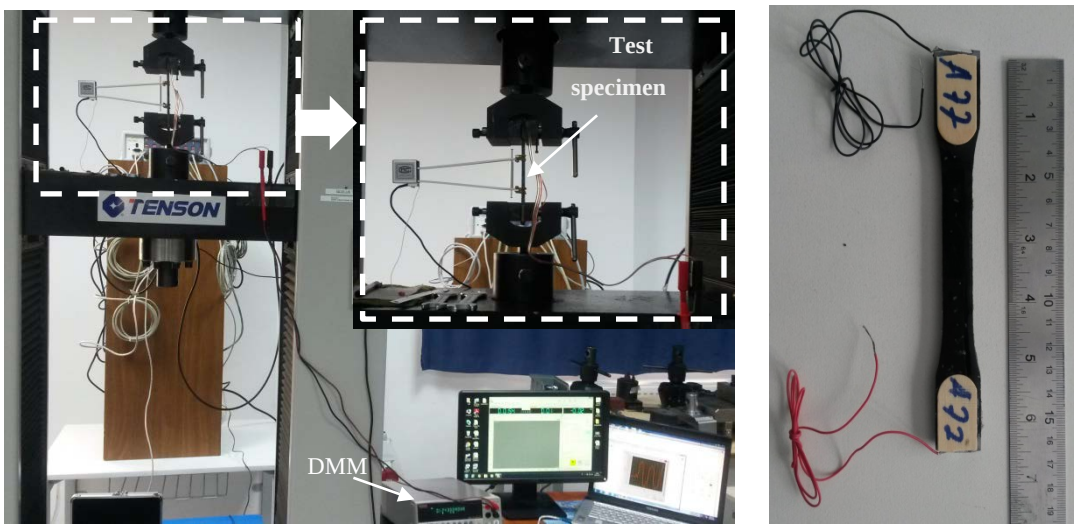

(a) (b)

Figure 9. (a) Tensile test set-up for studying the electrical resistance of CNT/epoxy nanocomposites under loading, (b) Composite test specimen

2.4 Results and discussion

2.4.1 Dispersion state of CNTs in epoxy matrix

Figure 11 shows the CNT clusters (darker areas) in epoxy matrix. The experiment labels state suspension mixing conditions. For instance, 500N10T20W denotes the sample mixed at 500 rpm for 10 minutes, with 0.2 wt. % of CNT. The results of CNT clusters distribution analysis based on clusters surface area are represented in Table 5 CNT clusters surface area distribution analyzes. The dispersion state of CNT clusters was represented by citing A_{50}, A_{90} and A_{occ}. A_{50} and A_{90} are extracted respect to the cumulative area distribution of CNT clusters and indicate that the 50 and 90 percent of the detected CNT clusters have an area equal or less than these values, respectively. A_{occ} indicates the fractional area occupied by CNT clusters.

Considering Table 5, the occupied surface by CNT clusters (A_{occ}) were measured less than 20% and more than 40% (except 500N10T50W) for samples involved 0.2 and 0.5 CNT wt.%, respectively. Although sample 500N10T50W contains 0.5 CNT wt.%, the surface area occupied by CNT clusters is 26.1%. The existence of large (A_{90} = 4000 μm^2) and dense (A_{occ} =26.1%) clusters implies that applying low mixing speed with low mixing time was not sufficient to disperse CNTs in epoxy matrix, effectively.

Figure 11-e shows the microscopic image of this sample where several large clusters can be seen in epoxy matrix. Also, a finer microstructure ($A_{50} < 90$ μm^2) can be obtained using higher mixing speed (2000 rpm) (Figure 11-d, g and h). The interaction effect of mixing time and CNT concentration on dispersion state can be noticed by considering the results obtained for samples which were mixed at 2000 rpm. Both 2000N10T50W and 2000N60T50W samples (at which 0.5 wt.% CNT was mixed at 2000 rpm for 10 and 60 minutes, respectively), although; the occupied area by the clusters (A_{occ}) and the observed clusters median area (A_{50}) are very close to each other; there is a noticeable difference in their respective A_{90} values. Using higher mixing speeds for longer periods of time is effective to obtain a finer macrostructure at higher CNT concentrations. However, the obtained morphology is similar for the low CNT-concentration samples that are mixed at 2000 rpm (2000N10T20W and 2000N60T20W) regardless of mixing time.

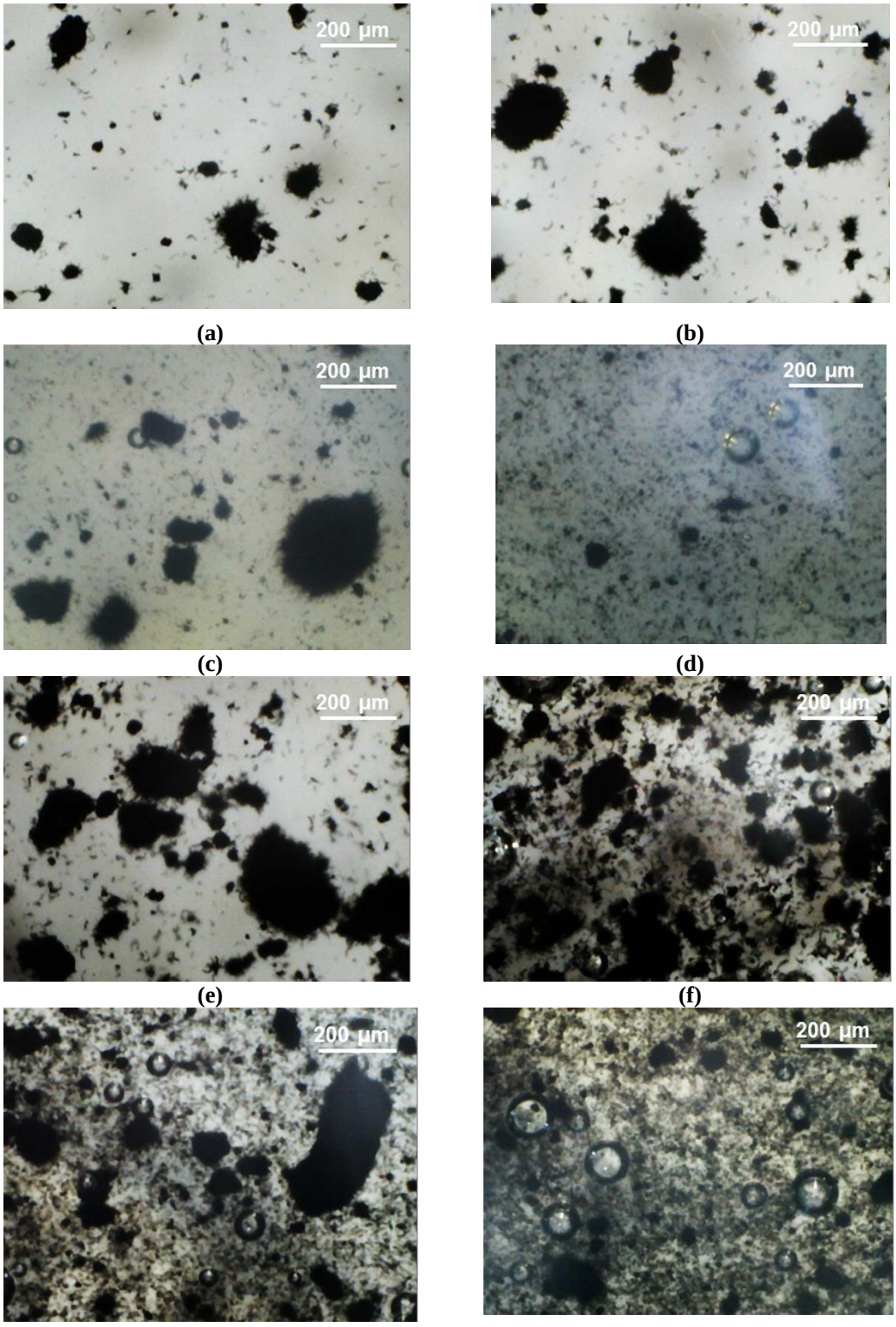

Figure 10 Microscopy imagery of CNT-epoxy suspensions (a) 500N10T20W, (b) 500N60T20W, (c) 2000N10T20W, (d) 2000N60T20W, (e) 500N10T50W, (f) 500N60T50W, (g) 2000N10T50W, (h) 2000N60T50W.

Table 5. CNT clusters surface area distribution analyzes

sample	Median area (A_{50}) - (μm^2)	A_{90} (μm^2)	Occupied area (Aocc) - (%)
500N10T20W	150	1600	8.4
2000N10T20W	90	700	16.3
500N60T20W	200	3000	17.1
2000N60T20W	70	500	18.6
500N10T50W	200	4000	26.1
2000N10T50W	90	1600	41.4
500N60T50W	200	3500	43
2000N60T50W	75	800	40.3
500N35T35W	150	2500	21
2000N35T35W	80	800	22.8
1250N10T35W	100	1200	22.9
1250N60T35W	100	2000	25.9
1250N35T20W	120	1500	14.3
1250N35T50W	120	1500	49.8
1250N35T35W	120	1300	24.5

2.4.2 Electric conductivity and tensile strength of CNT-epoxy nanocomposites

Three samples were prepared under same experimental conditions according to the design matrix (Table 4). The averages of calculated electric conductivity based on Equation (2) and measured tensile strength for each sample set, are shown in Table 6. Figure 12 presents the measured conductivity for the samples in which mixing speed, mixing duration and CNT concentration were set to their low and high levels. From Figure 12, it is seen that mixing parameters (speed and duration) and their interactions do not show considerable effect on electric conductivity when CNT concentration is at its lowest level (0.2 wt.%). However, maximum conductivity (3.340×10^{-3}(s/m)) was measured for the case where mixing was performed with the lower mixing speed (500 rpm) for 60 minutes. This implies that, low mixing speed can provide sufficient shear force for dispersing CNTs in low concentrated CNT-epoxy suspensions with less care about over dispersing [24]. At higher CNT concentrations, the electric conductivity of the samples mixed at 2000 rpm for 60 minutes is nearly six times that of other samples with the same CNT concentration. At high CNT concentration where viscosity of epoxy/CNT suspension is high and there are significant aggregates of CNTs, low mixing speeds cannot create sufficient

shear force to break down CNT agglomerates and disperse CNT's in epoxy matrix effectively (Figure 11e-f).

Tensile strength of CNT/ epoxy composites with varying CNT concentrations are presented in Figure 13. The maximum tensile strength (84 MPa) was measured for the sample at which 0.5 wt.% CNT was dispersed in epoxy matrix at 2000 rpm for 60 minutes (84 MPa). The minimum strength (52 MPa) was observed at sample prepared by mixing 0.5 wt.% CNT at 500 rpm for 60 minutes. Tensile strength of all samples prepared with low shear force (500 rpm), regardless of mixing time and CNT concentration, alter between 52 up to 61 MPa and indicate a decreasing in strength comparing to not reinforced epoxy resin.

Table 6. Tensile strength and electric conductivity of CNT-epoxy nanocomposites prepared with different mixing conditions and CNT concentrations

Run order	sample	tensile strength (MPa)	Electric conductivity (S/m)×10^{-3}
1	500N10T20W	55	0. 198
2	2000N10T20W	81	0. 102
3	500N60T20W	61	0. 250
4	2000N60T20W	78	0. 278
5	500N10T50W	58	4.230
6	2000N10T50W	74	4.950
7	500N60T50W	52	3.340
8	2000N60T50W	84	26.300
9	500N35T35W	52	1.660
10	2000N35T35W	84	2.310
11	1250N10T35W	63	1.200
12	1250N60T35W	75	2.240
13	1250N35T20W	71	0.185
14	1250N35T50W	66	5.980
15	1250N35T35W	76	1.460
16	1250N35T35W	72	2.140
17	1250N35T35W	79	2.500
18	1250N35T35W	72	2.300
19	1250N35T35W	80	2.680
20	1250N35T35W	75	2.420

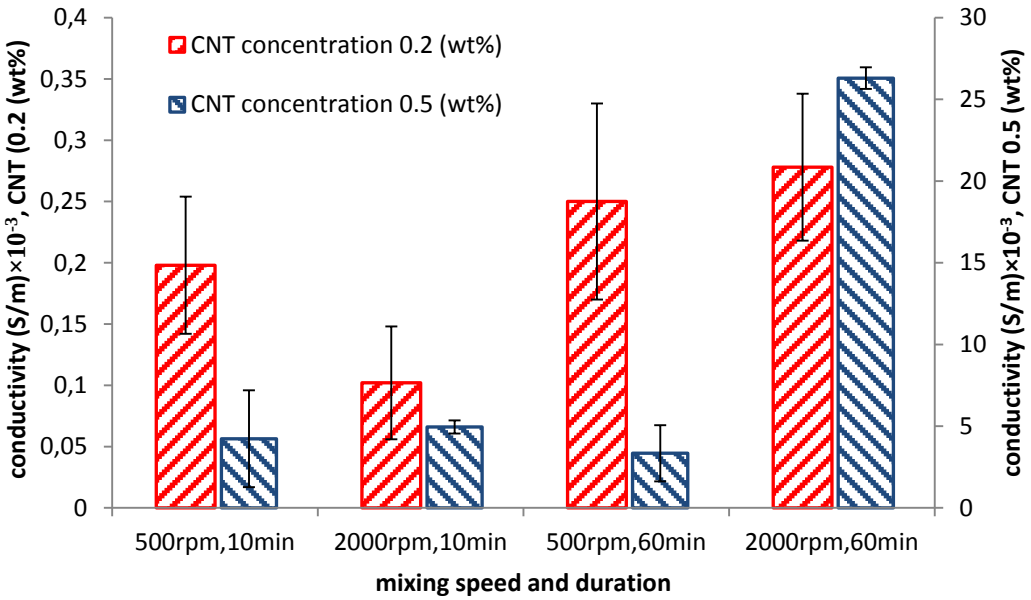

Figure 11. Effect of mixing conditions and CNT concentrations on electric conductivity

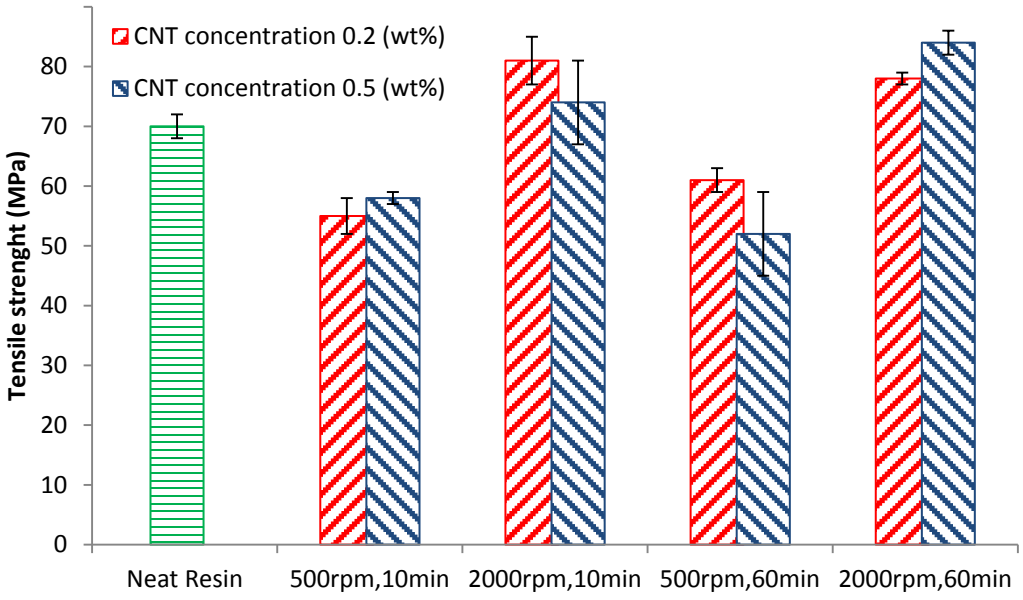

Figure 12. Tensile strength of CNT-epoxy composites prepared at different mixing conditions and varying amounts of CNT.

Figure 14 presents the SEM images of the fracture surfaces of tested nanocomposites. Here, the fractographic features are considerably varying. A smoother fracture surface with large CNT clusters is seen for the samples in which the mixing speed of suspension was low in Figure 14 a and d. Smaller CNT clusters and higher fracture surface roughness (Figure 14g and j) were obtained for samples where high mixing speed was used to prepare the suspension. Analyzing the CNT clusters on fractured surface with higher magnifications shows that a more uniform microstructure can be obtained using higher mixing speeds (Figure 14i and l). This result concurs with the obtained results through morphology study of CNT-epoxy suspension (Figure 11c and h).

Considering tensile test results and SEM results, it is seen that CNT-epoxy nanocomposites that have the higher strengths have finer structures (Figure 14j-l). Such a structure obtains by mixing the suspension with high shear speeds and for longer durations (Figure 11h). Conversely, existence of large CNT agglomerates, caused by dispersing CNT's at low mixing speeds and short times (Figure 11f and Figure 14d-f), resulted in forming stress concentration zones [34,61] which affects the strength of CNT-epoxy composite negatively. Similarly, it can be said that for any suspension mixing condition, there is an optimum CNT content above which the strength of nanocomposite is affected adversely due to ineffective dispersion process and existence macro-scale agglomerated CNT particles. These results confirm the effect of CNT dispersion state on mechanical properties of nanocomposites [38,43].

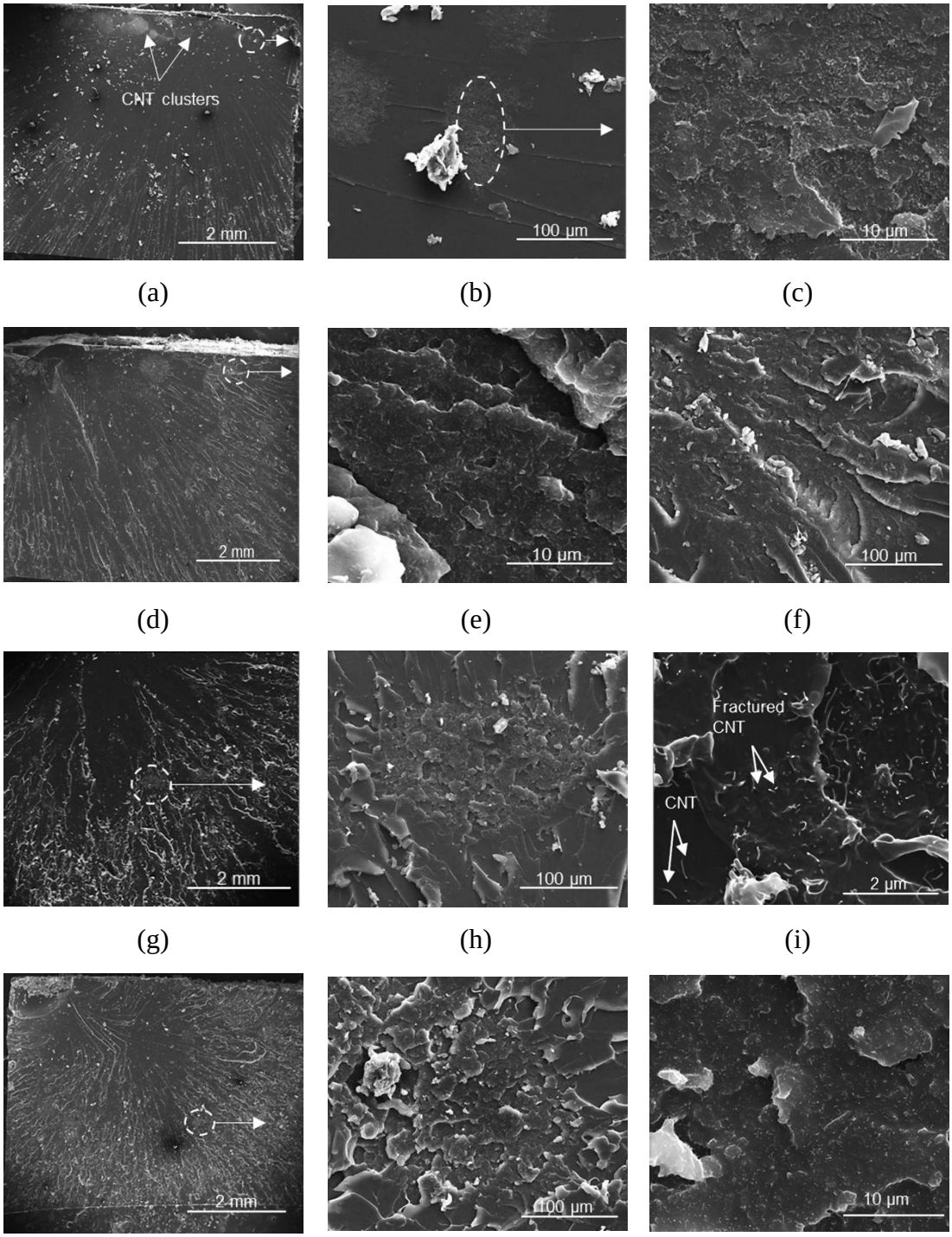

Figure 13. SEM images of CNT-epoxy nanocomposite fracture surface, (a-c) 500N10T20W, (d-f) 500N60T50W, (g-i) 2000N10T20W, (j-l) 2000N60T50W.

2.4.3 Analysis of variance (ANOVA) and regression models

In this study, a systematic approach was used to obtain a reliable mathematical relation to present the effect of suspension preparation parameters and CNT content on electric conductivity and tensile strength of CNT-epoxy nanocomposites. These models can then be used to optimize preparation parameters and CNT contents to achieve the desired electrical and/or mechanical properties. Based on RSM (Equation 1), such a model can be presented as:

$$y = \beta_0 + \beta_1 N + \beta_2 T + \beta_3 W + \beta_4 N^2 + \beta_5 T^2 + \beta_6 W^2 + \beta_7 N.T + \beta_8 N.W + \beta_9 T.W \quad (3)$$

where y is electric conductivity or tensile strength, N is the CNT-epoxy suspension mixing speed in rpm, T is the CNT-epoxy suspension mixing time in minutes, W is CNT concentration in in wt.% and β_1- β_9 are unknown coefficients which are estimated using least squares method. Equation 3 presents the effect of main factors (N, T and W), quadratic terms (N^2, T^2andW^2) and their interactions ($N.T$, $N.W$ and $T.W$) on electric conductivity and tensile strength of nanocomposite.

Finally, ANOVA was used to determine the effectiveness of the process parameters on properties of nanocomposite.

In ANOVA, significance of each term is evaluated using Fisher's variance ratio (F-value) and probability value (P-value) which are calculated based on Degrees of freedom (DF), sequential sums of squares (Seq SS), adjusted sums of squares (Adj SS), the adjusted mean square (Adj MS) [58]. P-value is defined as probability against null hypothesis which is denoted as H0 and stated as “Treatment does not have significant effect on response”. Terms with p-values less than significance level threshold ($\alpha = 0.05$) are considered as significant terms.

The analysis of variance on conductivity data (Table 6) is shown in Table 7. The respective regression model that fits the experimental data can be represented as:

$$\sigma = 23.53 - 0.014N - 0.38T - 83.50W + (1.0 \times 10^{-5})N^2 + (7.0 \times 10^{-4})T^2 + 80.1W^2 + (1.49 \times 10^{-4})N.T + (0.026)N.W + (0.674)T.W \quad (4)$$

Based on results of Table 7 there is a significant lack-of-fit in regression model (Equation 4), indicating this regression model is not able to describe the functional relationship between experimental factors and electric conductivity. This Lack-of-fit may occur due to existence of several large residuals result from fitting the model. Standardized residual for each observation is shown in Figure 15 where large residuals are calculated for the 1st and 8th observations. For the first observation at which 0.2 wt.% CNT was dispersed into epoxy with mixing speed of 500 rpm for 10 minute, the measured conductivity is 0.198×10^{-3} (S/m). For the same condition the calculated electric conductivity based on Equation 4 is 4.13×10^{-3} (S/m).

Table 7. Analysis of variance on conductivity (S/m), the analysis was done on uncoded units

Source	DF	Adj SS	Adj MS	F	P
Regression	9	515.953	57.328	6.48	0.004
Linear	3	297.805	99.268	11.22	0.002
mixing speed (rpm)	1	58.864	58.864	6.65	0.027
mixing time (min)	1	47.211	47.211	5.33	0.044
concentration (wt.%)	1	191.730	191.730	21.66	0.001
Quadratic	3	33.966	11.322	1.28	0.334
mixing speed (rpm)*mixing speed (rpm)	1	1.368	1.368	0.15	0.702
mixing time (min)*mixing time (min)	1	0.533	0.533	0.06	0.811
concentration (wt.%)*concentration (wt.%)	1	8.938	8.938	1.01	0.339
Interaction	3	184.181	61.394	6.94	0.008
mixing speed (rpm)*mixing time (min)	1	62.519	62.519	7.06	0.024
mixing speed (rpm)*concentration (wt.%)	1	70.496	70.496	7.96	0.018
mixing time (min)*concentration (wt.%)	1	51.167	51.167	5.78	0.037
Residual Error	10	88.514	8.851		
Lack-of-Fit	5	87.599	17.520	95.74	<0.001
Total	19	604.466			

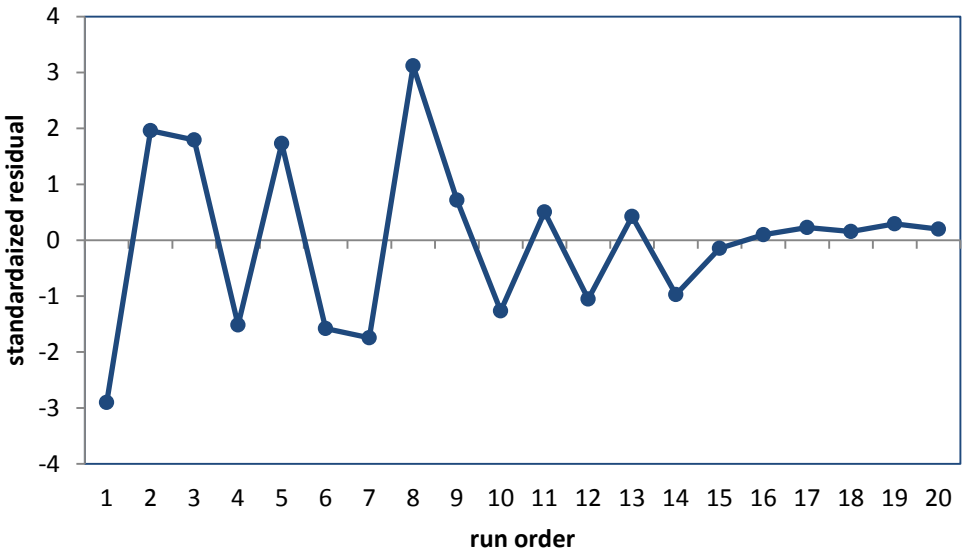

Figure 14. Standardized residual vs. observation order

Table 8. Fits and residuals for unusual observations

	conductivity×10^{-3} (S/m)			
Observation	Measured	Fit	Resid	Std Resid
1	0,20	4,13	-3,93	-2,90
8	26,30	22,08	4,22	3,12

Another large residual (3.12) is belong to the sample at which mixing speed and mixing time are set to 2000 rpm and 60 min, and CNT concentration is 0.5 wt.%. The measured electric conductivity and calculated conductivity based on Equation 4 and corresponding residuals for these two cases are presented in Table 8.

The Lack-of-fit issue can be resolved by using transformation of the response. The Box-Cox transformation [62] is the most commonly used technique at which an appropriate exponent (Lambda) is used to transform response data. The Box-Cox transformation is defined as:

$$y_i^{(\lambda)} = \begin{cases} \frac{y_i^{\lambda}-1}{\lambda}, & \lambda \neq 0 \\ \ln(y_i), & \lambda = 0 \end{cases} \quad (5)$$

where y_i is original data and $y_i^{(\lambda)}$ is transformed data. The optimal value for exponent Lambda was found by analyzing data in Minitab and then response data were transformed using Equation (5) by specifying Lambda equals to zero.

$$\sigma_t = \ln(\sigma) \tag{6}$$

where σ is the electric conductivity and σ_t is the transformed electric conductivity. The transformed electric conductivities are represented in Table 9.

Analysis of variance on transformed response (σ_t) considering all experimental factors, their interactions and quadratic terms shows that quadratic terms of mixing speed, mixing time and interaction of mixing time and CNT concentration have greater p-values than significance level threshold ($\alpha = 0.05$) (Table 10). These terms are removed from the model and respective analysis of variance is represented in Table 11.

Table 9. Electric conductivity and transformed conductivity of CNT-epoxy nanocomposite samples

Run order	sample	Electric conductivity $\times 10^{-3}$ (S/m)	σ_t $\times 10^{-3}$ (S/m)
1	500N10T20W	0. 198	-1.6195
2	2000N10T20W	0. 102	-2.2828
3	500N60T20W	0. 250	-1.3863
4	2000N60T20W	0. 278	-1.2801
5	500N10T50W	4.230	1.4422
6	2000N10T50W	4.950	1.5994
7	500N60T50W	3.340	1.2060
8	2000N60T50W	26.300	3.2696
9	500N35T35W	1.660	0.5068
10	2000N35T35W	2.310	0.8372
11	1250N10T35W	1.200	0.1823
12	1250N60T35W	2.240	0.8064
13	1250N35T20W	0.185	-1.6874
14	1250N35T50W	5.980	1.7884
15	1250N35T35W	1.460	0.3784
16	1250N35T35W	2.140	0.7608
17	1250N35T35W	2.500	0.9163
18	1250N35T35W	2.300	08329
19	1250N35T35W	2.680	09858
20	1250N35T35W	2.420	0.8838

Table 10. Analysis of Variance on transformed conductivity data (σ_t)

Source	DF	Adj SS	Adj MS	F	P
Regression	9	36.0541	4.0060	79.33	<0.001
Linear	3	32.3238	10.7746	213.38	<0.001
mixing speed (rpm)	1	0.3976	0.3976	7.87	0.019
mixing time (min)	1	1.0850	1.0850	21.49	0.001
concentration (wt.%)	1	30.8412	30.8412	610.77	0.000
Quadratic	3	1.8658	0.6219	12.32	0.001
mixing speed (rpm)*mixing speed (rpm)	1	0.0087	0.0087	0.17	0.686
mixing time (min)*mixing time (min)	1	0.0405	0.0405	0.80	0.392
concentration (wt.%)*concentration (wt.%)	1	0.8784	0.8784	17.40	0.002
Interaction	3	1.8645	0.6215	12.31	0.001
mixing speed (rpm)*mixing time (min)	1	0.8950	0.8950	17.72	0.002
mixing speed (rpm)*concentration (wt.%)	1	0.9646	0.9646	19.10	0.001
mixing time (min)*concentration (wt.%)	1	0.0049	0.0049	0.10	0.762
Residual Error	10	0.5050	0.0505		
Lack-of-Fit	5	0.2698	0.0540	1.15	0.442
Total	19	36.5591			
R^2 =98.6%	R^2_{pred} = 97.4%			R^2_{adj} = 87.6%	

Table 11. Analysis of Variance for transformed conductivity (Lambda = 0), some predictors have been eliminated

Source	DF	Adj SS	Adj MS	F	P
Regression	6	36.0084	6.0014	141.67	0.000
Linear	3	32.3238	10.7746	254.35	0.000
mixing speed (rpm)	1	0.3976	0.3976	9.39	0.009
mixing time (min)	1	1.0850	1.0850	25.61	0.000
concentration (wt.%)	1	30.8412	30.8412	728.05	0.000
Quadratic	1	1.8249	1.8249	43.08	0.000
concentration (wt.%)*concentration (wt.%)	1	1.8249	1.8249	43.08	0.000
Interaction	2	1.8596	0.9298	21.95	0.000
mixing speed (rpm)*mixing time (min)	1	0.8950	0.8950	21.13	0.001
mixing speed (rpm)*concentration (wt.%)	1	0.9646	0.9646	22.77	0.000
Residual Error	13	0.5507	0.0424		
Lack-of-Fit	8	0.3156	0.0394	0.84	0.608
Total	19	36.5591			
R^2 =98.5%	R^2_{pred} = 97.8%			R^2_{adj} = 94.6%	

According to Table 11 mixing time is shown to have no significant effect on electric conductivity as an individual parameter. However, the interaction of mixing time and mixing speed has significant effect on composite conductivity as the calculated p-value is less than the significance level threshold ($\alpha = 0.05$).

The regression model that fits the experimental data based on the results of Table 9 can be represented as:

$$\sigma_t = -5.341 - 0.001N - 0.009T + 26.65W - 26.85W^2 + (0.309 \times 10^{-2})N.T + (0.003)N.W \quad (7)$$

where N is the CNT-epoxy suspension mixing speed in rpm, T is the CNT-epoxy suspension mixing time in minutes and W is CNT concentration in in wt.%. Hence, electric conductivity (10^{-3}×S/m) is represented as:

$$\sigma = \exp(-5.341 - 0.001N - 0.009T + 26.65W - 26.85W^2 + (0.309 \times 10^{-2})N.T + (0.003)N.W) \quad (8)$$

The adjusted R^2_{adj} (which denotes how successfully the experimental data fits the model) for the regression model has been calculated as 94.6%, indicating the improvement in the fit by the logarithmic model.

Figure 16 shows the residuals normality test. The calculated p-value is 0.135 which indicates that residuals come from a normally distributed population.

A similar analysis has been employed for the effect of production parameters on CNT-epoxy nanocomposite strength and the results are given in Table 12. Based on results, no significant terms are removed and respective analysis of variance on tensile test results considering the main factors and quadratic term of concentration is presented in Table 13. Considering the calculated P-values, mixing speed has the greatest effect on tensile strength of the samples. On the other hand, mixing duration does not show a significant effect on tensile strength.

Ultimate tensile strength (UTS, MPa) of CNT-epoxy can be represented using a regression model as follow:

$$UTS = -216.3 + 26.59N + 0.02T + 0.08W - 141.85W^2 \qquad (9)$$

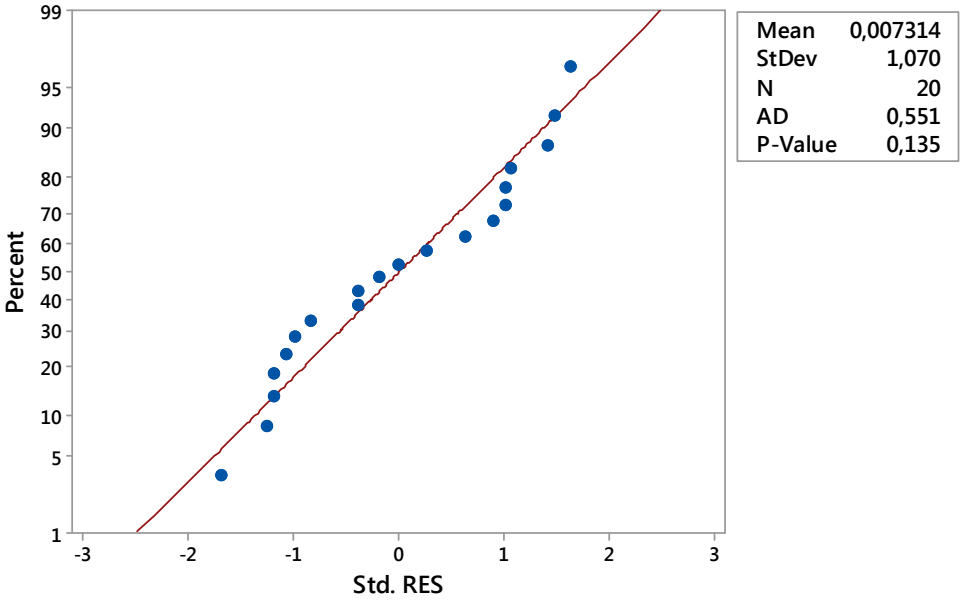

Figure 15. Normality test for residuals

Table 12. Analysis of Variance on tensile strength of CNT-epoxy nanocomposite

Source	DF	Seq SS	Adj SS	Adj MS	F	P
Regression	9	1707.6	1707.6	189.733	6.48	0.004
Linear	3	1537.56	128.08	42.694	1.46	0.284
mixing speed (rpm)	1	1480.28	69.98	69.981	2.39	0.153
mixing time (min)	1	36.74	4.53	4.525	0.15	0.702
concentration (wt.%)	1	20.54	7.21	7.211	0.25	0.63
Quadratic	3	160.86	160.86	53.621	1.83	0.205
mixing speed (rpm)*mixing speed (rpm)	1	128.36	21.26	21.258	0.73	0.414
mixing time (min)*mixing time (min)	1	18.21	6.44	6.44	0.22	0.649
concentration (wt.%)*concentration (wt.%)	1	14.3	14.3	14.299	0.49	0.5
Interaction	3	9.18	9.18	3.059	0.1	0.956
mixing speed (rpm)*mixing time (min)	1	5.84	5.84	5.837	0.2	0.665
mixing speed (rpm)*concentration (wt.%)	1	2.92	2.92	2.92	0.1	0.759
mixing time (min)*concentration (wt.%)	1	0.42	0.42	0.42	0.01	0.907
Residual Error	10	292.59	292.59	29.259		
Lack-of-Fit	5	235.38	235.38	47.076	4.11	0.073
Total	5	57.21	57.21	11.442		
R^2 =85.37%	$R^2_{pred} = 0.00\%$			$R^2_{adj} = 72.21\%$		

Table 13. Analysis of Variance on tensile strength, some predictors have been eliminated

Source	DF	Seq SS	Adj SS	Adj MS	F	P
Regression	4	1655.98	1655.98	414	18.04	<0.001
Linear	3	1537.56	1618.63	539.54	23.51	<0.001
mixing speed (rpm)	1	1480.28	1480.28	1480.28	64.51	<0.001
mixing time (min)	1	36.74	36.74	36.74	1.6	0.225
concentration (wt.%)	1	20.54	101.61	101.61	4.43	0.053
Quadratic	1	118.42	118.42	118.42	5.16	0.038
concentration (wt.%)*concentration (wt.%)	1	118.42	118.42	118.42	5.16	0.038
Residual Error	15	344.21	344.21	22.95		
Lack-of-Fit	10	287	287	28.7	2.51	0.161
Total	5	57.21	57.21	11.44		
R^2 =82.8%	R^2_{pred} = 68.3%		R^2_{adj} = 78.2%			

2.4.4 Validation of the Mathematical Models of Conductivity and Composite Strength

To investigate the accuracy and robustness of the found regression models for conductivity and composite strength, 8 further experiments were carried out within the range of explored experimental parameters. Each “experiment” is the production of a new nanocomposite sample that has different production parameters (mixing conditions for preparation of the CNT-epoxy suspensions that are later cast and cured). These samples were then tested for conductivity and tensile strength as outlined before. The results are compared with the predicted results from the regression models of section 2.4.3. Table 14 presents the predicted values and the experimental values (average of 3 samples) with the corresponding standard deviation. The tabulated results are shown in graphical form in Figure 17. The estimated values are all within scattering range, indicating the developed regression models have acceptable robustness and accuracy within the range of explored experimental parameters (suspension mixing speed: 500 to 2000 rpm, suspension mixing duration: 10 to 60 min and CNT concentration: 0.2 to 0.5 wt.%). The high residuals observed in some of the experiments based on which the regression models were developed in earlier analysis, did not prevent the acceptability of the developed models.

Table 14. Validation tests

Exp. No.	Sample ID	Tensile strength (Mpa)			Electric conductivity (S/m)×10^{-3}		
		Predicted	Experimental	2Std.	Predicted	Experimental	2Std.
1	800N10T30W	63.5	66	±4	0.88	0.78	±0.16
2	800N60T30W	67.2	70	±8	1.14	1.29	±0.52
3	1600N10T30W	76.4	80	±6	0.68	0.648	±0.30
4	1600N60T30W	80.2	78	±6	1.79	1.57	±0.60
5	800N10T40W	62.5	66	±4	2.48	1.96	±0.50
6	800N60T40W	66.3	71	±8	3.21	2.76	±0.52
7	1600N10T40W	75.4	79	±4	2.43	2.33	±0.64
8	1600N60T40W	79.3	76	±6	6.42	5.87	±0.78

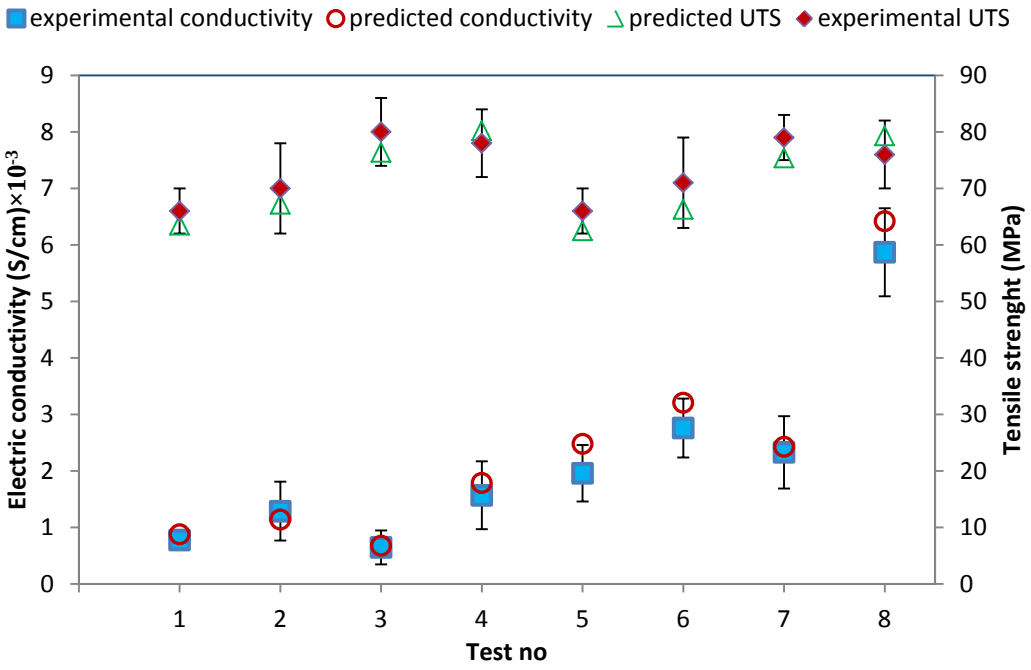

Figure 16. Estimated and experimental Electric conductivity of samples presented in Table 14.

2.4.5 Strain sensing behavior of CNT-epoxy nanocomposites under tensile loads

Strain in a conductive nanocomposite during service can be related to the electrical conductivity of nanocomposite. The variation in electrical resistance can be used for measuring and monitoring the amount of strain in composite during service, if the conductivity of nanocomposite has sufficient sensitivity to strain. The sensitivity of a strain gauge to sense strain can be expressed quantitatively using

$$k = \frac{\Delta R/R_0}{\varepsilon} \tag{10}$$

where k is gauge factor, $\Delta R/R_0$ is the change of the electrical resistance ΔR normalized by the initial resistance R_0 and ε is strain [63]. The fractional change in electrical resistance ($\Delta R/R_0$) versus the strain during the testing of the samples is presented in Figure 18a and 18b. Gauge factor is obtained by curve-fitting a straight line to the experimental data of Figure 18.

Bias and nonlinearity are used to determine the accuracy of (nanocomposite) sensors in sensing the strain. The % bias value is given as:

$$Bias = \left(\frac{1}{n}\sum_{i=1}^{n}\frac{|\varepsilon_i - \hat{\varepsilon}|}{\varepsilon_{max}}\right) \times 100\ \% \tag{11}$$

and indicates how much gauge bias explains the overall process variation [64]. Here, ε_i is the measured strain, $\hat{\varepsilon}$ is the predicted strain (based on composite electrical resistance) and ε_{max} is the maximum measured strain.

Deviation from linearity is calculated using

$$Nonlinearity = \frac{|k\varepsilon - \Delta R/R_0|}{\varepsilon} \times 100\% \tag{12}$$

and describes how accurate the measurements are through the expected range of measurements [63]. The effect of CNT filler concentration and dispersing scenario on sensory properties of the CNT-epoxy nanocomposites is presented in Table 15.

Regardless of mixing factors, gauge factor of nanocomposites with low CNT concentration (0.2 wt.%) varies between 1.5 and 2.9 which is too wide comparing to scattering in k-factor of the high CNT loaded composites (1.3 up to 1.6). This can be observed in Figure 18 where for low concentrated samples; a significant difference between the responses of the composite sensors ($\Delta R/R_0$) under tensile strain can be observed (Figure 18a). On the other hand, the fractional change in electrical resistance ($\Delta R/R_0$) of the samples containing high amount of CNT under axial tensile strain is significantly close to each other. Considering above discussion, it can be say that sensitivity (k-factor) of high CNT concentrated is not affected by mixing

scenario in contrast to low concentrated nanocomposites where other sensory properties (bias, nonlinearity) are also affected by mixing parameters.

According to Table 15, considering bias less than 10%, the maximum sensitivity (k=2.9) was observed for the sample at which 0.2 wt.% CNT was dispersed in epoxy matrix at 2000 rpm for 60 minutes. It implies that finer morphologies are more sensitive to strain and are more suitable for strain sensing applications.

Table 15. Effect of mixing parameters and CNT concentration on sensory properties of CNT-epoxy nanocomposites

Mixing speed (rpm)	Mixing time (min)	CNT concentration (wt.%)	Gauge factor (k)	Bias max	Bias (%)	Nonlinearity (%)
500	10	0.2	-	-	-	-
2000	10	0.2	1.8	32.2	11.8	20.4
500	60	0.2	2.0	28.1	10.6	24.7
2000	60	0.2	2.9	12.1	5.4	13.0
500	10	0.5	1.4	22.8	10.1	26.2
2000	10	0.5	1.6	11.0	5.7	14.0
500	60	0.5	1.5	9.7	6.6	16.5
2000	60	0.5	1.5	19.1	7.5	18.5

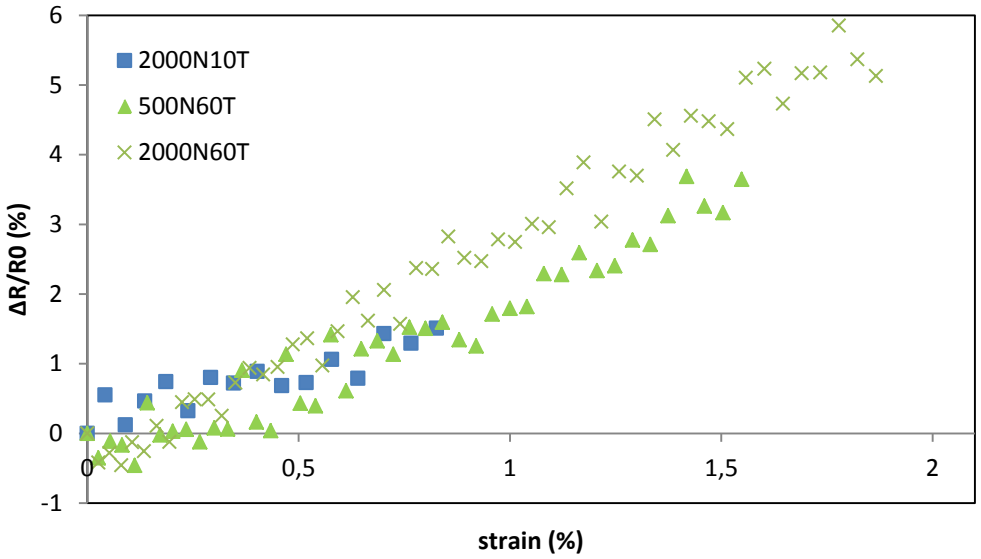

(a)

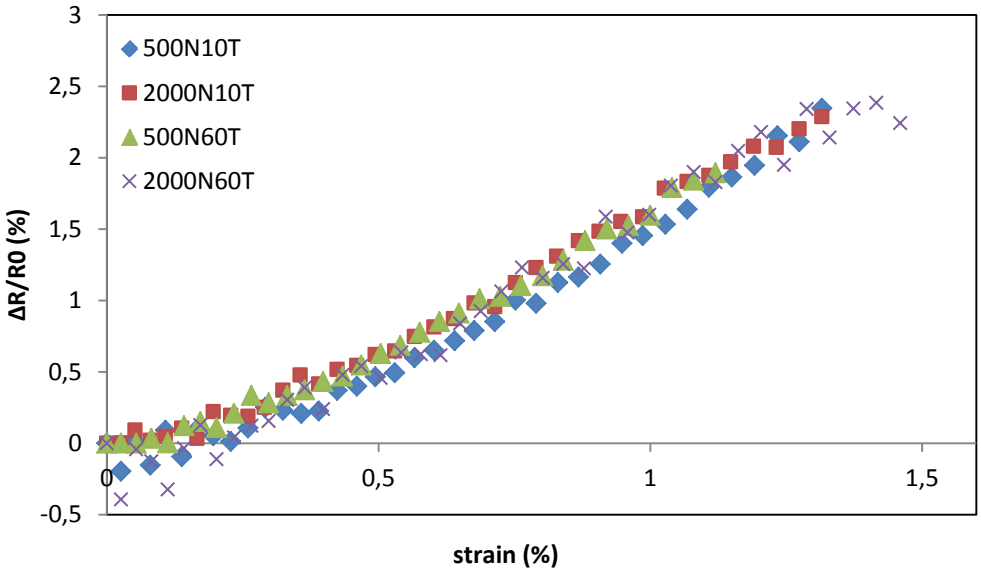

(b)

Figure 17. The fractional change in electrical resistance ($\Delta R/R_0$) verses strain of the samples containing (a) 0.2 and (b) 0.5 wt.% CNTs.

CHAPTER 3

PRODUCTION OF ALIGNED CNT/EPOXY NANOCOMPOSITES VIA MAGNETIZATION OF CNT'S

3.1 Production of Aligned CNT composites via Magnetization

The alignment of CNTs can improve the mechanical (fracture resistance [65] and tensile strength [66]) and physical (thermal [65] and electrical [67] conductivities) properties of nanocomposites in the direction of CNT orientation. Various alignment techniques have been proposed. The application of electric and magnetic fields is an effective approach to compel CNTs to align in a matrix [66]. Although an electric field can properly draw desired anisotropic behavior from CNTs with proper alignment, doing so requires an extremely high field strength (600–1000 V/cm) and frequency (10–100 MHz), confine it to small-scale applications [67,68]. Although using magnetic fields to align CNTs has a distinct advantage over electric field alignment [68], ultra-strong magnetic fields of 7–25 T are often required, which are unavailable in most research laboratories. To overcome this issue, CNTs have been modified by metal fillers or with attached magnetic particles [66,69]. This allows CNT alignment under low magnetic fields. Furthermore, due to the residual catalysts such as Fe, Ni, or Co, used in fabricating CNTs, incompletely purified CNTs can respond well to low magnetic fields (typically 0.1–0.6 T) and are hence aligned in the polymer matrix with improved physical properties [65,66].

In this study, in order to improve the electrical conductivity of CNT/epoxy nanocomposites, the magnetic field approach was used to align CNTs. A magnetic

field of 0.2 T was generated using a solenoid. The composition of CNTs used is shown in Table 16. A CNT/epoxy suspension was prepared by dispersing 0.5 wt.% CNT into an epoxy matrix using shear mixing. The suspension was then mixed at 2000 rpm for 1 h. Finally, to release trapped air the suspension was degassed under vacuum for 10 min.

Three samples were prepared by injecting CNT/epoxy suspension into plastic tubes of diameter 2 mm and length 80 mm. Two of the samples were placed into a solenoid as a core. The solenoid was powered with 25 VDC at 2 A and samples were kept under the magnetic field for 4 h.

3.2 Characterization of Aligned CNT composites

The morphologies of the fracture surfaces of the CNT/epoxy samples were examined using scanning electron microscopy (SEM). The samples for morphology inspection were prepared by cutting a small segment of maximum length 2 mm from a master sample (Figure 19, sec A-A). These small pieces were then split into two (Figure 19, sec B-B).

Table 16. Element composition of CNT

C (at%)	O (at%)	Fe (at%)	Co (at%)	Cu (at%)	Zn (at%)
>90	3.01	1.27	<0,50	3.51	1.72

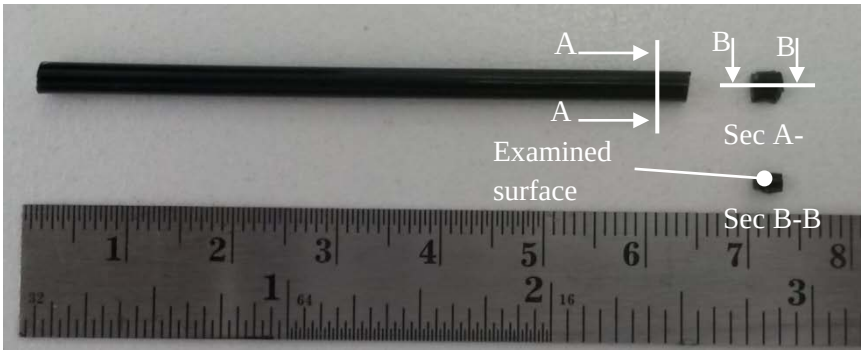

Figure 18. Preparing a fractured surface for SEM characterization

SEM images were analyzed using the ImageJ (v 1.50b) software. The images of the samples prepared with and without an applied magnetic field differ based on the geometry of the detected CNTs. Most of the detected CNTs on the fractured surface of the samples that were not subjected to a magnetic field are in the form of a circle. On the other hand, by applying a magnetic field, the CNTs lay on the fractured surface. This can be quantified by counting the observed circles. According to ISO 9276-6, circularity is defined as the degree to which the object is similar to a circle, taking into consideration the particle form and roughness. Circularity is a dimensionless value and calculated using following equation:

$$C = \sqrt{\frac{4\pi A}{P^2}} \tag{13}$$

where C is the circularity, A is the area, and *P* is the perimeter of the object.

Analysis of the SEM images (Figure 20) using ImageJ shows that the ratio of detected CNTs with circularity greater than 0.7 to the number of total detected CNTs for the samples subjected to a magnetic field varied between 0.21 and 0.30. The same ratio for nanocomposite samples not subjected to a magnetic field was in the range 0.55–0.68.

Figure 20 to Figure 22 show the SEM images, ImageJ-processed images, and histogram of CNT orientation angles of the composites, respectively. Histograms were plotted in MATLAB® using processed SEM micrographs from ImageJ. The histograms of the samples subjected to the magnetic field show CNTs aligned to the direction of the magnetic field. Note that the high viscosity of the CNT/epoxy suspension makes the alignment of CNTs difficult under the low 0.3 T magnetic field [65].

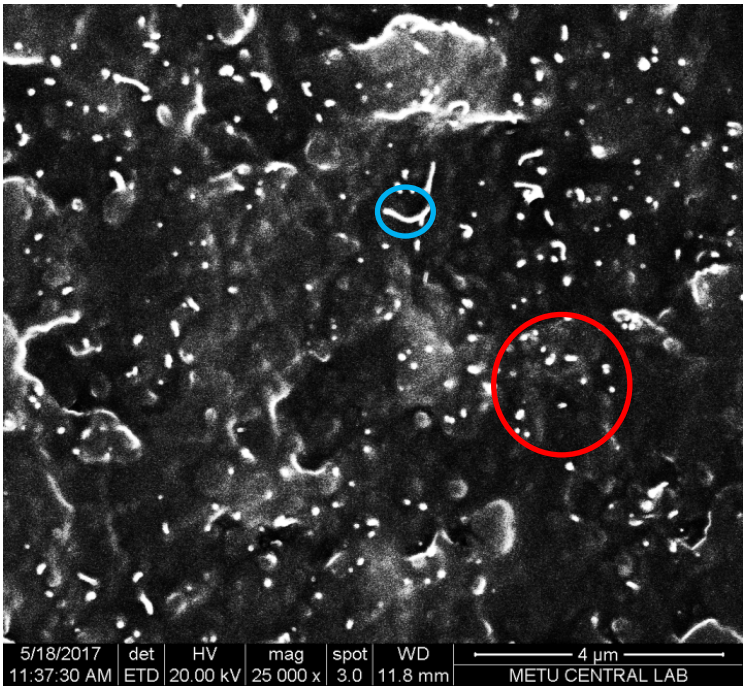
5/18/2017
11:37:30 AM
det
ETD
HV
20.00 kV
mag
25 000 x
spot
3.0
WD
11.8 mm
4 µm
METU CENTRAL LAB

(a)

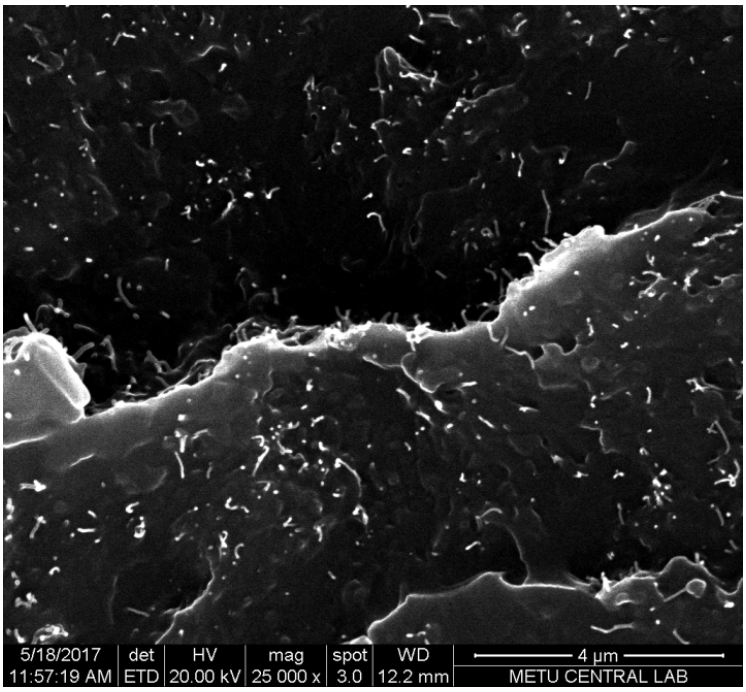
5/18/2017
11:57:19 AM
det
ETD
HV
20.00 kV
mag
25 000 x
spot
3.0
WD
12.2 mm
4 µm
METU CENTRAL LAB

(b)

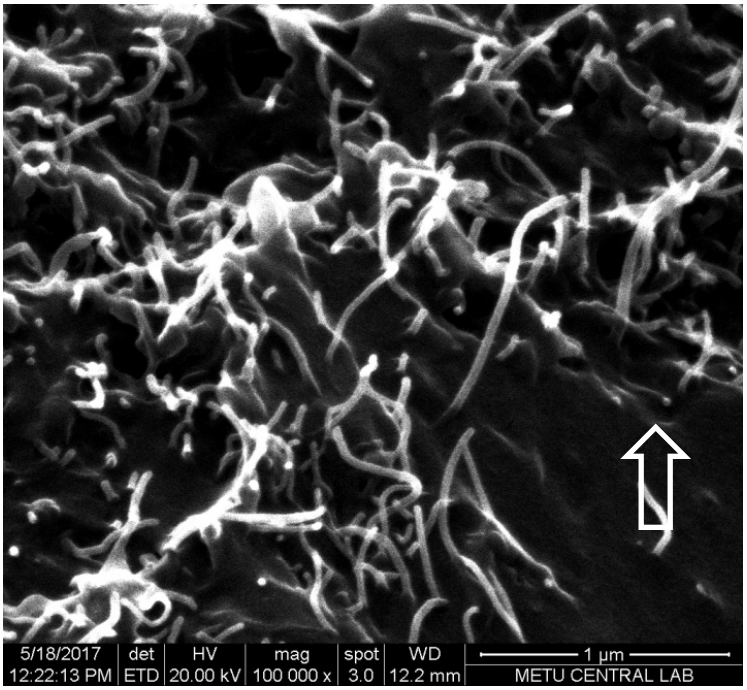

(c)

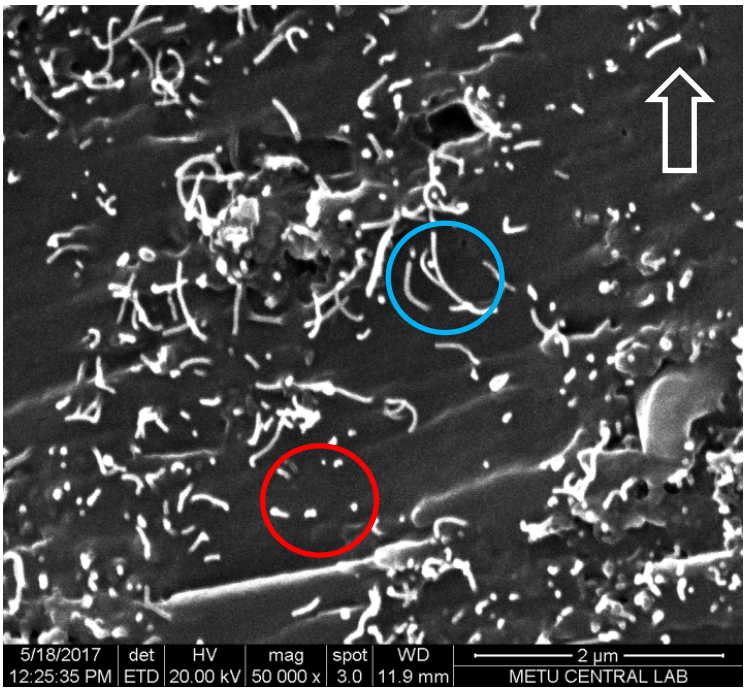

(d)

Figure 19. SEM micrographs of fracture surfaces of CNT epoxy containing 0.5 wt. % CNT. (a - b) Not magnetized. (c-d) Magnetized. Surfaces are parallel to magnetic field. Arrows show the direction of magnetic field.

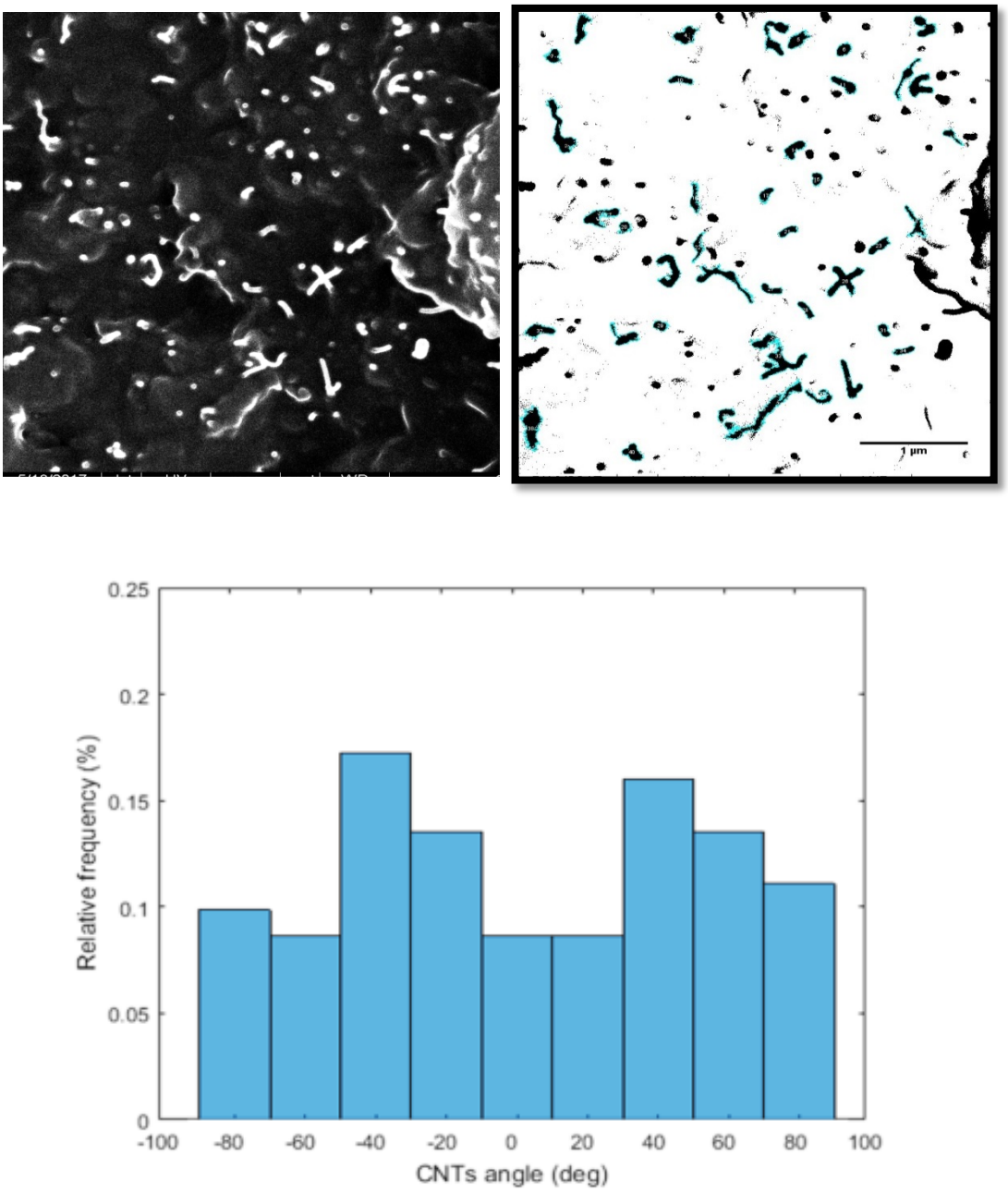

Figure 20. Histograms of CNT orientation angles of CNTs in the composites not subjected to the magnetic field.

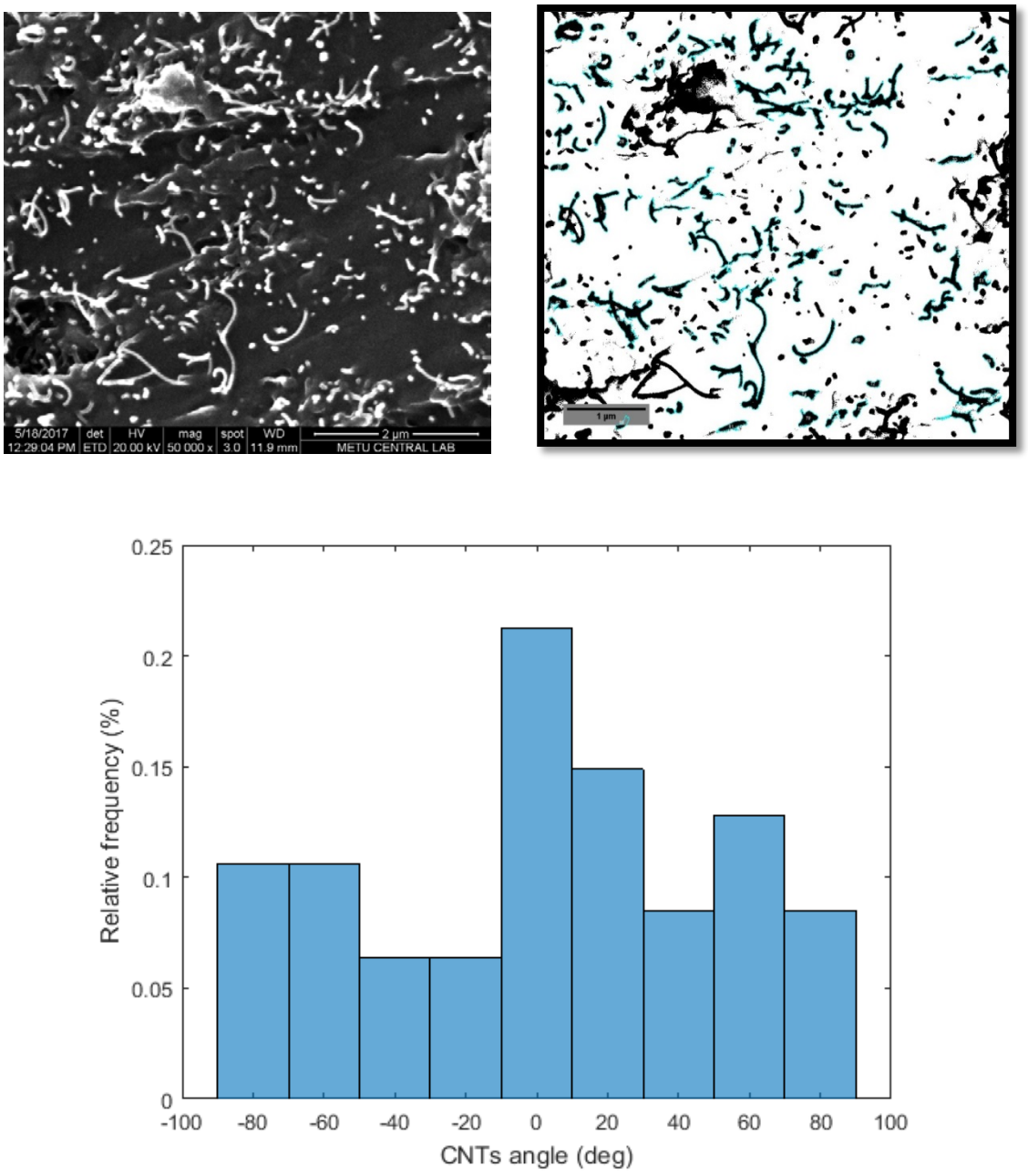

Figure 21. Histograms of CNT orientation angles of CNTs in the composites subjected to a magnetic field (magnetized sample 1).

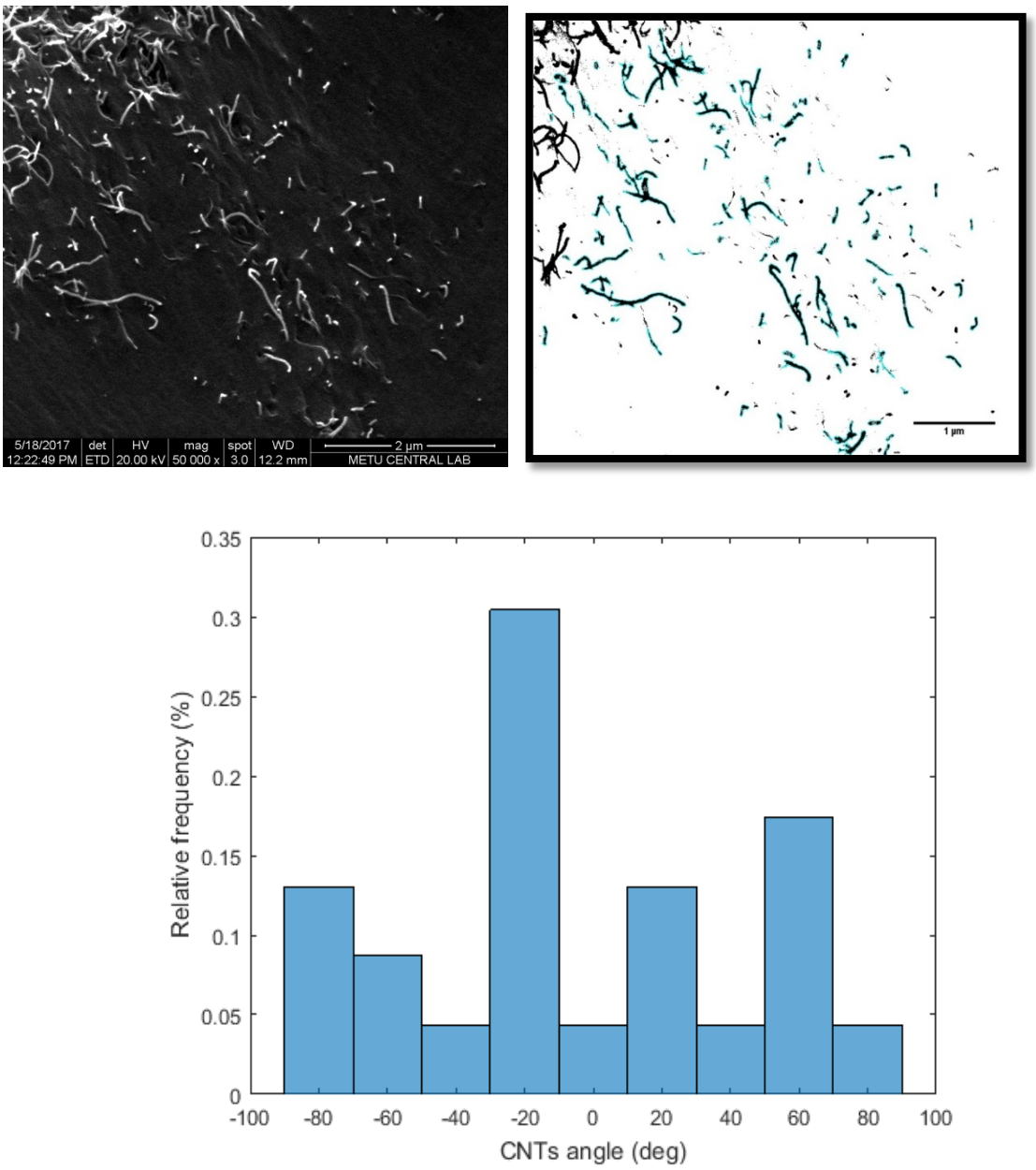

Figure 22. Histograms of CNT orientation angles of CNTs in the composites subjected to a magnetic field (magnetized sample 2).

3.3 Comparison of Aligned and Randomly Distributed CNT Composite Electrical Conductivities and Discussion

Magnetized CNT/epoxy samples were cut and polished at their ends and then painted using silver paint. The electrical resistance of the samples along their length was measured using a two-point-probe technique [60] with a Keithley 2000 Digital Multimeter. The electrical resistance of the samples was measured as 170±30 kΩ, nearly half of the measured resistance of the control samples (380±50 kΩ). Thus, a significant improvement in the electrical conductivity of the CNT/epoxy nanocomposite was obtained by applying a magnetic field.

CHATER 4

MODELING OF THE PIEZORESISTIVITY OF CNT EPOXY NANOCOMPOSITES WITH ALIGNED CNTs

The electrical and electromechanical properties of CNT nanocomposites are strongly affected by CNT characteristics such as the aspect ratio, dispersion state, and alignment of CNTs in the polymer matrix. Several studies in literature have proposed numerical models to predict the nominal electrical conductivity and electromechanical behavior of CNT nanocomposites.

Behnam et al. [70] investigated the effect of CNT resistance, length, density, and alignment on the electrical resistivity of nanocomposites. Hu et al. [71] set up a 3D numerical model to predict the nominal electrical conductivity of agglomerated CNTs obeying a normal distribution. Bao et al. [72] developed a 3D model by applying periodic boundary conditions to analyze the electrical conductivity of a CNT nanocomposite with a uniform or aligned, distributed, and agglomerated CNTs. Additionally, several subsequent studies have utilized these models to investigate the strain sensing behavior of a CNT nanocomposite [73,74]. Note that the uniform distribution of CNTs is a key assumption of these models [71,73–75].

In this chapter, a Monte Carlo process is adapted to a straight forward 2D percolation-based model of [73,74]. This makes it possible to analyze the piezoresitivity of CNT nanocomposites with any CNT distribution, whether uniform or aligned. It is worth noting that despite the simplicity of the mentioned 2D model, its capability to predict the electrical and electromechanical behavior of CNT nanocomposites has been proved by experimental results [73].

4.1 Percolation based models

In a CNT nanocomposite where CNT-conductive particles are embedded in an insulating matrix, three cases can be expected for insulator-to-conductor phase transitions:

- The concentration of conductive tubes in the matrix is too low, so there is not a continuous conductive pathway for electrical current to flow from one end to the other (source to drain).
- As the concentration of nanotubes reaches a critical threshold, electrically conductive clusters form by direct contact between the CNTs or the transporting electrons between neighboring CNTs (tunneling phenomena). Finally, these clusters connect and form an electrically conductive path between source and drain (electrodes). By adding more CNTs, the electrical conductivity of the nanocomposite increases dramatically.
- Finally, at high CNT concentrations, the electrical conductivity increases gradually and then saturates due to the existence of several electrically conductive paths.

These three cases are shown schematically in Figure 23. The percolation threshold is defined as the minimum concentration of CNTs that result in a remarkable increase in nanocomposite electrical conductivity (Figure 24).

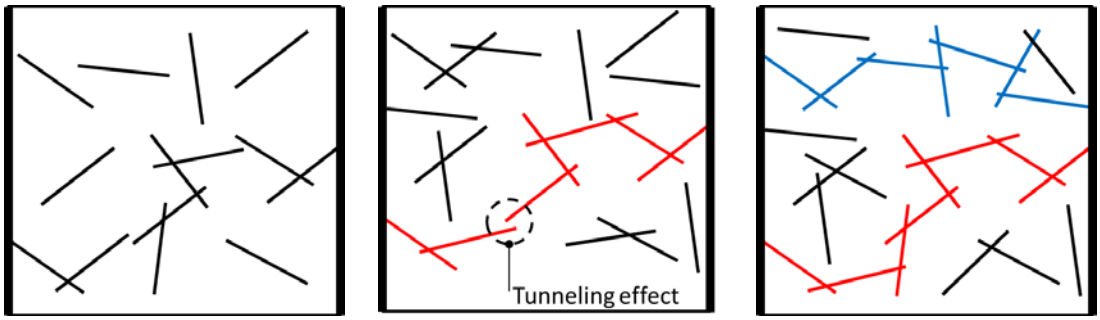

(a) (b) (c)

Figure 23. Electrical conductivity of CNT nanocomposites based on percolation theory, a) an electrically insulating state where CNT concentration is lower than percolation threshold, b) electric conductivity is increased dramatically due to existence of conductive pathway(s) between opposite electrodes, c) electrically conductive nanocomposite consists of several conductive paths.

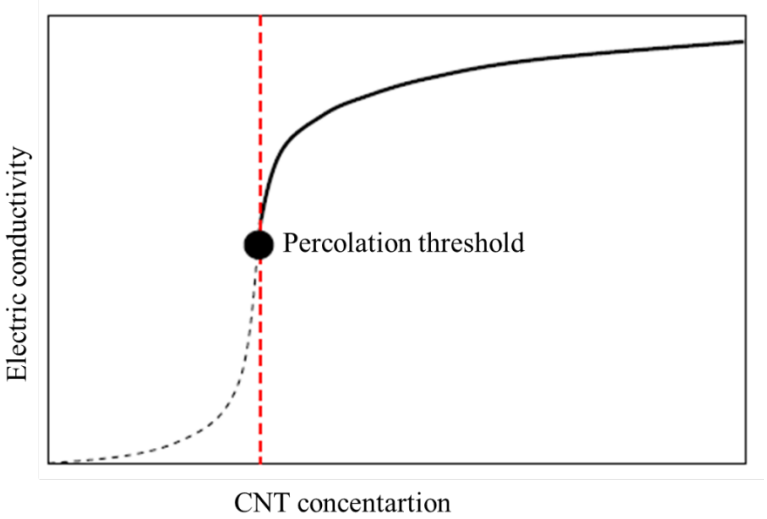

Figure 24. Electrical conductivity of CNT/epoxy nanocomposite at various CNT concentrations

In this study, a 2D resistor network model was used to investigate the electrical and electromechanical properties of CNT-filled nanocomposites. In a resistor network model, each CNT is considered as a resistor. Therefore, a CNT-filled nanocomposite above the percolation threshold can be modeled as a network of resistors that form conductive paths between two surfaces, or source and drain electrodes. This concept is shown in Figure 26.

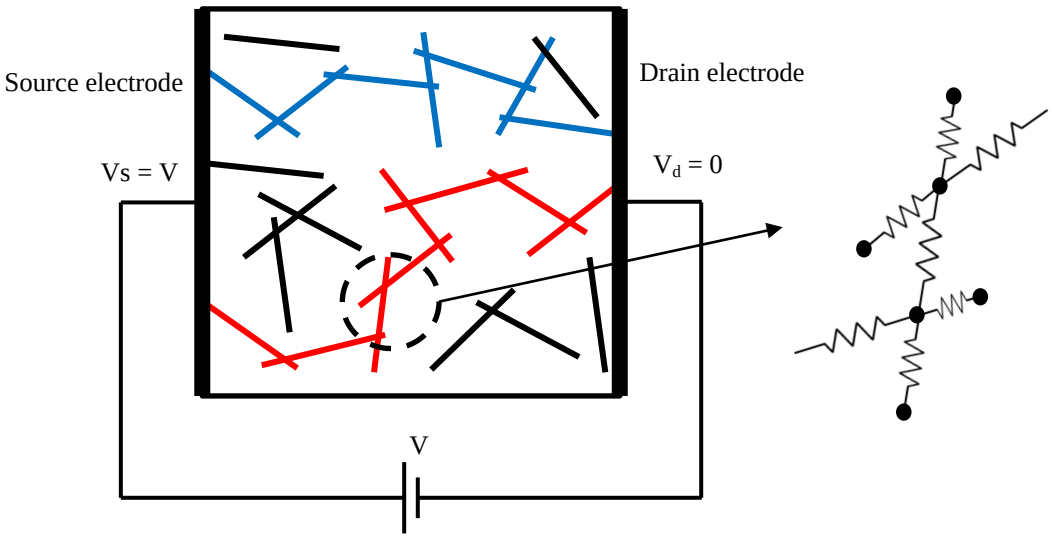

Figure 25. Schematic of resistor network model

Here, CNTs were simulated as straight lines of length L_{cnt} and were distributed on a representative 2D area of length L and width W. Each nanotube was located by determining its two endpoints in a Cartesian coordinate system whose origin was fixed at the left-bottom corner of the representative area. The first endpoint location (x_1,y_1) was determined randomly, with x_1 and y_1 random numbers in [0,L] and [0,W], respectively. The other endpoint position, (x_2,y_2), was then calculated using the following equations:

$$x_2 = x_1 + L_{cnt}\cos\theta \qquad , -\frac{\pi}{2} \le \theta \le \frac{\pi}{2} \qquad (14)$$

$$y_2 = y_1 + L_{cnt}\sin\theta \qquad , -\frac{\pi}{2} \le \theta \le \frac{\pi}{2} \qquad (15)$$

where θ is the nanotube's orientation angle. Note that in a random distribution, the orientation angle is generated randomly and for oriented cases this angle is defined with respect to the CNT's orientation function. Using this procedure, each nanotube is represented as a straight line.

Upon generating CNTs with a concentration N, the locations of intersecting points (junctions) were identified by solving sets of linear equations. Then, graph theory was used to find the available paths between any two points, or between source (S) and drain (D) electrodes. As illustrated in Figure 27, the graph model assumes that each CNT includes a graph vertex and the junction between nanotubes is an edge between two corresponding vertices.

In Figure 27, the parameter of interest is the total electrical resistance between source and drain electrodes. The resistance of segments between junctions can be calculated as [70]:

$$R = R_t\left(1 + \frac{l_c}{\lambda}\right) + R_{jct} \qquad (16)$$

where R_t is the theoretical contact resistance at the ballistic limit with an approximate value of 6.5 kΩ and 100 kΩ for SWCNT and MWCNT respectively, λ is the electron mean free path (assumed to be 1 μm), l_c is the length of the conductor (nanotube segment between neighboring junctions), and R_{jct} is the nanotube-nanotube junction contact resistance. Figure 28 shows the modeling of nanotube resistance using equivalent resistors.

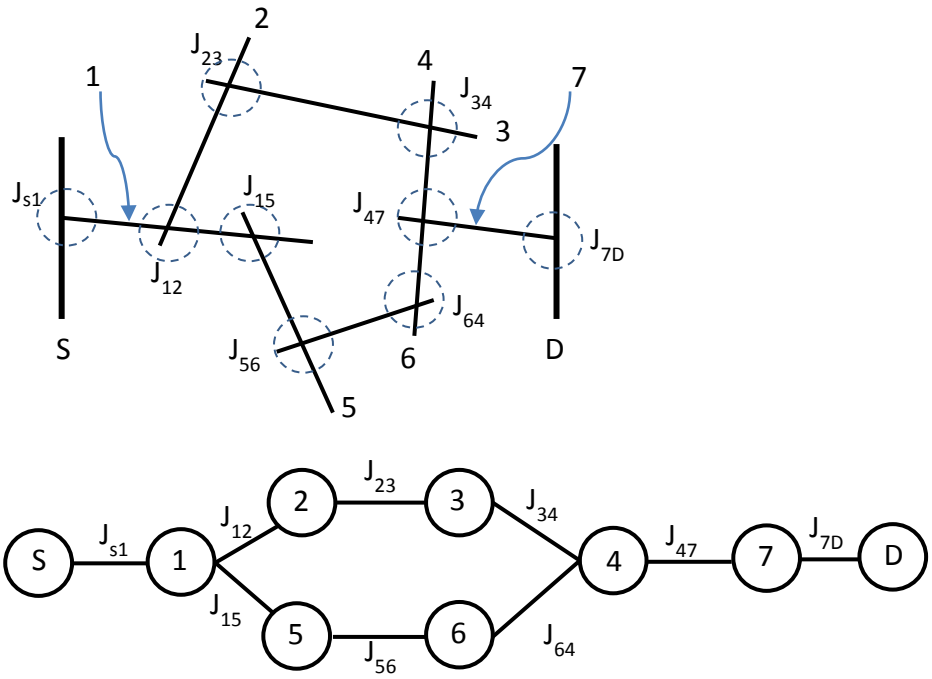

Figure 26. Equivalent graph of a nanotube network, a) randomly distributed nanotube network between source (S) and drain (D) electrodes, b) equivalent graph for resistance analysis of nanotube network.

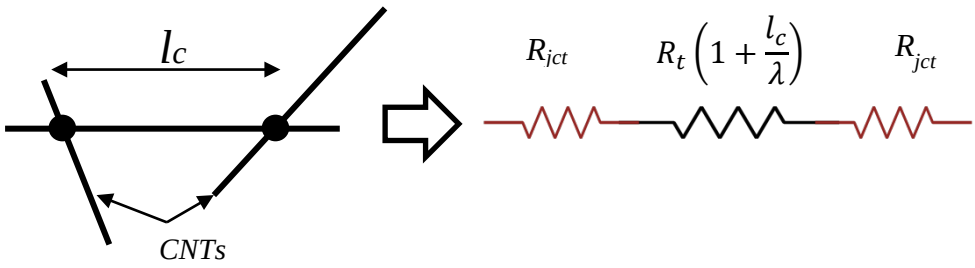

Figure 27. Equivalent resistance of a nanotube segment between two junctions

Finally, network resistance can be calculated using nodal analysis, i.e., Kirchhoff's current law, [70,73,74] or graph conductance theory [76].

In this study, the entire network resistance was calculated using graph conductance theory. First, the resistance of all available paths along the length of the representative element (L) was calculated. In other words, the nanotube network was considered as a circuit consisting of several connected resistors (in parallel or series) that form conductive paths between the source and drain electrodes. Then, the

network overall resistance can be calculated using Ohm's law. In this study, the simulation code was implemented in *MATLAB* (Mathworks, Inc.).

4.2 Model validation with randomly oriented CNTs

In order to verify the accuracy of the model, a simulation was done with the same properties as [74]. Nanotubes of length 0.16 μm were distributed randomly on a 1 μm×1 μm representative area, with a nanotube density of 300. The intrinsic resistance of the nanotubes and junction resistance were set at $R_t = 6.5\ \text{k}\Omega$ and$R_{jct} = 98\ \text{k}\Omega$, respectively. With these conditions, the entire resistance of network was predicted to be around 500 kΩ. Figure 29 illustrates a network consist of 300 CNTs distributed in a 1×1 μm^2 area along with their intersections. The equivalent resistor network for this simulation is shown in Figure 30. The total resistance of the network was calculated to be 534 kΩ, which is very close to the predicted value from [74] for the same nanotube network. Considering this, the presented model could be considered as validated and thus utilized for different conditions.

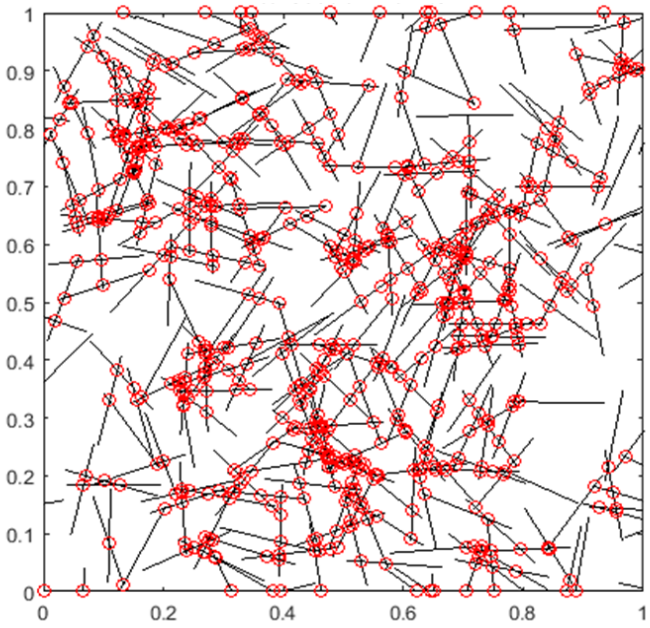

Figure 28. CNTs uniformly distributed in a representative area (1×1 μm^2) with a concentration of *N = 300*. Intersections are marked by red circles.

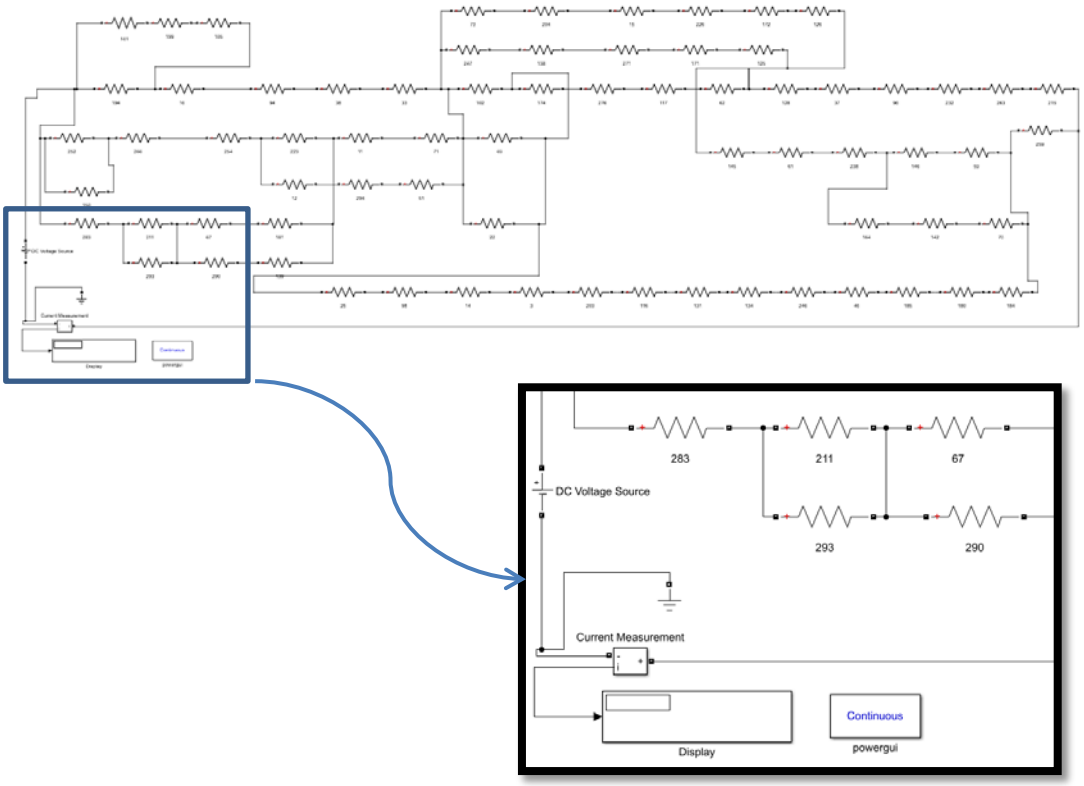

Figure 29. Equivalent resistor network.

4.3 Effect of CNT alignment on strain sensing

In CNT nanocomposites, carbon nanotubes are significantly stiffer than the polymer matrix material. For instance, the elastic modulus of a typical epoxy resin is around 3 GPa, nearly 300 times less than that of CNTs [77]. Thus, when nanocomposites are subjected to tensile or compression strain, the amount of strain at the nanotubes can be neglected compared to the matrix strain [76]. Therefore, when the matrix is deformed, nanotubes are just displaced from their initial positions in the matrix, and consequently, the conductive network reconfigures itself and the nanocomposite resistance changes. To be specific, if a strain ε is applied to a representative area along *y* axis, the new location and orientation of nanotubes can be updated using following equations:

$$x_1' = x_1(1 - \varepsilon\vartheta) \quad (17)$$

$$y_1' = y_1(1 + \varepsilon) \quad (18)$$

$$\theta' = \tan^{-1}\left[\frac{1+\varepsilon}{1-\vartheta\varepsilon}\tan(\theta)\right] \quad (19)$$

where x_1' , y_1' ,and θ' are the updated coordinates and direction of nanotubes and ϑ is the Poisson ratio of the matrix (here, ϑ = 0.35).

Upon doing so, the electrical resistance of reconfigured CNT network is then calculated using the same procedure outlined at section 4.1. Finally, strain sensitivity (*k*) or strain gauge factor is calculated as:

$$k = \frac{(\Delta R/R_0)}{\varepsilon} \quad (20)$$

where R_0 is the initial resistance when unstrained, and ΔR is the change in electrical resistance of the nanocomposite for strained and unstrained cases.

In this section, a Monte Carlo process is used to study the effect of nanotube orientation on the strain sensitivity of CNT nanocomposites. The distribution pattern of CNTs was captured from the histograms presented in Figure 20 to Figure 22.

4.4 Discussion of the Results

Using the proposed percolation model, the effect of CNT alignment on percolation probability of nanocomposites was simulated. The percolation probability is calculated using Equation 21:

$$P = \frac{N_c}{N_{ts}} \quad (21)$$

where N_{ts} is the total number of simulations, and N_c is the number of cases in which the model is electrically conductive. To calculation percolation probability, CNTs

with length of 1.5 μm were distributed in a 7.5×7.5 μm^2 area [70] with presented distribution functions at Figure 20 to Figure 22 and the simulation was conducted 100 times for each cases. The simulation results are shown in Figure 30. According to simulation results, nanocomposite with aligned nanotubes reaches to percolation threshold (50% percolation probability) at lower CNT concentrations than nanocomposites with random nanotubes.

Figure 31 shows that, the electrical resistance of the percolated CNT networks (*N = 250*) with a random distribution is much higher than the networks consist of aligned CNTs. In case of random distribution, the resistance of simulated CNT network is 748 kΩ and for the cases in which CNTs were distributed according to the presented distribution patterns in Figure 21 and Figure 22, the resistance of model is 512 kΩ and 497 kΩ, respectively. In another word, the simulation results show that the electrical conductivity of CNT networks with the same morphology as Figure 21 and Figure 22 is 1.5 times higher than the nanocomposite with random CNT distribution. This finding is in good agreement with the presented experimental results in Chapter 3.

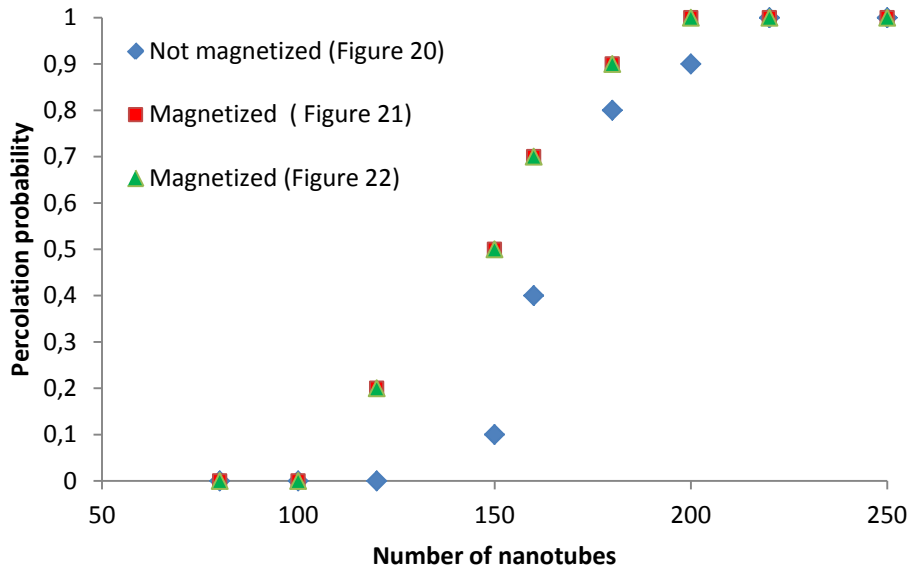

Figure 30. The effect of nanotubes distribution on the calculated percolation characteristics of 7.5×7.5 µm^2 CNT based nanocomposite models. $L_{CNT} = 1.5\ \mu m, R_t = 100\ k\Omega, R_{jct} = 1\ k\Omega$.

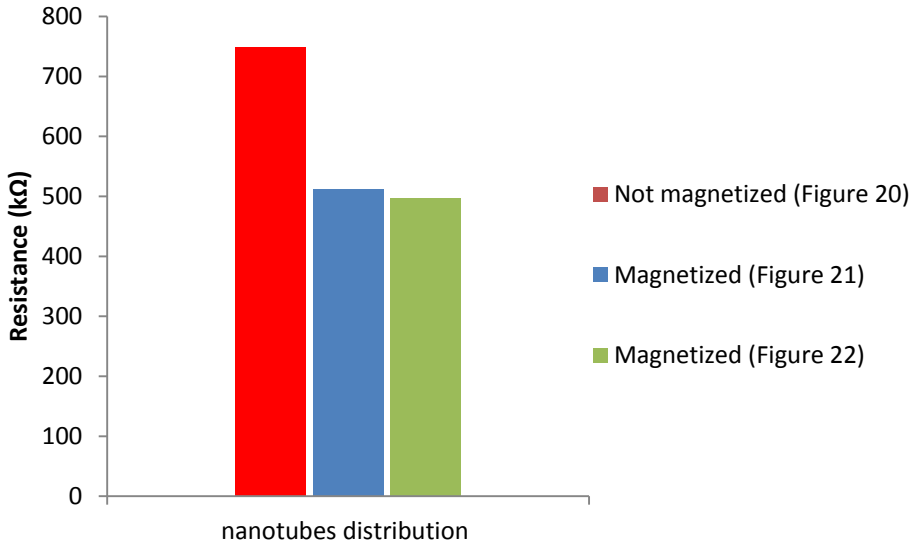

Figure 31. Effect of nanotubes distribution on the calculated electrical resistance of 7.5×7.5 µm2 CNT based nanocomposite models. N=250 and $L_{CNT} = 1.5\ \mu m, R_t = 100\ k\Omega, R_{jct} = 1\ k\Omega$.

Figure 32 shows the fractional change in electrical resistance ($\Delta R/R_0$) of the CNT networks with random and aligned nanotubes distributions as a function of applied strains. From Figure 32, it can be observed that the nanocomposite with random CNT distribution shows higher strain sensitivity ($k = 34.2$) comparing nanocomposite with aligned nanotubes ($k = 26.0$, $k = 21.1$).

This means that although the magnetized nanocomposites have higher electrical conductivity; the nanocomposites with random nanotube distribution are more sensitive to strain.

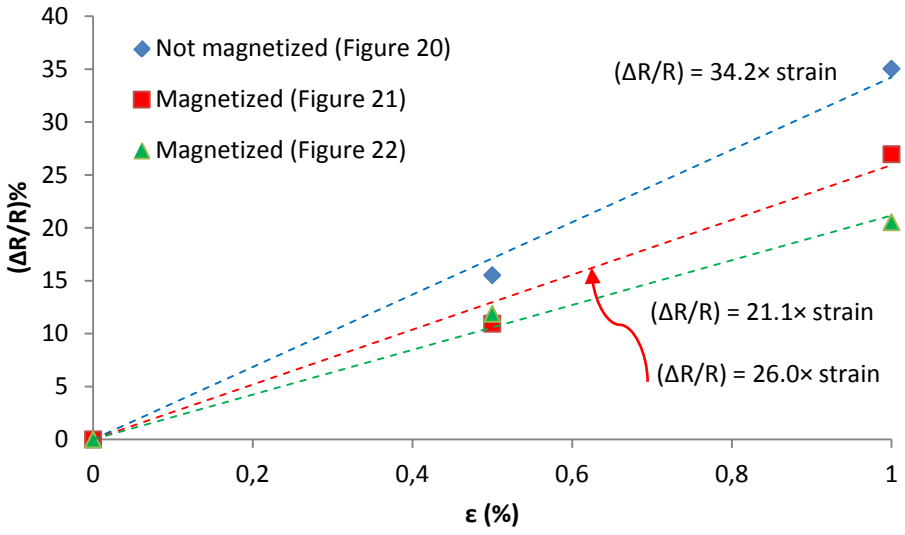

Figure 32. Fractional change in electrical resistance (ΔR/R0) of the CNT network model under tensile strain. The model assumed that N= 250, Lcnt =1.5 µm, $R_t = 100\ k\Omega$, $R_{jct} = 1\ k\Omega$.

CHAPTER 5

MANUFACTURING OF ELECTRICALLY CONDUCTIVE COMPOSITES VIA MICROVASCULAR CHANNELS

5.1 Chemical treatment of sacrificial fibers

The PLA fibers which were used as sacrificial fibers in the vaporizing of sacrificial components process must be chemically modified for ease of burn-out. For this purpose, the commercial PLA fibers are treated with tin(II) oxalate (SnOx) catalyst to decrease their thermal degradation temperature from approximately 280 °C to 200 °C. Figure 34 presents the Thermo-gravimetric analysis (TGA) of unmodified PLA which has been done at METU Central Laboratory. According to TGA results, thermal degradation of unmodified PLA fibers starts at 280 °C which is too high to apply on epoxy resin based fiber reinforced composite structures.

5.1.1 Treating PLA using Trifluoroethanol: H2O: SnOx suspension

Esser Kahn et al.[10,78,79] established a process to chemical treatment of the PLA fibers. In this process, the commercial PLA fibers are wound on a reel and placed in a catalyst treatment (Table 17) bath. The beaker containing the catalyst solution is suspended in a temperature-controlled water bath and the reel is attached to a mechanical mixer, which agitates the solution at 400–450 RPM for 24 h at 37 °C. Following the treatment process, the fibers are dried in an oven for 24 h at 35 °C.

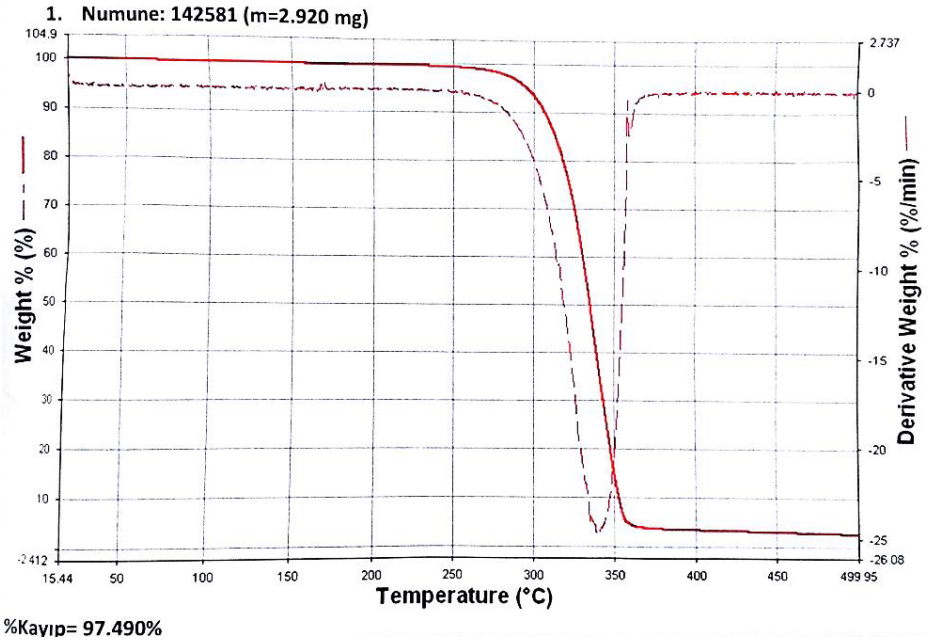

Figure 33. Thermo-gravimetric analysis (TGA) of unmodified PLA fibers

Table 17. Composition of catalyst treatment bath

Item	Ingredient	Reference			
		[78]	[10]	[79]	[11]
1	Trifluoroethanol (TFE)	480 mL	67 vol.%	480 mL	480 mL
2	deionized water	320 mL	33 vol.%	320 mL	320 mL
3	SnOx	10 wt.%	2 wt.%	1.3 g (0.1 wt.%)	13 g (1 wt.%)
4	DISPERBYK-130	--	--	40 mL	40 mL
5	Rhodamine 6G dye	1 g	1 g	1 g	1 g

In this process, the amount of catalyst (tin(II) oxalate) entrapped in the fiber determines the efficiency of the process. Solvent composition (the ratio of TFE to water) and fiber soaking time are introduced as the process parameters which can affect the treatment efficiency.

Exposing fibers to a solution of TFE/water ratio of 60:40 for 24 h has been reported as the optimum solvent for PLA fibers with diameter of 500 micrometer [11,78,79]. However, our preliminary experiments showed that this chemical solvent and treating time may not proper for all grades of PLA. For instance, PLA grade Ingeo 6062D is dissolved in TFE/water solvent ratio of 60:40 after 6 hours. Thus, it was necessary to find proper solution combination (TFE: H2O) and treating time for the available PLA grade.

In this study, two solvent solutions with TFE:H_2O ratio of 50:50 and 60:40 were prepared and both solutions were reached with tin (II) oxalate catalyst in the same concentration (5 wt.%). For this purpose, the treatment suspension was prepared by mixing 100 ml deionized water with 10 ml of DISPERBYK-130 in a closed bottle and shook until a homogenous solution was obtained. Then TFE was added considering TFE:H_2O ratio and suspension was mixed until uniform. Finally, 10 g of tin (II) oxalate (SnOx) catalyst was added slowly to the mixture and pH value of the mixture was adjusted to 7 by adding NaOH. The process steps are shown in Figure 35. Note that the catalyst particles easily settle down, agglomerate and make clusters. The clusters adhere to the tube wall and not disappear even by violent shaking (Figure 35e). Adjusting pH value to 7 was found very useful for destroying the catalyst clusters and make a homogeny suspension (Figure 35f). Figure 36 shows the setup designed and prepared for chemical treatment of PLA fibers. This setup consists of four glass tubes which mounted on a fixture and attached to a mechanical stirrer horizontally. Tubes are filled with treatment suspensions and a PLA fiber (length of 30 cm) is cut and placed in each tube. To eliminate the adverse effect of the centrifugal force on dispersion of tin (II) oxalate particles, rotational speed is set as low as 50 rpm.

In this study, two types of PLA filaments were used, filaments which have been prepared by extruding of the PLA pellets grade Ingeo 6062D (NatureWorks ^{LLC}) and the others those sized by re-extruding of PLA filaments diameter of 1.75 mm (7Hillsfilament, Turkey). PLA filaments were chemically treated with different conditions as shown in Table 18. Thermo-gravimetric analysis (TGA) was used to study the effect of treatment operation on de-polymerization temperature of PLA samples. TGA tests were run with heating rate of 10 ºC/min. Figure 37a shows the variation in the samples weight in 140 ºC up to 400 ºC temperature interval and Figure 37b shows reduction rate in the weight of the samples in the same temperature interval.

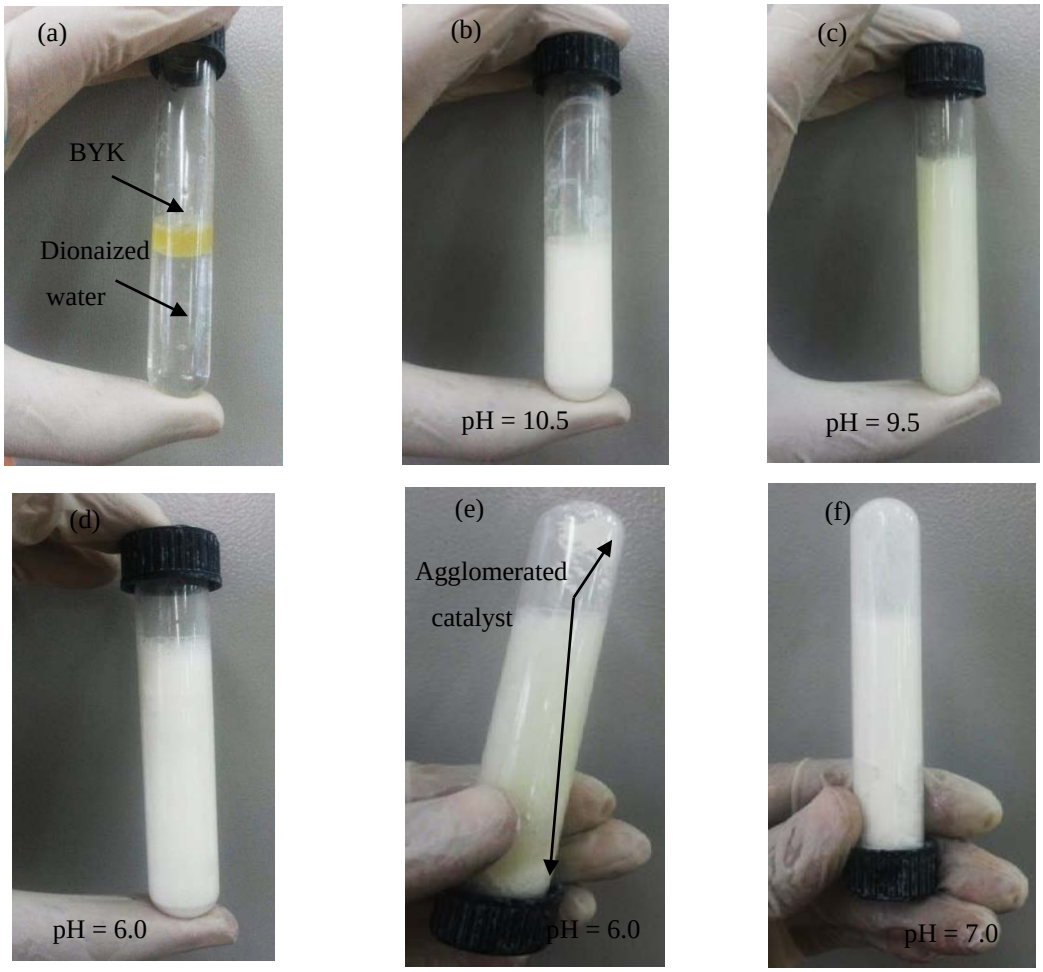

Figure 34. Chemical treatment suspension, (a) adding DISPERBYK-130 to deionized water with ratio of 10:1, (b) shaking to obtain a homogenous solution, (c) adding TFE to the water solution with ratio of 60:40, (d) adding 5 g of tin (II) oxalate (SnOx) catalyst, (e) agglomerated tin (II) oxalate in the solution,(f) adjusting pH value of the mixture to 7 by adding NaOH.

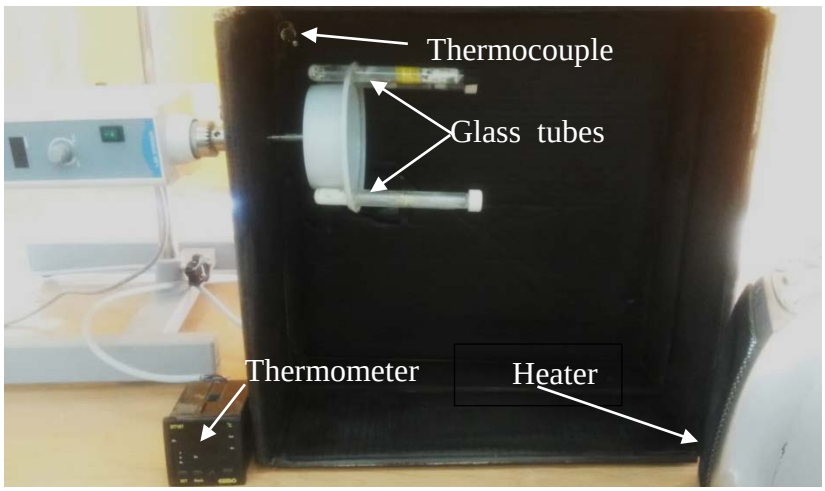

Figure 35. Designed setup for chemical treatment of PLA fibers.

Table 18. Chemically treating of the PLA fibers with various solvent compositions and soaking times. Catalyst concentration was 5 wt. % for all samples

Sample code	TFE:H_2O	Soaking time (h)
control	--	0
control-P	--	0
60-20-P	60:40	20
50-12	50:50	12
60-06	60:40	6

According to the results of the TGA tests (Figure 37a), mass loss in untreated PLA samples begins at 280 °C and 290 °C for control and control-P, respectively; where a sudden increase in mass loss rate (Figure 37b) can also be seen at these temperatures. Similar reduction in mass is seen around 220 °C for 60-06 and 50-12 samples and around 240 °C for 60-20-P. Although de-polymerization temperature of the commercial PLA filaments which are used as 3D printer filament could be significantly decreased; Ingeo 6062D is still better choice for using as sacrificial fiber. Also, treating PLA filaments in TFE:H_2O solvent ratio of 60:40 for 6 hours results in higher decomposition rate. Considering the above discussion PLA filament was prepared by extruding of PLA pellets (Ingeo 6062D, NatureWorks ^{LLC}) and then treated in TFE:H_2O ratio 60:40 with tin (II) oxalate concentration of 5 wt% for 6 hours.

5.1.2 Melt compounding of SnOx and PLA

Gergely et al [80] used a twin screw compounder to make the sacrificial material (PLA, 5%wt SnOx). In this study, the same procedure was followed to infuse SnOx catalyst into PLA. PLA pellets and SnOx (5 wt% respect to PLA) were melt compounded using a twin screw micro compounder (Figure 38). The mixing chamber of compounder was heated to 180 °C and rotational speed of the mixing screw was set to 30 rpm. Then PLA pellets (20 gr, Ingeo 6062D) was added and let to melt. SnOx catalyst (1 gr) was added into the mixing chamber and let to mix for 10 min. Finally, the melt compounded material was extruded through a 1.5 mm

nozzle and wound on a spool. The diameter of extruded filament was set to 0.8 mm by adjusting the rotational velocity of the spool.

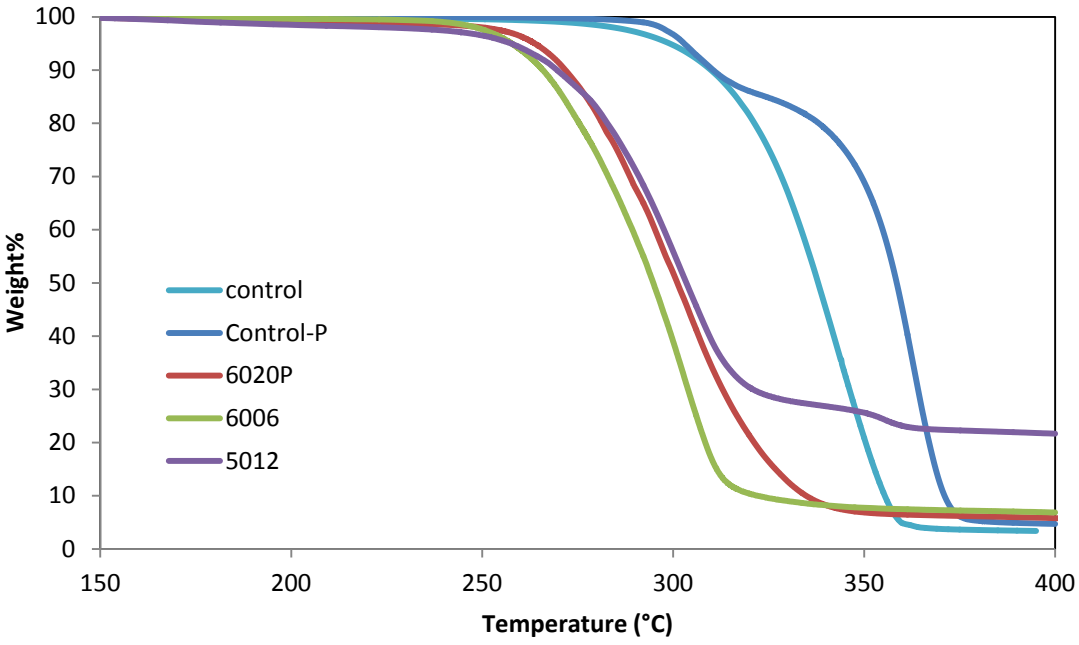

(a)

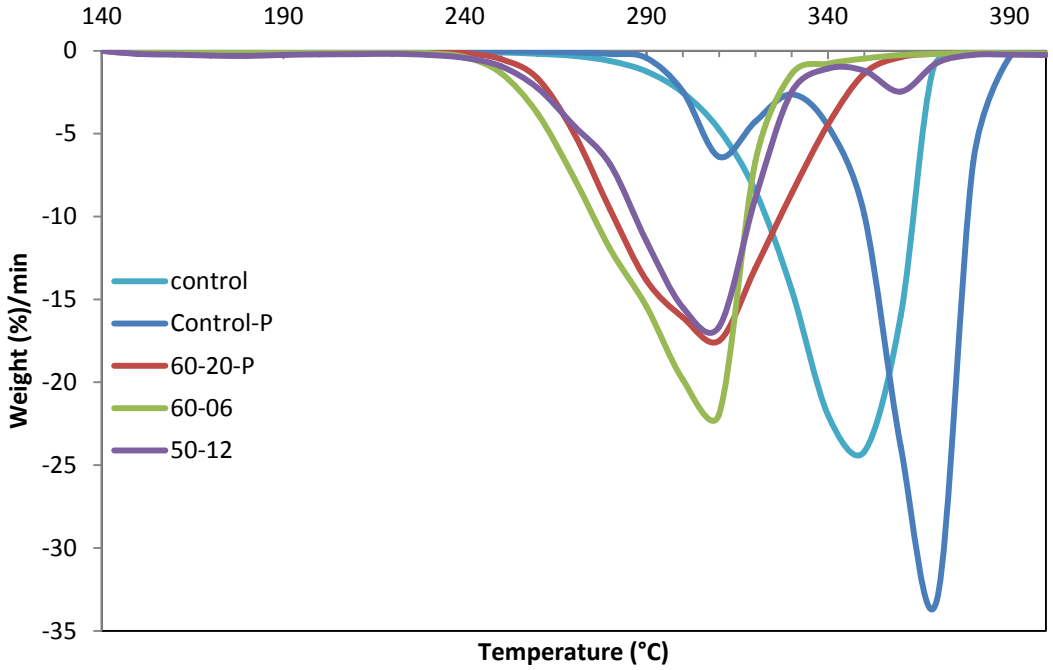

(b)

Figure 36. Thermo-gravimetric analyses (TGA) of untreated and treated PLA filaments, (a) variation in weight (%) vs temperature, (b) weight reduction rate vs temperature.

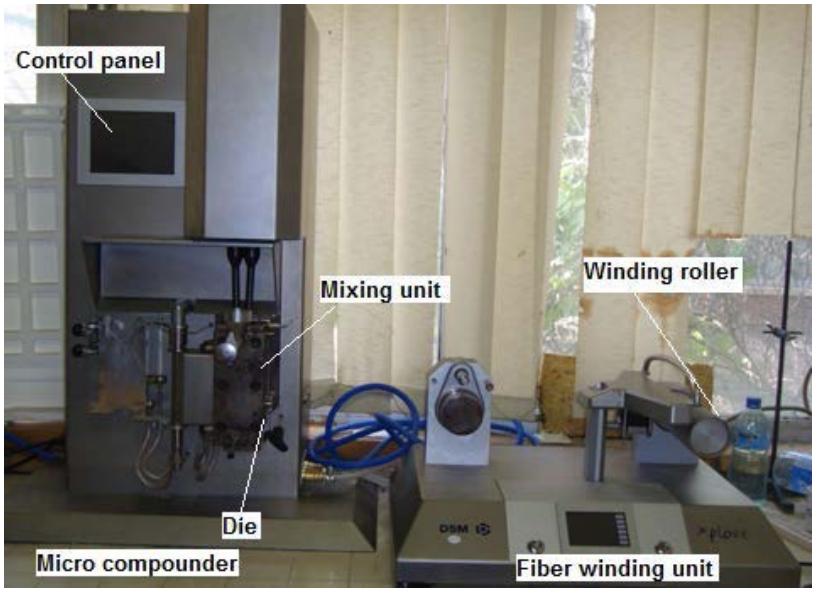

Figure 37. Twin screw micro compounder

5.2 Choosing the proper polymeric matrix

In this study composite laminates are produced by impregnating of unidirectional glass fabrics with a thermoset resin via VRTM process. For this purpose the resin should have low viscosity, long gel time and high glass transition temperature (Tg). Table 19 presents specifications of some epoxy resins and hardeners which could be meeting the mentioned requirements. As it is shown in Table 19, the maximum Tg for these resins is 150 °C which is lower than the necessary temperature to remove sacrificial fibers (200 °C). Thus, it is important to study the effect of post treatment process on the mechanical properties of the epoxy matrix. In this study, Araldite564 /Aradur2954 was selected and subjected to uniaxial tensile tests to study the post treatment effect on their mechanical properties.

Dog bone tensile test samples are prepared according to the ASTM D638 by casting epoxy/hardener solution into Aluminum molds. Samples are cured according to the mentioned scenarios in Table 19. Also, some samples are post treated in an oven for 24 hr at 200 °C. Figure 39 shows the post treated samples. As it is shown in Figure 39 post treated samples are darker which may be due to oxidation that occurs at non-vacuumed oven atmosphere.

Table 19. specifications of some proper epoxy system suitable for making vascularized composites

Resin/Hardener	Curing Cycle	Mixed Viscosity (mPa.s) @25 °C	Gel Time (min) @60°C	Tg (°C)
Araldite1564 Aradur2954	1 hr. 80ºC + 4h 160ºC	500-700	90-120	153
Araldite564 Aradur2954	1 hr. 80ºC + 4h 160ºC	500-700	90-120	153
Araldite8605 Aradur8605	24 hr. 25ºC+2 hr. 120ºC+ 3 hr. 177º C	500-700	90-120	153
Araldite5052 Aradur5052	24 hr. 25ºC+8 hr. 80ºC	500-700	40-50	125

After de-molding, the samples were marked and their cross sections are measured at different sections using micrometer (Figure 40). Tensile test applied to the samples using universal tensile test machine under displacement control at a rate of 0.5 mm/min. To measure strain an extensometer with gauge length of 50 mm was used.

Figure 38. Post treated (24 hrs. @ 200C) epoxy resin (Araldite564/ Aradur2954) samples

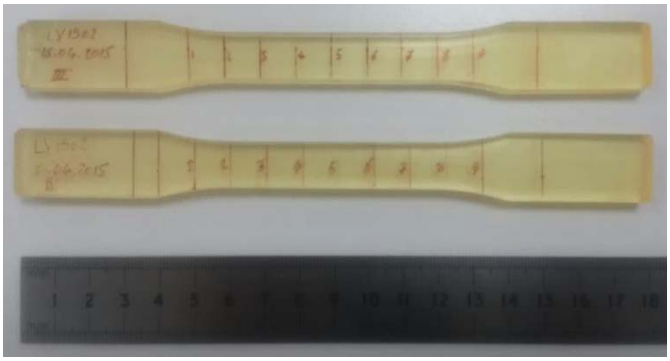

Figure 39. Prepared samples for tensile test

During tensile tests we faced with some issues. Slipping of the tensile sample during tensile test was an issue that frequently observed. This issue affects the amount of calculated strain. In this study, tensile tests were done on two tensile machines (TENSON at University of Turkish Aeronautical Association and ZWICK at METU) with different grips (Figure 41). Figure 42 presents the results of a test which was done on TENSON and Figure 43 is related to the test which was done on ZWICK. Although it was not seen any slippage using self-tightening wedge grips on ZWICK, there was big difference between the calculated strain based on extensometer data and grips displacement.

(a) (b)

Figure 40. Two types of grips those used in this study, (a) ZWICK with self-tightening wedge grips, (b) TENSON with pre-stressed self-tightening wedge-screw grips.

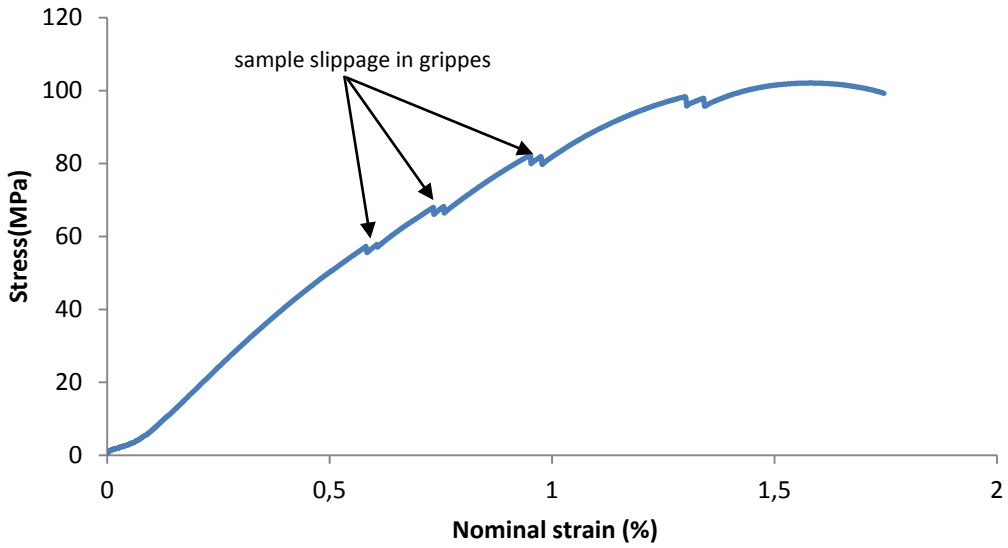

Figure 41. Slippage during tensile test using TENSON.

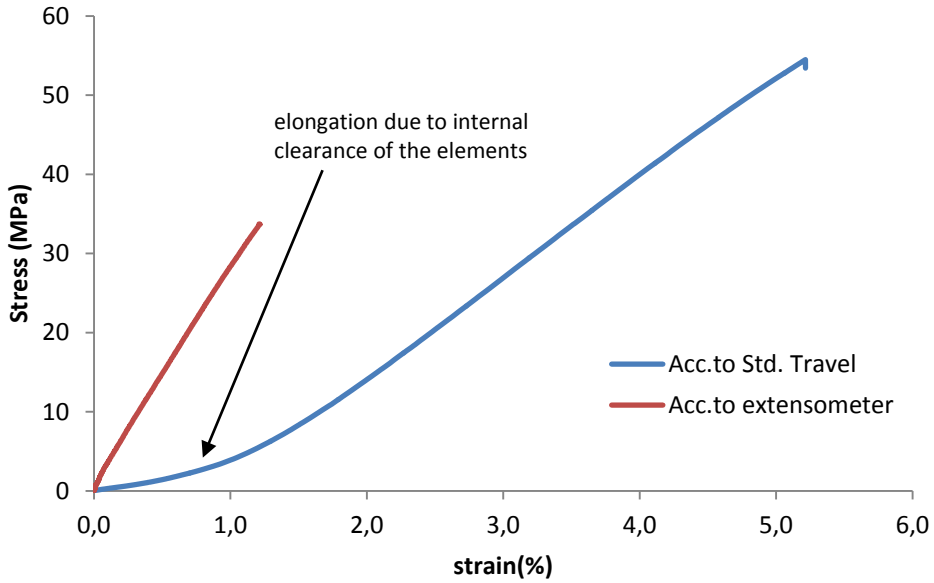

Figure 42. Effect of using extensometer on strain data. Test was done using ZWICK

Note that according to the ASTM D638 and ISO 527-2 for the specimens which show uniform deformation (necking does not occur during test) elongation values should be reported. Percent elongation is defined as the change in gage length relative to the original specimen gage length, expressed as a percent. Percent elongation is calculated using the captured data by extensometer. However,

extensometer is generally removed before breaking of the test sample. This was done for the safety considerations. Therefore, the elongation data via extensometer could be captured just for portion of test up to 1.0% of strain (Figure 43). According to ISO527-1, stress-strain diagrams (for the material which are in ISO527 scope) can be represented using by combination of the percent elongation data those captured by extensometer and nominal strain which calculated using displacement of the grips (Figure 44). However, as it is shown in Figure 43, for the samples which were tested using ZWICK there is an obvious difference between the strain calculated via extensometer data and nominal strain calculated via displacement of the grips. This may because of calibration problem or existence of large clearance between the mechanical joints.

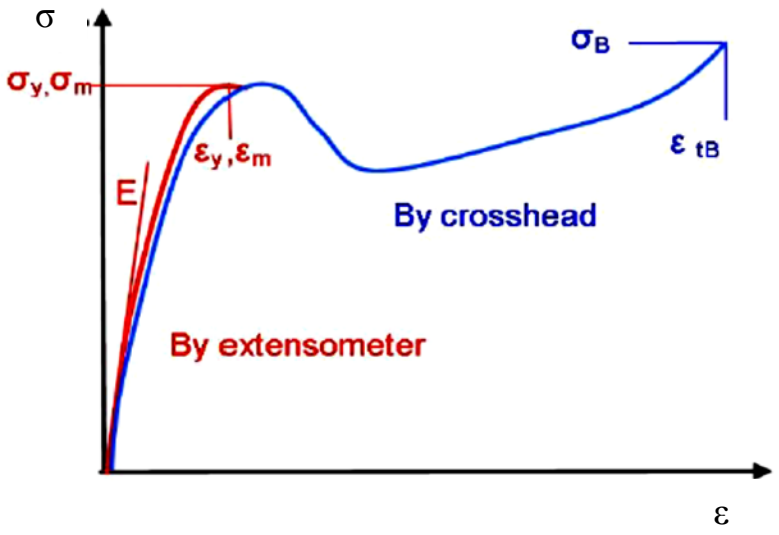

Figure 43. Stress-strain diagram with respect to the ISO 527

Another issue is the specimen alignment which causes problems such as inaccurate tensile modulus and premature failures. Bending may occur as a result of misaligned grips or from specimens themselves if improperly installed in the grips. Figure 45 shows gripping issue at a sample at which braking occurred at gripping zone instead of test length (narrow section of the specimen). Also the breakage form of the samples which have been tested on ZWICK differs from whose tested through TENSON. The Samples which tested via ZWICK were broken in ´V´ shape but the

breakage of the specimen those tested using TENSON occurred on a straight line (Figure 46). This may be due to different breaking mechanisms where at ZWICK the breakage was occurred due to moment instead of pure tension. Existence of moment can result in breakage at lower stresses. Therefore, the tests were continued on TENSON at University of Turkish Aeronautical Association.

Figure 44. Premature failure at gripping area.

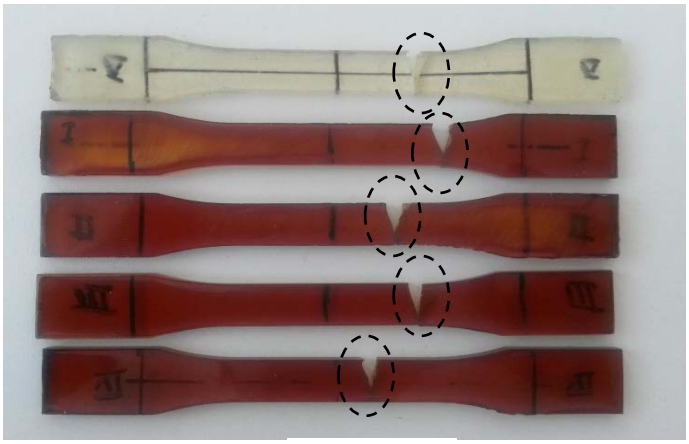

(a)

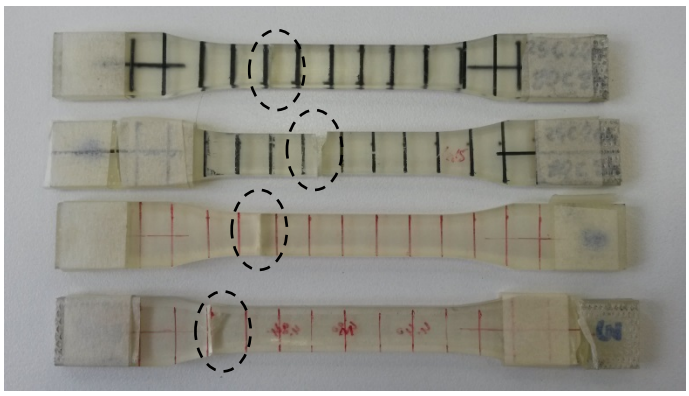

(b)

Figure 45. The Samples with different breakage form (shape), (a) tested via ZWICK, (b) tested using TENSON.

Table 20 presents the results of tensile tests for the epoxy samples subjected and not subjected to post treatment process. Both groups of samples are cured at 80 ºC for 8 hours followed by curing in the oven at 160 °C for 4 hours. Considering the presented results at Table 20, post curing treatment does not show any adverse effect on tensile strength, break point elongation and modulus of elasticity.

Table 20. effect of post treatment process on mechanical properties of Araldite LY564 / Aradur 2954 polymer matrix

Curing cycle	Post treatment	σ_m (MPa)	ϵ_b (%)	E (GPa)
1 hr at 80ºC + 4hrs at 160ºC	--	80±5	6.0±0.5	2.3±0.2
1 hr at 80ºC + 4hrs at 160ºC	24 hrs at 200ºC	78±3	6.5±0.5	2.4±0.2

5.3 Fabrication of epoxy/glass continuous fiber reinforced composite specimens with Vascular Channels

Specimens of UD glass fiber reinforced composite laminates were fabricated containing vascular channels (0.8 mm diameter) along the laminate mid-plane. The laminates were made using 12 plies (4 mm thickness) uni-directional glass fabrics (areal weight of 190 g/m2) with two stacking sequences ($[0/90]_{3s}$ and $[90/0]_{3s}$). Fabrics were cut and laid in an Aluminum mold (with dimensions 280 mm × 205 mm and thickness of 4 mm) respect to the designed stacking sequence. Four PLA filaments with diameter of 0.8 mm and 290 mm length were located on the 6^{th} ply with 50 mm apart each other (Figure 47). To keep the filaments straight along the mold cavity, both ends were adhered to the mold surface. Mold setup is shown in Figure 48. The nominal fiber volume fraction was 55%. Finally, the mold was closed and fabrics were impregnated with epoxy resin (Aradur 564: Araldite 2954, 100:37 wt%, Huntsman) using Vacuum Assisted Resin Transfer Molding (VARTM). Composites were cured in an oven at 80 ºC for one hour then at 160 ºC for 4 hours. Following the cure, composite plates were trimmed around the edges and cut along PLA filaments into the individual tensile test specimens (dimension of 250 mm × 25 mm).

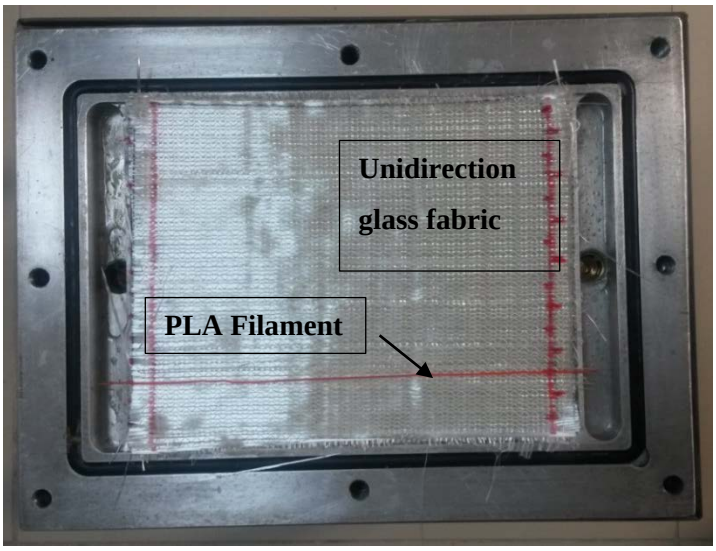

Figure 46. Locating PLA on 6th fabric

Figure 47. Mold setup

Figure 49 shows the cross section of a test specimen. Samples were put in a vacuum oven at 200 ºC for 24 hours to vaporize the sacrificial component (PLA filament). In order to remove depolymerized PLA which was in form of powder, Acetone was injected into the channels.

Figure 50 shows the composite specimens with a hollow channel with 0.8 mm diameter. Cross-sectional optical micrographs of vascularized laminates (Figure 50) shows that the geometrical form of the composite laminate surrounding vascule is affected by stacking sequence.

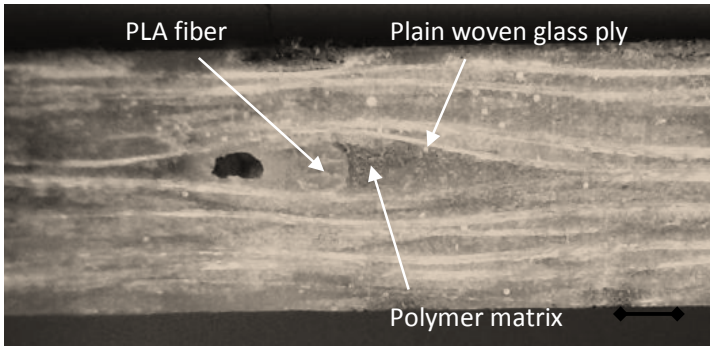

Figure 48. Cross section of the PLA fibers 0.8 mm diameter examined using optical microscope (15× lens). Scale bar represents 1 mm.

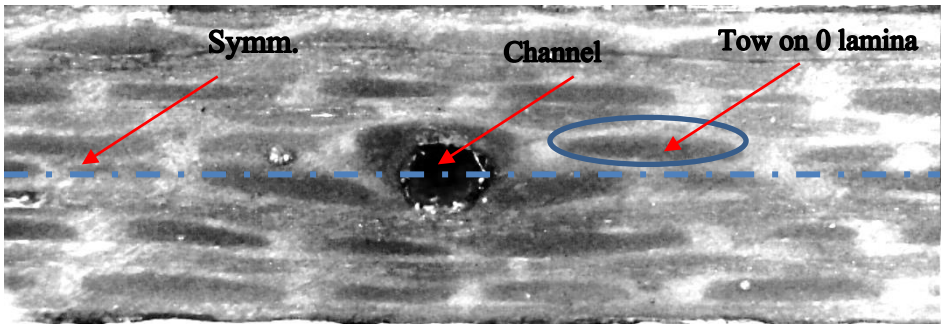

(a)

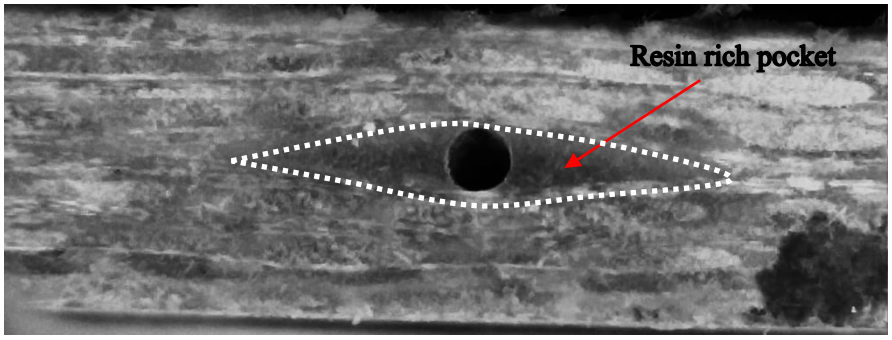

(b)

Figure 49. Optical image (15× lens).of a hollow channel with 0.8 mm diameter in a glass fiber reinforced composite specimen. Stacking, a) $[90, 0]_{3s}$, b) $[0, 90]_{3s}$.

In case of [0/90] stacking, a larger resin reach pocket is observed around channel in comparison with [90/0] where tows on zero plies adjacent to vascular channel cover the channel surround. This issue is shown in Figure 51, graphically. It is worth noting that the geometry and dimensions of the resin reach area should be considered

in modeling of vascularized composites. Huang et. al. [14] defined four parameters as resin pocket length (L_{RP}), fiber disturbance angle (θ_d), fiber disturbance height (h_d), resin pocket area (A_{RP}) to make a 2D model of composite laminate with embedded circular vasculature (Figure 52). In order to measure the mentioned geometric parameters, the cross section of the fabricated composite laminates was examined using optical microscopy (Veho VMS-004D). The results are presented in Table 21.

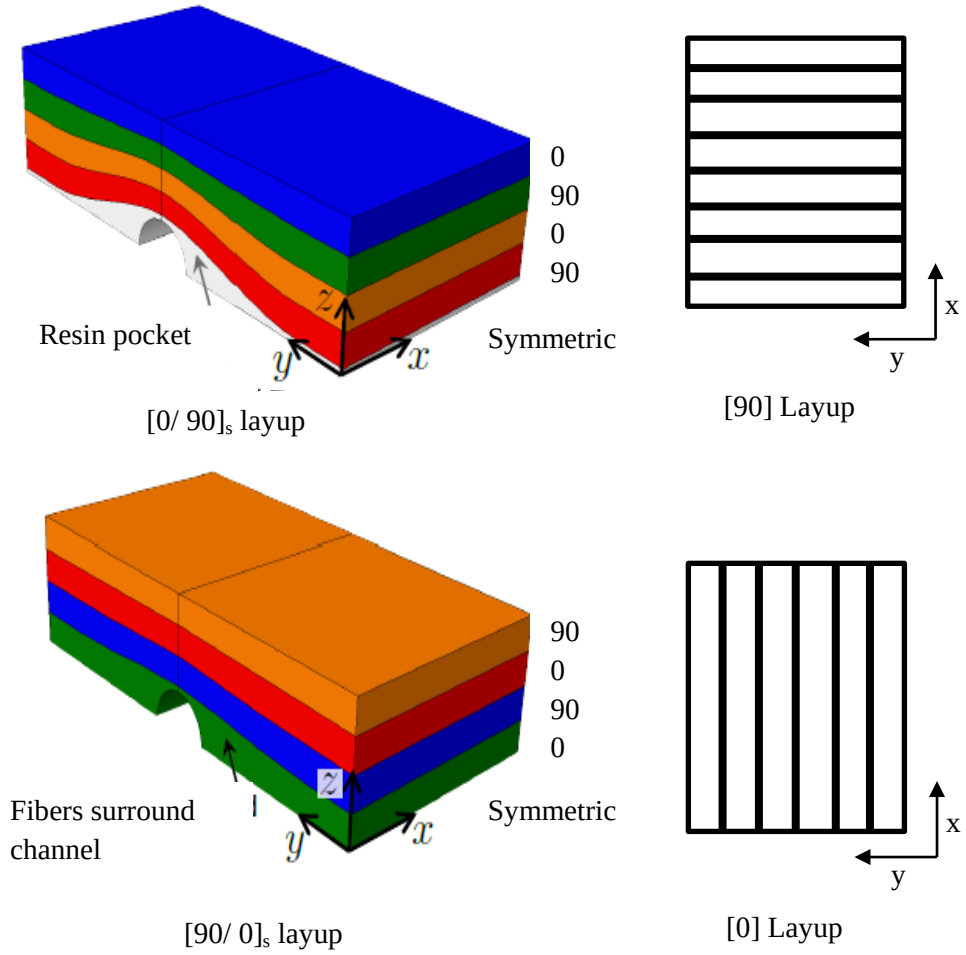

Figure 50. Graphical description of the effect of existence of a circular vascular channel on cross section of a laminate with [0/90] and [90/0] stacking.

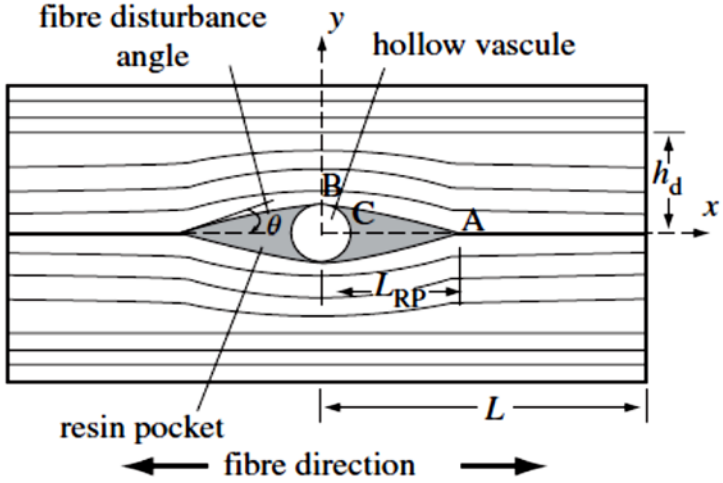

Figure 51. Conceptual model of laminate with embedded circular vascule surrounded by a resin pocket.

Table 21. Geometric parameters of circular channel diameter of 0.8 mm

Stacking	number of plies	resin pocket length (L_{RP}) (mm)	Fiber disturbance angle (θ_d)	Fiber disturbance height (h_d) (mm)
[0/90]	12	3.5±0.2	25±1	1.4±0.2
[90/0]	12	1.6±0.2	10±0.5	0.6±0.1

5.4 Injection of CNT/epoxy slurry into vascular channels for conductive pathway formation

A syringe pump (Figure 53) was used to inject the CNT/epoxy suspension as an electrically conductive medium into the vascular channels with a flow rate of 2cc/min through a veterinary luer needle (21-gauge, d_{out}=0.8 mm, d_{in}=0.5 mm). When the channel was filled completely, the injection process was halted. Then, the inlet valve was closed and the sample was allowed to cure under a solenoid magnetic field for 6 h (Figure 54). Figure 55 shows the optical images of vascularized composite laminates with vascular channels that have been filled with CNT/epoxy.

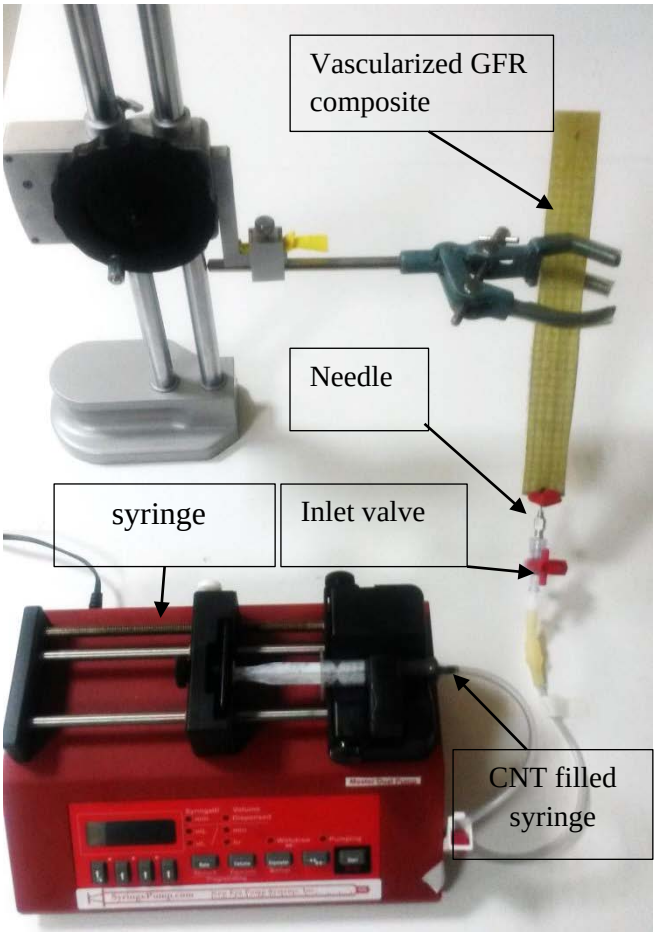

Figure 52. Filling the microvascular channel with CNT/epoxy conductive suspension.

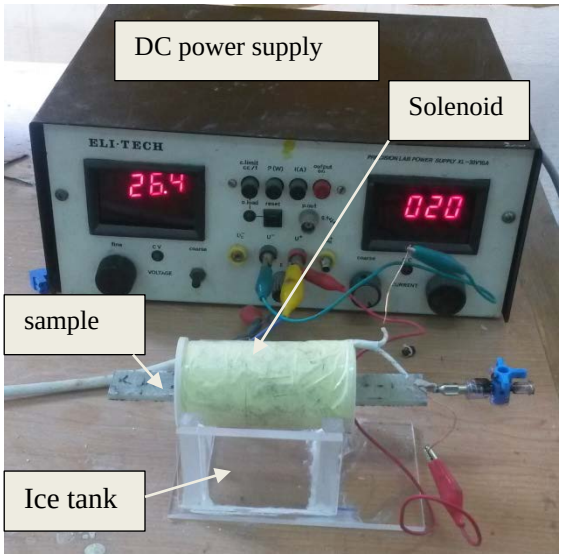

Figure 53. Curing CNT/epoxy conductive suspension inside microvascular channel under magnetic field .

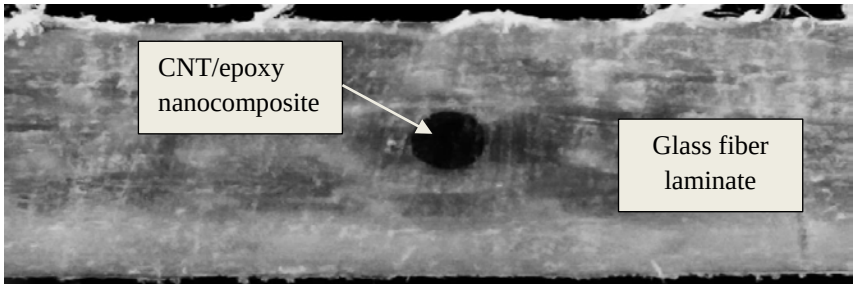

(a)

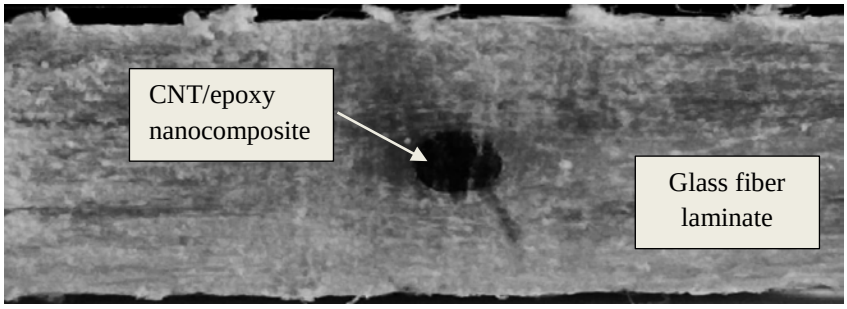

(b)

Figure 54. Optical image (15× lens) of a vascularized composite laminate. Macro channel (0.8 mm diameter) was filled with CNT/epoxy. Stacking, a) $[90, 0]_{3s}$, b) $[0, 90]_{3s}$.

5.5 Characterization of electrically conductive epoxy/glass fiber reinforced composites and Results

5.5.1 Measurement of electrical conductivity

The electrical resistance of the samples along their length was measured using the two-point-probe technique [60] with a Keithley 2000 Digital Multimeter. Both ends of the composite samples were polished using sand paper and washed with acetone, then painted with a conductive silver paint. The average electrical resistance measured along the macro-channel (diameter 0.8 mm, length 150 mm) for three samples was 18±2 MΩ.

5.5.2 Comparison of the mechanical properties

A uniaxial tensile test was performed according to ISO 527-4 under displacement control by straining at a rate of 0.5 mm/min using a universal tensile test machine (Zwick Z250). Clamping used hydraulic grips with a clamping pressure of 100 bar. To measure strain, an extensometer with a gauge length of 50 mm was used. The experimental setup and test specimen are shown in Figure 56. Table 22 presents the modulus of elasticity, ultimate tensile strength, and strain at breaking point for samples under the uniaxial tensile test. Note that the presented results are the mean of three successful tests. In addition, Young's modulus was measured in the linear portion of stress-strain curve between 0.1% and 0.5% strain. From Table 22, the modulus of elasticity, tensile strength, and fracture strain of the composite laminates containing a 0.8-mm-diameter vascular channel on their symmetry plane are the same as the control samples, regardless to the stacking sequence or whether the channel was hollow or filled with CNT/epoxy nanocomposite. In other words, the ratio of the vascular channel diameter (0.8 mm) to the fabricated laminate thickness (4 mm) is small enough so as to not affect the composite strength. Injecting the CNT/epoxy high viscous suspension into channels with diameters less than 0.8 mm is not feasible. Therefore, the minimum vascular channel diameter in this study was limited to 0.8 mm.

Table 22. Uniaxial tensile test result

Sample	Vascular channel	Modulus of elasticity (GPa)	Tensile strength (MPa)	Fracture strain (%)
[0/90]	No	16.5±0.2	298±10	2.3±0.2
[90/0]	No	17.0±0.4	316±15	2.4±0.1
[0/90]	hollow	16.7±0.2	302±10	2.1±0.1
[90/0]	hollow	17.4±0.4	320±10	2.4±0.1
[0/90]	Filled with CNT/epoxy	16.9±0.2	305±10	2.4±0.2
[90/0]	Filled with CNT/epoxy	17.4±0.1	325±4	2.4±0.1

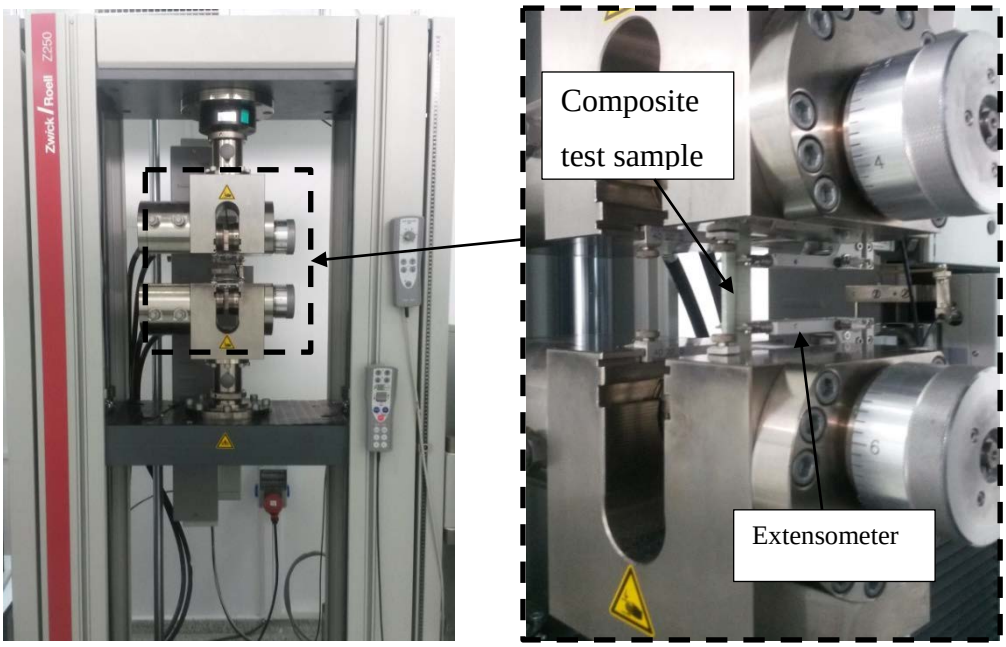

Figure 55. Tensile test setup for measuring tensile strength.

5.6 Strain sensing behavior of electrically conductive epoxy/glass fiber reinforced composites under tensile load

In order to obtain the relationship between the electrical resistance of the conductive composites and the mechanical load, the change in electrical resistance along the vascular channel was measured. Samples were prepared as described in section 5.5.1, and two electric cables were attached to their ends. The electrical resistance of each sample through their vascular channel was measured during the tensile test. Figure 57 shows the piezoresistive response of the vascularized electrically conductive composite samples with $[0,90]_s$ and $[90,0]_s$ stacking configurations. Note that the tests were halted when the electrical conductivity through the channels was missed. In both cases, the relation between the variation in electrical resistance, normalized by the resistance measured for the unloaded condition $\left(\frac{\Delta R}{R_0}\right)$ and tensile strain(ε), can be represented by a linear equation. In Table 23, the calculated gauge factor ($k = (\Delta R/R_0)/\varepsilon$), the maximum measured normalized resistance change, and its respective strain value for the $[0,90]_s$ and

$[90,0]_s$ vascularized conductive laminates are shown. Theoretically, there is no difference between the mechanical properties of these laminates made with $[0, 90]_s$ and $[90, 0]_s$ stacking sequences. This is addressed during the discussion of experimental results in section 5.5.2, since here the conductive path for the $[0, 90]_s$ configuration was cut at a lower strain than the $[90,0]_s$ configuration. As presented in Table 23, for the case when 90 plies surround the vascular channel at a tensile strain of 1.0%, the conductive path was cut. However, for the case where 0 plies were placed at the mid-plane, the resistance through the vascular channel was measured up to 1.9% of the strain.

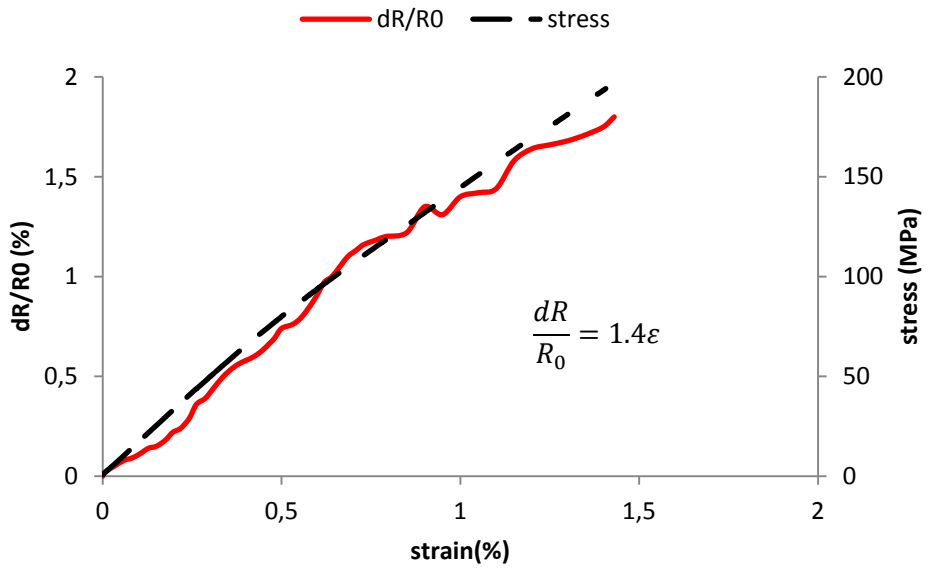

(a)

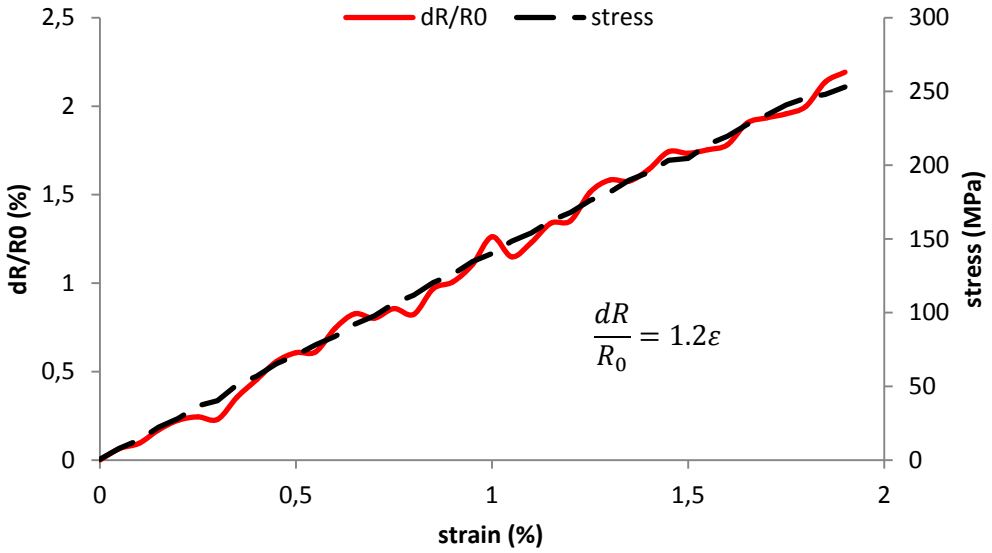

(b)

Figure 56. Normalized changes in resistance and tensile stress vs. strain, for stacking configuration (a) [0,90], (b) [90,0].

Table 23. Calculated gauge factor and measured normalized resistance change at different stacking configurations

Stacking sequence	Gauge factor	$\left(\frac{\Delta R}{R_0}\right)_{max}$	$(\varepsilon)_{max}$
[0,90]	1.4±0.1	1.3±0.4	1.0±0.3
[90,0]	1.2±0.1	2.1±0.1	1.9±0.1

5.7 Applying correction coefficient to gauge factor

In this study, tensile strain of the samples was measured using an extensometer with gauge length L_{gauge} of 50 mm. However, the effectively stressed length of the internal sensor is $L_{channel}$ = 200 mm, resulting from the sum of the length of the sample between grips (150 mm) plus twice the half length of the sample inside grips (25 mm). Assuming direct proportionality between the length and the electric conductivity of the CNT nanocomposite, the following equations can be established [63]:

$$\frac{L_{gauge}}{R_{gauge}} = \frac{L_{channel}}{R_{channel}} \tag{21}$$

$$\Delta R_{gauge} \cong \Delta R_{channel} \tag{22}$$

$$\frac{\Delta R_{gauge}}{\mathrm{R}_{gauge}} = \frac{L_{channel}}{L_{gauge}} \times \frac{\Delta R_{channel}}{\mathrm{R}_{channel}} \tag{23}$$

$$\frac{\Delta R_{gauge}}{\mathrm{R}_{gauge}} = \frac{L_{channel}}{L_{gauge}} \times k\varepsilon \tag{24}$$

$$k_{gauge} = \frac{L_{channel}}{L_{gauge}} \times k = \frac{200}{50} \times k \tag{25}$$

Thus the presented strain sensitivities in are considerably increased by applying a correction coefficient $\frac{L_{channel}}{L_{gauge}} = 4$. In another word, the fabricated conductive pathways through vascular channels are about two times more sensitive to sense strain than conventional strain gauges.

5.8 Discussion of Results

In this chapter, electrically conductive composites were fabricated by forming vascular channels embedded in continuous-glass, fiber-reinforced composites using the vaporization of sacrificial components. The sacrificial fiber PLA was used. Two different techniques, chemical treatment and melting, were used to reduce the degradation temperature of the PLA fibers. In both techniques, a catalyst (SnOx) was

infused into the PLA. The effectiveness of these techniques was tested via thermogravimetric analysis of the treated samples. From a review of section 5.1, treating the PLA with a melting compound is cheaper and requires less effort than chemical treatment.

The mechanical properties of the Araldite LY 564/Aradur 2954 epoxy system with a nominal glass transition temperature of 150°C were not affected by treating this polymeric matrix at 180°C for 24 h.

Optical inspection of the cross-section of the vascularized laminates with [0,90] and [90,0] stacking configurations showed that the dimensions and form of the resin that reached a pocket surrounding the vascular channel varies with respect to the stacking configuration. A larger resin pocket formed around the channel for the [0,90] configuration. Despite this, the mechanical properties found from the uniaxial tensile test were the same for vascularized and not vascularized samples regardless of the stacking configuration used.

For both stacking configurations, the electrical resistance of the composite samples through their vascular channel varied with respect to the applied uniaxial tensile strain with an acceptable sensitivity. The maximum detected strain for the samples with [0,90] stacking was around 1.0%. For samples with the [90,0] configuration, it was around 2.1%. In another word, the electrical conductivity via vascular channel was cut-off under lower strain at with the [0,90] configuration. This severing of the electrical conductivity through the vascular channel may be resulted by two phenomena: a permanent, plastic deformation in the CNT/epoxy matrix, driving the CNTs apart and destroying the conductive path between the two ends of the channel, or a failure of the CNT/epoxy matrix. Note that, theoretically, the amount of strain at the midplane of the composite laminates with [0,90] and [90,0] stacking sequences is the same. Thus, the early cutoff for the [0,90] case implies that an early failure of the CNT/epoxy matrix is more probable than when using the [90,0] configuration. This may be due to manufacturing issues. As mentioned before, using [0,90] stacking results in the formation of a large resin reach volume around the vascular channel. By applying vacuum pressure during the fabrication process, the trapped air bubbles in the resin tend to pass through this highly permeable

volume. By ending the process when the inlet and outlet ports are closed, the air bubbles are trapped inside this resin volume, forming several micro- and macroscopic voids in the cured composite. Finally during the service, cracks are initiated from these discontinuities. Propagation of these cracks causes the CNT/epoxy matrix to fail. On the other hand, for the [90,0] configuration the compact resin pocket around the vascular channel minimizes the risk of the formation of macroscopic cracks.

5.9 Potential for use of wax filament in sacrificial fiber production

The potential for using PLA as a sacrificial component is limited to matrices with high glass transition temperatures (Tg). The maximum Tg for typical epoxy polymers is 150ºC, which can be achieved by curing the epoxy polymer at high temperatures. That is, PLA cannot be used for polymers with low Tg or in fiber-reinforced composites those are cured at room temperature.

Here we introduce a potential application of hydrocarbon-based wax filaments to form microchannels embedded in fiber-reinforced composites. As filaments, Print2Cast by Machinablewax, USA were used. A Print2Cast filament is a hybrid plasticized wax blend, and its technical specification is presented in Table 24. The filament used is available in 1.75 and 3 mm diameters, and its well-known application is in making 3D models by fused deposition modeling (FDM) for use in lost wax casting.

In this study we used wax filaments and introduced a cost-effective process for fabricating microchannel-embedded fiber-reinforced composites. The fabricated laminate consists of 8-ply ±45-glass fabrics. Fabrics were cut and laid in an aluminum mold of dimensions 280 mm × 205 mm and 4 mm thick. Two Print2Cast filaments 1.75 mm in diameter were placed on the mid ply in the form of S-shaped curves (Figure 57). After closing the mold, fabrics were impregnated with epoxy resin (Araldite 564: Aradur 3486, 100:35 wt%, Huntsman) using vacuum assisted resin transfer molding. Composites were cured in an oven at 80ºC for 8 h. Following the cure, the laminate was trimmed around the edges. In order to remove wax fibers,

each composite plate was treated in a vacuum oven at 130ºC for 4 h. Note the oblique positioning of the plate inside the oven which allowed molten wax to run out ease. Figure 58 shows an S-shaped hollow channel embedded in the composite plate.

Table 24. Technical specifications of Print2Cast filament

Hardness	50 (Shore "D" Scale)
Specific Density	0.9137 $\frac{gr}{cm^3}$
Flash Point	300 ºC
Melt Point	117 ºC
Viscosity 130 ºC	3,000 cP
Volumetric Shrinkage (for recycling, from melting point to room temp)	5% typical
Ash content for lost wax casting applications	0.004%

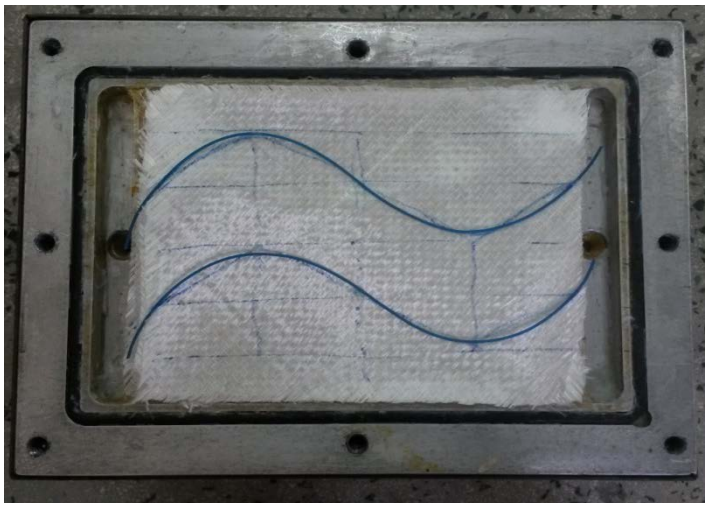

Figure 57. Placing wax filaments inside the mold mid-ply.

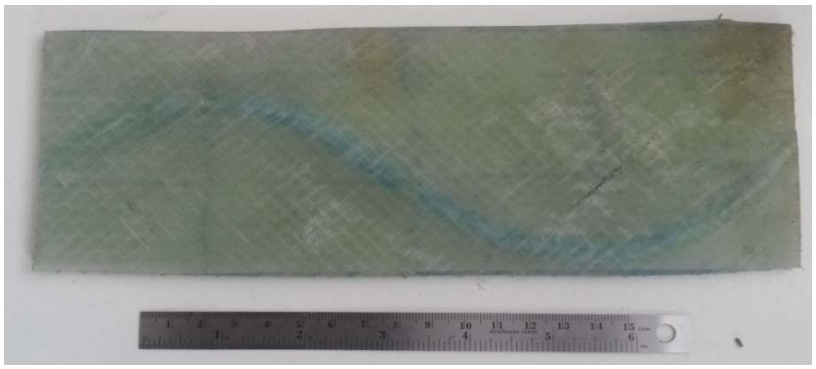

Figure 58. S--shaped hollow channel embedded in the composite.

CHAPTER 6

CONCLUSIONS AND FUTURE WORK

In this study, a novel approach was introduced to make electrically conductive fiber reinforced composites. In the proposed approach, microvascular channels were produced in glass fiber reinforced laminates and then these hallow channels were filled with CNT-epoxy suspension. These electrically conductive paths were then used as internal strain sensors. CNT-epoxy suspension was prepared using shear mixing process. The effectiveness of the process parameters on electric conductivity and tensile strength of nanocomposite was studied using ANOVA. Furthermore, the effect of fabrication parameters on strain sensing properties of the nanocomposites was also investigated by citing sensitivity, bias and nonlinearity of the prepared nanocomposites.

The electrical properties of nanocomposites were significantly increased by subjecting CNT-epoxy suspension in a magnetic field during curing cycle. A 2D percolation based model was also used to simulate electrical conductivity of CNT nanocomposites as well as their behavior under tensile strain. The distribution state of CNTs was captured from SEM analysis of experimental samples and integrated into model through Monte Carlo process.

Vaporization of sacrificial fibers was used to make hollow vascular channels in glass fibers reinforced composites. The effect of stacking configuration was also investigated by fabricating hollow vascular channels in laminates with [0,90]s and [90,0]s stacking sequences. Tensile tests were performed for mechanical characterization of vascularized composites. These hollow vascular channels were then filled with CNT-epoxy suspension to make electrical conductive paths in

composite laminate. The use of such conductive pathways for in situ strain monitoring of a composite specimen was also investigated.

The following have been found and concluded in this thesis

- The suspension dispersion homogeneity is not affected by mixing time at low CNT concentration (0.2 wt.%). However, for high concentrated samples (0.5 wt.%) using higher mixing speed with longer periods of mixing time is resulted in finer structure (lower A_{50} and A_{90} values and higher A_{occ}).
- Electric conductivity of the high concentrated nanocomposites is strongly affected by mixing parameters. On the other hand, mixing parameters do not show significant effect on electric conductivity when the CNT loading was set to its low value.
- Tensile strength of the nanocomposites those are prepared using low mixing speed, regardless of mixing time and CNT concentration is significantly lower than the strength of not reinforced epoxy.
- Strain sensory behavior of the nanocomposite gauges containing higher amount of CNTs is not affected by mixing speed and time. Respect to the obtained high gauge sensitivity with acceptable bias and nonlinearity, the nanocomposites fabricated by dispersing of low amount of CNT (0.2 wt.%) with high mixing speed and long mixing time are more suitable for strain sensing applications.
- The electrical properties of nanocomposites are increased near two times by subjecting CNT-epoxy suspension in a magnetic field of 0.2T during curing cycle. The following morphological study of theses samples show that CNTs have been aligned to the direction of the magnetic field.
- Simulation results demonstrate that the electrical conductivity of nanocomposites with aligned nanotubes is around 1.5 times greater than those have randomly distributed nanotubes in their microstructures. Despite this improvement in electrical conductivity, the variation in electrical resistance was more pronounced for randomly distributed microstructures. Strain sensitivity factor (Gauge factor) as high as 35 and

27 were predicted for nanocomposites made from random and aligned nanotube microstructures, respectively.

- Mechanical characterization of composite laminates with and without a vascular channel show that tensile strength and elastic module of composite are not affected by making a 0.8 mm vascular channel on its symmetry plane.
- Filling vascular channels imbedded in fiber reinforced composites with CNT-epoxy is introduced as a novel method to fabricate electrical conductive composites.
- These conductive paths are proper tools for in situ strain monitoring. The fabricated conductive pathways through vascular channels are about two times more sensitive to sense strain than conventional strain gauges.

The following are recommended for future work related to this thesis topic

- The experimental analysis can be extended to other mechanical properties such as flexural strength and interlaminar shear strength. This analysis would give a more complete picture of mechanical characteristics of electrical conductive composites via embedded vascular channels.
- The process of filling the vascular channels with CNT-epoxy can be improved by either developing the proposed technique or using new methods. This would be essential in case of filling very long vascular channels or channels with complex geometries.

REFERENCES

[1] Phillips DM, Ryan Pierce M, Baur JW. Mechanical and thermal analysis of microvascular networks in structural composite panels. Compos Part A Appl Sci Manuf 2011;42:1609–19. doi:10.1016/j.compositesa.2011.07.008.

[2] Soghrati S, Najafi AR, Lin JH, Hughes KM, White SR, Sottos NR, et al. Computational analysis of actively-cooled 3D woven microvascular composites using a stabilized interface-enriched generalized finite element method. Int J Heat Mass Transf 2013;65:153–64. doi:10.1016/j.ijheatmasstransfer.2013.05.054.

[3] Norris CJ, Meadway GJ, O'Sullivan MJ, Bond IP, Trask RS. Self-Healing Fibre Reinforced Composites via a Bioinspired Vasculature. Adv Funct Mater 2011;21:3624–33. doi:10.1002/adfm.201101100.

[4] Patrick JF, Hart KR, Krull BP, Diesendruck CE, Moore JS, White SR, et al. Continuous self-healing life cycle in vascularized structural composites. Adv Mater 2014;26:4302–8. doi:10.1002/adma.201400248.

[5] Wu AS, Coppola AM, Sinnott MJ, Chou T-W, Thostenson ET, Byun J-H, et al. Sensing of damage and healing in three-dimensional braided composites with vascular channels. Compos Sci Technol 2012;72:1618–26. doi:10.1016/j.compscitech.2012.06.012.

[6] Coppola AM, Warpinski LG, Murray SP, Sottos NR, White SR. Survival of actively cooled microvascular polymer matrix composites under sustained thermomechanical loading. Compos PART A 2016;82:170–9. doi:10.1016/j.compositesa.2015.12.010.

[7] Barton DP. Comparative vacuum monitoring: a new method of in-situ real-time crack detection and monitoring. 2004.

[8] Roach D. Real time crack detection using mountable Comparative Vacuum monitoring sensors. Smart Struct Syst 2009;5:317–28. doi:10.12989/sss.2009.5.4.317.

[9] Kousourakis a., Bannister MK, Mouritz a. P. Tensile and compressive properties of polymer laminates containing internal sensor cavities. Compos Part A Appl Sci Manuf 2008;39:1394–403. doi:10.1016/j.compositesa.2008.05.003.

[10] Esser-kahn AP, Thakre PR, Dong H, Patrick JF, Vlasko-vlasov VK, Sottos NR, et al. Three-Dimensional Microvascular Fiber-Reinforced Composites. Adv Mater 2011;23:3654–8. doi:10.1002/adma.201100933.

[11] Coppola AM, Thakre PR, Sottos NR, White SR. Tensile properties and damage evolution in vascular 3D woven glass/epoxy composites. Compos Part A Appl Sci Manuf 2014;59:9–17. doi:10.1016/j.compositesa.2013.12.006.

[12] Janowski MM and UKV and GM. Parametric studies on self-repairing approaches for resin infused composites subjected to low velocity impact. Smart Mater Struct 1999;8:623.

[13] Williams HR, Trask RS, Bond IP. Self-healing sandwich panels: restoration of compressive strength after impact. Compos Sci Technol 2008;68:3171–7.

[14] Huang C, Trask RS, Bond IP. Characterization and analysis of carbon fibre-reinforced polymer composite laminates with embedded circular vasculature. R Soc Interface 2010:1229–41.

[15] Swait TJ, Jones FR, Hayes SA. A practical structural health monitoring system for carbon fibre reinforced composite based on electrical resistance. Compos Sci Technol 2012;72:1515–23. doi:10.1016/j.compscitech.2012.05.022.

[16] Pyrzanowski P, Olzak M. Numerical modelling of resistance changes in symmetric CFRP composite under the influence of structure damage. Compos Sci Technol 2013;88:99–105. doi:10.1016/j.compscitech.2013.08.023.

[17] Krückel J, Weck C, Schubert DW. Rheology and conductivity of carbon fibre composites with defined fibre lengths. Compos Sci Technol 2013;85:58–64. doi:10.1016/j.compscitech.2013.06.006.

[18] Liu L, Ma P, Xu M, Ullah S, Kim J. Strain-sensitive Raman spectroscopy and electrical resistance of carbon nanotube-coated glass fibre sensors. Compos

Sci Technol 2012;72:1548–55. doi:10.1016/j.compscitech.2012.06.002.

[19] Devalve C, Pitchumani R. Experimental investigation of the damping enhancement in fiber-reinforced composites with carbon nanotubes. Carbon N Y 2013;63:71–83. doi:10.1016/j.carbon.2013.06.041.

[20] Domingues D, Logakis E, Skordos AA. The use of an electric field in the preparation of glass fibre / epoxy composites containing carbon nanotubes. Carbon N Y 2012;50:2493–503. doi:10.1016/j.carbon.2012.01.072.

[21] Sandler J, Shaffer MSP, Prasse T, Bauhofer W, Schulte K, Windle AH. Development of a dispersion process for carbon nanotubes in an epoxy matrix and the resulting electrical properties. Polymer (Guildf) 1999;40:5967–71.

[22] Martin CA. Formation of percolating networks in multi-wall carbon-nanotube – epoxy composites. Compos Sci Technol 2004;64:2309–16. doi:10.1016/j.compscitech.2004.01.025.

[23] Schüler R, Petermann J, Schulte K WH. Agglomeration and electrical percolation behaviour of carbon black dispersed in epoxy resin. J Appl Polym Sci 1997;63:1741–6.

[24] Hu N, Masuda Z, Yamamoto G, Fukunaga H. Effect of fabrication process on electrical properties of polymer / multi-wall carbon nanotube nanocomposites. Compos Part A Appl Sci Manuf 2008;39:893–903. doi:10.1016/j.compositesa.2008.01.002.

[25] Grammatikos SA, Paipetis AS. On the electrical properties of multi scale reinforced composites for damage accumulation monitoring. Compos Part B 2012;43:2687–96. doi:10.1016/j.compositesb.2012.01.077.

[26] Wichmann MHG, Meyer LO, Schulte K. Load and health monitoring in glass fibre reinforced composites with an electrically conductive nanocomposite epoxy matrix. Compos Sci Technol 2008;68:1886–94. doi:10.1016/j.compscitech.2008.01.001.

[27] Loos MR, Coelho LAF, Pezzin SH, Amico SC. Effect of Carbon Nanotubes Addition on the Mechanical and Thermal Properties of Epoxy Matrices. Mater Res 2008;11:347–52.

[28] Yamamoto N, Guzman de Villoria R, Wardle BL. Electrical and thermal

property enhancement of fiber-reinforced polymer laminate composites through controlled implementation of multi-walled carbon nanotubes. Compos Sci Technol 2012;72:2009–15. doi:10.1016/j.compscitech.2012.09.006.

[29] Ma P-C, Liu M-Y, Zhang H, Wang S-Q, Wang R, Wang K, et al. Enhanced Electrical Conductivity of Nanocomposites Containing Hybrid Fillers of Carbon Nanotubes and Carbon Black. ACS Appl Mater Interfaces 2009;1:1090–6. doi:10.1021/am9000503.

[30] Lin Y, Gigliotti M, Lafarie-frenot MC, Bai J. Effect of carbon nanotubes on the thermoelectric properties of CFRP laminate for aircraft applications. J Reinf Plast Compos 2015. doi:10.1177/0731684414565940.

[31] Wen X, Wang Y, Gong J, Liu J, Tian N, Wang Y, et al. Thermal and fl ammability properties of polypropylene / carbon black nanocomposites. Polym Degrad Stab 2012;97:793–801. doi:10.1016/j.polymdegradstab.2012.01.031.

[32] Huang G, Wang S, Song P, Wu C, Chen S, Wang X. Combination effect of carbon nanotubes with graphene on intumescent flame-retardant polypropylene nanocomposites. Compos Part A Appl Sci Manuf 2014;59:18–25. doi:10.1016/j.compositesa.2013.12.010.

[33] Hossain MK, Hossain ME, Hosur MV, Jeelani S. Flexural and compression response of woven E-glass/polyester–CNF nanophased composites. Compos Part A Appl Sci Manuf 2011;42:1774–82. doi:10.1016/j.compositesa.2011.07.033.

[34] Zhou YX, Wu PX, Cheng Z, Ingram J, Jeelani S. Improvement in electrical , thermal and mechanical properties of epoxy by filling carbon nanotube. Express Polym Lett 2008;2:40–8. doi:10.3144/expresspolymlett.2008.6.

[35] Tang L-C, Wan Y-J, Peng K, Pei Y-B, Wu L-B, Chen L-M, et al. Fracture toughness and electrical conductivity of epoxy composites filled with carbon nanotubes and spherical particles. Compos Part A Appl Sci Manuf 2013;45:95–101. doi:10.1016/j.compositesa.2012.09.012.

[36] Gracia J De, Vargas G. In-plane shear behaviour of multiscale hybrid composites based on multiwall carbon nanotubes and long carbon fibres. J

Reinf Plast Compos 2015. doi:10.1177/0731684415603491.

[37] Jangam S, Raja S, Gowd BUM. Influence of multiwall carbon nanotube alignment on vibration damping of nanocomposites. J Reinf Plast Compos 2016. doi:10.1177/0731684415626285.

[38] Siddiqui NA, Li EL, Sham M, Zhong B, Lin S, Mäder E, et al. Tensile strength of glass fibres with carbon nanotube – epoxy nanocomposite coating : Effects of CNT morphology and dispersion state. Compos Part A 2010;41:539–48. doi:10.1016/j.compositesa.2009.12.011.

[39] Ma PC, Siddiqui NA, Marom G, Kim JK. Dispersion and functionalization of carbon nanotubes for polymer-based nanocomposites: A review. Compos Part A Appl Sci Manuf 2010;41:1345–67. doi:10.1016/j.compositesa.2010.07.003.

[40] Kim S, Lee WI, Park CH. Assessment of carbon nanotube dispersion and mechanical property of epoxy nanocomposites by curing reaction heat measurement. J Reinf Plast Compos 2016. doi:10.1177/0731684415613704.

[41] Overbeck A, Linke S, Kwade A, Schilde C, Schl M. Thermal , mechanical and electrical properties of highly loaded CNT- epoxy composites e A model for the electric conductivity. Compos Sci Technol 2015;117:183–90. doi:10.1016/j.compscitech.2015.06.013.

[42] Bauhofer W, Kovacs JZ. A review and analysis of electrical percolation in carbon nanotube polymer composites. Compos Sci Technol 2009;69:1486–98. doi:10.1016/j.compscitech.2008.06.018.

[43] Xie X, Mai Y, Zhou X. Dispersion and alignment of carbon nanotubes in polymer matrix : A review. Mater Sci Eng A 2006;49:89–112. doi:10.1016/j.mser.2005.04.002.

[44] Ma PC, Siddiqui NA, Marom G, Kim JK. Dispersion and functionalization of carbon nanotubes for polymer-based nanocomposites: A review. Compos Part A Appl Sci Manuf 2010;41:1345–67. doi:10.1016/j.compositesa.2010.07.003.

[45] Guru K, Mishra SB, Shukla KK. Effect of temperature and functionalization on the interfacial properties of CNT reinforced nanocomposites. Appl Surf Sci 2015;349:59–65. doi:10.1016/j.apsusc.2015.04.196.

[46] Cha J, Jin S, Hun J, Soo C, Jin H, Hyung S. Functionalization of carbon

nanotubes for fabrication of CNT / epoxy nanocomposites. JMADE 2016;95:1–8. doi:10.1016/j.matdes.2016.01.077.

[47] Fan Z, Hsiao K-T, Advani SG. Experimental investigation of dispersion during flow of multi-walled carbon nanotube/polymer suspension in fibrous porous media. Carbon N Y 2004;42:871–6. doi:10.1016/j.carbon.2004.01.067.

[48] Geng Y, Liu MY, Li J, Shi XM, Kim JK. Effects of surfactant treatment on mechanical and electrical properties of CNT / epoxy nanocomposites. Compos Part A 2008;39:1876–83. doi:10.1016/j.compositesa.2008.09.009.

[49] Pillai S, Ray S. Epoxy-based carbon nanotubes reinforced composites. Adv Nanocomposites - Synth Charact Ind Appl Ed by Dr Boreddy Reddy 2011:727.

[50] Yum SH, Roh JU, Park JM, Park JK, Kim SM, Lee W Il. Assessment of particle distribution in particle-containing composite materials using an electron probe microanalyzer. Compos Sci Technol 2013;82:38–46. doi:10.1016/j.compscitech.2013.04.008.

[51] Castellino M, Chiolerio A, Shahzad MI, Jagdale PV, Tagliaferro A. Electrical conductivity phenomena in an epoxy resin–carbon-based materials composite. Compos Part A Appl Sci Manuf 2014;61:108–14. doi:10.1016/j.compositesa.2014.02.012.

[52] Kovacs JZ, Velagala BS, Schulte K, Bauhofer W. Two percolation thresholds in carbon nanotube epoxy composites. Compos Sci Technol 2007;67:922–8. doi:10.1016/j.compscitech.2006.02.037.

[53] Knite M, Teteris V, Kiploka A, Kaupuzs J. Polyisoprene-carbon black nanocomposites as tensile strain and pressure sensor materials. Sensors Actuators A Phys 2004;110:142–9. doi:10.1016/j.sna.2003.08.006.

[54] Ma P, Siddiqui NA, Marom G, Kim J. Dispersion and functionalization of carbon nanotubes for polymer-based nanocomposites : A review. Compos Part A 2010;41:1345–67. doi:10.1016/j.compositesa.2010.07.003.

[55] Kumaresan T, Nere NK, Joshi JB. Effect of internals on the flow pattern and mixing in stirred tanks. Ind Eng Chem Res 2005;44:9951–61. doi:10.1021/ie0503848.

[56] Jirout T, Rieger F. Impeller design for mixing of suspensions. Chem Eng Res Des 2011;89:1144–51. doi:10.1016/j.cherd.2010.12.005.

[57] Paul EL, Atiemo-obeng VA, Kresta SM. HANDBOOK OF INDUSTRIAL MIXING Edited by. n.d.

[58] Montgomery DC. Design and Analysis of Experiments. John Wiley & Sons; 2006.

[59] Schneider CA, Rasband WS, Eliceiri KW. NIH Image to ImageJ: 25 years of image analysis. Nat Meth 2012;9:671–5.

[60] Schroder DK. Semiconductor Material and Device Characterization. Wiley-Interscience; 2006.

[61] Korayem AH, Barati MR, Simon GP, Zhao XL, Duan WH. Reinforcing brittle and ductile epoxy matrices using carbon nanotubes masterbatch. Compos Part A Appl Sci Manuf 2014;61:126–33. doi:10.1016/j.compositesa.2014.02.016.

[62] Kowalski SM, Montgomery DC. Design and Analysis of Experiments: MINITAB Companion. J. Wiley & Sons; 2011.

[63] Häntzsche E, Matthes A, Nocke A, Cherif C. Physical Characteristics of carbon fiber based strain sensors for structural-health monitoring of textile-reinforced thermoplastic composites depending on the textile technological integration process. Sensors Actuators A Phys 2013;203:189–203. doi:10.1016/j.sna.2013.08.045.

[64] Pyzdek T, Keller PA. Quality Engineering Handbook. Taylor & Francis; 2003.

[65] Ma C, Liu H, Du X, Mach L, Xu F, Mai Y. Fracture resistance , thermal and electrical properties of epoxy composites containing aligned carbon nanotubes by low magnetic field. Compos Sci Technol 2015;114:126–35. doi:10.1016/j.compscitech.2015.04.007.

[66] Moaseri E, Karimi M, Baniadam M, Maghrebi M. Improvements in mechanical properties of multi-walled carbon nanotube-reinforced epoxy composites through novel magnetic-assisted method for alignment of carbon nanotubes. Compos PART A 2014;64:228–33. doi:10.1016/j.compositesa.2014.05.014.

[67] Arguin M, Sirois F, Therriault D, Arguin M. Electric field induced alignment of multiwalled carbon nanotubes in polymers and multiscale composites Electric field induced alignment of multiwalled carbon nanotubes in polymers and multiscale composites. Adv Manuf Polym Compos Scince 2015;340. doi:10.1179/2055035914Y.0000000003.

[68] Park C, Wilkinson J, Banda S, Ounaies Z, Wise KE, Sauti G, et al. Aligned single-wall carbon nanotube polymer composites using an electric field. J Polym Sci Part B Polym Phys 2006;44:1751–62.

[69] Tyagi PK, Singh MK, Misra A, Palnitkar U, Misra DS, Titus E, et al. Preparation of Ni-filled carbon nanotubes for key potential applications in nanotechnology. Thin Solid Films 2004;470:127–30. doi:10.1016/j.tsf.2004.08.070.

[70] Ashkan Behnam AU. Computational study of geometry-dependent resistivity scaling in single-walled carbon nanotube films. Phys Rev 2007. doi:10.1103/PhysRevB.75.125432.

[71] Hu N, Karube Y, Yan C, Masuda Z, Fukunaga H. Tunneling effect in a polymer/carbon nanotube nanocomposite strain sensor. Acta Mater 2008;56:2929–36.

[72] Bao WS, Meguid S a., Zhu ZH, Pan Y, Weng GJ. A novel approach to predict the electrical conductivity of multifunctional nanocomposites. Mech Mater 2012;46:129–38. doi:10.1016/j.mechmat.2011.12.006.

[73] Lee BM, Loh KJ. Carbon nanotube thin fi lm strain sensors : comparison between experimental tests and numerical simulations. Nanotechnology 2017;28:155502. doi:10.1088/1361-6528/aa6382.

[74] Lee BM, Loh KJ. A 2D percolation-based model for characterizing the piezoresistivity of carbon nanotube-based films. J Mater Sci 2015;50:2973–83. doi:10.1007/s10853-015-8862-y.

[75] Wang Z, Ye X. A numerical investigation on piezoresistive behaviour of carbon nanotube/polymer composites: mechanism and optimizing principle. Nanotechnology 2013;24:265704. doi:10.1088/0957-4484/24/26/265704.

[76] Amini A, Bahreyni B. Behavioral model for electrical response and strain

sensitivity of nanotube-based nanocomposite materials. J Vac Sci Technol B 2012;30. doi:http://dx.doi.org/10.1116/1.3691654.

[77] Singh AK, Harsha SP, Parashar A. Finite Element Analysis of CNT reinforced epoxy composite due to Thermo-mechanical loading. Procedia Technol 2016;23:138–43. doi:10.1016/j.protcy.2016.03.009.

[78] Dong H, Esser-kahn AP, Thakre PR, Patrick JF, Sottos NR, White SR, et al. Chemical Treatment of Poly (lactic acid) Fibers to Enhance the Rate of Thermal Depolymerization. ACS Appl Mater Interfaces 2012:503–9.

[79] Nguyen DT, Leho YT, Esser-Kahn AP. Process of Making Three-dimensional Microstructures using Vaporization of a Sacrificial Component. JoVE (Journal Vis Exp 2013:e50459--e50459. doi:10.3791/50459.

[80] Gergely RCR, Pety SJ, Krull BP, Patrick JF, Doan TQ, Coppola AM, et al. Multidimensional Vascularized Polymers using Degradable Sacrifi cial Templates. Adv Funct Mater 2015:1043–52. doi:10.1002/adfm.201403670.

CURRICULUM VITAE

Name: Hamed Tanabi

Email: tanabi.hamed@metu.edu.tr tel.:0553 222 38 13

Degree	University	From/To	CGPA
B.S	Tabriz	1998-2002	3.05
M.S	Tabriz	2002-2005	3.35
PhD	METU	2011-2017	3.78

PhD Thesis Title:

DESIGN AND MANUFACTURING OF ELECTRICALLY CONDUCTIVE COMPOSITES VIA MICROVASCULAR CHANNELS

Publications:

- K. Poorghasemi, F Ommi, V. Esfahanian and H. Tanabi " Investigation of the Soot and NO Emission Reduction Mechanism in DI Diesel Engines by Means of Split Injection Strategy." Journal of Fuel and Combustion,3,pp 91-103,2011
- V. Poormostagimi and H. Tanabi " Investigation of the Effect of Tool Wear on Chip Radii by using of the Neural Networks" ICME 2010 Conf., Tabriz, Iran,2010
- H. Tanabi, N. Babaei, D. Khanlari "Evaluation of Machinability Rating of ADI in Comparison with Forged Steels" ICME 2010 Conf., Tabriz, Iran,2010
- N. Babaei,A. Babaei, H. Tanabi “Evaluation of process parameters effect on hardness of HPT disks and hardness prediction using fuzzy logic and regression” ICME 2010 Conf., Tabriz, Iran,2010
- H. Tanabi, N. Babaei, D. Khanlari " Evaluation of Mechanical Properties and Machinability Rating of ADI in Comparison with Casting Steels “ National Mechanical Engineering Conference, Marvdasht, Iran,2011
- H. Tanabi, N. Babaei,A. Babaei " Real-time tool wear monitoring based on feed motor current in chuck- center mounting condition" Advanced Materials

Research Vols. 341-342 (2012) pp 307-312

- N. Babaei,A. Babaei, H. Tanabi " Investigation of Grinding Surface Temperature: Experimental Measurements and Numerical Modeling" Advanced Materials Research Vols. 341-342 (2012) pp 147-151
- T. Aydil, H. Tanabi, M. Erdal," Modeling of Compression Resin Transfer Molding for Manufacturing Particle-Filled Advanced Composites", 28th American Society for Composites, Pennsylvania, USA, 2013.
- T. Aydil, H. Tanabi, M. Erdal," Particle Deposition In Resin Transfer Molding Of Advanced Composites", 16th International Conference on Machine Design and Production (UMTIK 2014), Izmir, Turkey, 2014.
- T. Aydil, H. Tanabi, M. Erdal," Resin Transfer Molding Of Particle-Filled, Continuous-Fiber Reinforced Composites", American Society for Composites 29th Technical Conference,16th USJapan Conference on Composite Materials, ASTM-D30 Meeting, California, USA, 2014.

Relevant work experiences:

- Atash Su, Tabriz, Mechanical Engineer,2002-2003, Responsibility included die design .
- Sarmad Tabriz, Auditor,2003-2004, Audit to ISO TS, ISO 9000
- Iran Fareh, Tabriz, , Mechanical Engineer,2004-2006, CNG kits design, getting TA for NGV (Pride, Nissan) and CNG kit's components. Also, responsibility included operating with CMM, Profile Projector, and Hardness Testing Machine.
- Iran Tractor Manu. Co., Tabriz, 2006-2010, R & D Engineer, responsibility included front axle assembly design (ITM285-4WD and ITM399-4WD).
- Azad University, Tabriz, Iran, Instructor, 2010-2011.
- Middle East Technical University, Teaching Assistant, 2012-2013.
- Middle East Technical University, Researcher, BAP entitled ''Kompozit Malzemelerde Mikrovasküler Kanallar Yardımıyla Elektrik İletkenliği Oluşturulması'', 2015-2016.
- University of Turkish Aeronautical Association, Instructor, 2013.

Awards:

- The Best Engineering Team of Iran, Awarded by Ministry of Labor and Social Affairs, 2011.
- The grand prize awarded by the Elginkan Foundation, The 13th annual New Businesses New Ideas (YFYİ) program, 2017.